NYO-9660
MITNE-13

MEASUREMENTS OF THE MATERIAL BUCKLINGS OF LATTICES OF NATURAL URANIUM RODS IN D_2O

by

P.F. PALMEDO, I. KAPLAN and T.J. THOMPSON

January 20, 1962

Contract AT(30-1) 2344
U.S. Atomic Energy Commission

Department of Nuclear Engineering
Massachusetts Institute of Technology
Cambridge, Massachusetts

MASSACHUSETTS INSTITUTE OF TECHNOLOGY
DEPARTMENT OF NUCLEAR ENGINEERING
Cambridge 39, Massachusetts

MEASUREMENTS OF THE MATERIAL BUCKLINGS OF LATTICES OF NATURAL URANIUM RODS IN D_2O

by

P. F. PALMEDO, I. KAPLAN and T. J. THOMPSON

January 20, 1962

NYO-9660
AEC Research and Development Report
UC-34 Physics
(TID-4500, 16th Edition)

Contract AT(30-1)2344
U.S. Atomic Energy Commission

DISTRIBUTION

NYO - 9660
AEC Research and Development Report
UC - 34 Physics
(TID - 4500, 16th Edition)

1. USAEC, New York Operations Office (D. Richtmann)
2. USAEC, Division of Reactor Development (I. Zartman)
3. USAEC, New York Patents Office (H. Potter)
4. USAEC, New York Operations Office (S. Strauch)
5. USAEC, Division of Reactor Development, Reports and Statistics Branch
6. USAEC, Maritime Reactors Branch
7. USAEC, Civilian Reactors Branch
8. USAEC, Army Reactors Branch
9. USAEC, Naval Reactors Branch
10. Advisory Committee on Reactor Physics (E. R. Cohen)
11. ACRP (G. Dessauer)
12. ACRP (D. de Bloisblanc)
13. ACRP (M. Edlund)
14. ACRP (R. Ehrlich)
15. ACRP (I. Kaplan)
16. ACRP (H. Kouts)
17. ACRP (F. C. Maienschein)
18. ACRP (J. W. Morfitt)
19. ACRP (B. I. Spinrad)
20. ACRP (P. F. Zweifel)

21. ACRP (P. Gast)

22. ACRP (G. Hansen)

23. ACRP (S. Krasik)

24. ACRP (T. Merkle)

25. ACRP (T. M. Snyder)

26. ACRP (J. J. Taylor)

27. - 29. O.T.I.E., Oak Ridge, for Standard Distribution, UC-34, TID-4500 (16th Edition)

30. - 49. P. F. Palmedo

50. - 100. Internal Distribution

ABSTRACT

The experimental and analytical bases of the determination of the material bucklings of uranium-D_2O lattices are presented. Techniques which were developed, particularly with the intent of measuring material bucklings in the MIT lattice facility, are described.

The design considerations and experiments dealing with the spatial distribution and magnitude of the neutron source in the lattice facility are discussed. The source distribution was analyzed as it entered the subcritical assembly tank when the tank contained only D_2O and when the tank contained a lattice of uranium rods in D_2O. The detailed investigation of the over-all flux distributions in lattices included a study of the non-separability of the macroscopic and microscopic radial distribution.

A set of computer codes was developed to reduce and analyze fully the data from flux distribution measurements.

The bucklings of three lattices of 1.010-inch diameter natural uranium rods in D_2O were measured. These measurements are shown to be in good agreement with measurements made in similar lattices at other laboratories.

This report is based on a dissertation submitted by Philip F. Palmedo to the Nuclear Engineering Department of the Massachusetts Institute of Technology, in partial fulfillment of the requirements for the degree of Doctor of Philosophy. The work was performed in part at the MIT Computation Center

ACKNOWLEDGMENTS

The success of a project of this order of magnitude is due to the combined work of a number of individuals and groups. The results of this particular report are primarily due to the work of the principal author, Philip Palmedo, who has submitted substantially this same report in partial fulfillment for the requirements of the Ph.D. degree at M.I.T. He has been assisted by other students working on the project as well as by those mentioned specifically below. Mr. A. E. Profio has been responsible for much of the work of the project as a whole and has contributed many ideas and given direction in the design of the facility, methods of carrying out the experiments, and the over-all program. Over-all direction of the project is shared by A. E. Profio and two of the authors, I. Kaplan and T. J. Thompson. Mr. Joseph Barch has been of invaluable assistance in setting up experiments and in the construction and operation of the facility. Miss Barbara Kelley has assisted with the preparation and counting of foils and in many other ways. Mr. M. Quinteiro was responsible for the development of the automatic flux scanner system and the miniature fission chambers. Mr. F. Becker carried out the two-group reflector analysis summarized in Appendix A-2.

Staffs of the M.I.T. Reactor and the Reactor Machine Shop have provided daily assistance to the project and advice during the experimental portion of the work. The development of the computer codes utilized in this work was made possible by the efficient cooperation of the M.I.T. Computation Center.

All of these individuals and groups were essential to the completion of this work.

TABLE OF CONTENTS

TABLE OF CONTENTS (continued)

TABLE OF CONTENTS (continued)

LIST OF FIGURES

LIST OF FIGURES (continued)

LIST OF TABLES

CHAPTER I
INTRODUCTION

1.1 PURPOSES OF THE WORK

The work which will be reported was undertaken with several purposes in mind. Generally, it was initiated with the intent of studying the methods of measuring material bucklings of heterogeneous systems. Specifically, the study was to be applied and exemplified in preparing for, and in making, buckling measurements in lattices of uranium rods in D_2O at MIT. The specific purposes can be distinguished as follows:

a) The investigation of present techniques of measuring the bucklings of lattices with an eye to improving these techniques where possible.

b) The establishing of experimental and analytical techniques which would allow the convenient and accurate determination of the bucklings of various lattices to be studied by the MIT Lattice Project.

c) The design of aspects of the MIT lattice facility directly related to the measurement of bucklings in the facility.

d) The investigation and "adjustment" of the source flux distribution to make it satisfactory for the various types of experiments to be performed.

e) The investigation of the details of flux distributions in lattices which are related to the measurement of bucklings.

f) The determination of the material bucklings of three spacings of 1.010 inch diameter natural uranium rods in D_2O.

The measurements of bucklings are an important part of the MIT Heavy Water Lattice Project. The project is one of the research programs of the Nuclear Engineering Department at MIT and is being carried out under a contract with the U.S. Atomic Energy Commission. A preliminary description of the project, the first annual report, has

already been published (H6).

The first stage of the work consisted of the design and construction of the lattice facility. During this period, the author was particularly concerned with those aspects of the design directly related to the buckling measurements. Chapter II of this report is devoted to a description of the studies made to design a flux-shaping pedestal for the experimental tank. The experiments designed to examine the resultant flux distributions in the tank are described in Chapter III.

Chapter IV is devoted to a discussion of the theoretical bases of buckling measurements. Particular emphasis is given to the assumptions made when the theory is applied in particular experiments. A detailed investigation of the various contemporary approaches to the measurement of buckling was made and is summarized in Chapter V. On the basis of this investigation, the combination of experimental methods and analytical techniques to be used at MIT were chosen. A description of these methods, the equipment used, and the analytical techniques employed is given in Chapter VI. In choosing the methods to be used, consideration was given, not only to the accurate determination of the bucklings of the systems to be studied, but also to the investigation of some of the details of such measurements.

For purposes of accuracy, completeness, and convenience, a set of IBM-709 computer codes was developed to analyze experimental data. Brief descriptions of the various codes, their theoretical basis, and their operation are given in Chapter VI, while detailed descriptions of the codes are presented in Appendix A1.

Various aspects of the flux distribution in lattices were investigated experimentally and are reported in Chapter VII. The material bucklings of three lattices of natural uranium rods in D_2O were measured and are also reported in Chapter VII. Chapter VIII summarizes the work performed and suggests the experimental methods to be used in future buckling measurements at the MIT Lattice Project.

1.2 THE EXPONENTIAL EXPERIMENT

Exponential experiments have played an important and changing role in the history of nuclear reactor physics. Early in the development of the field, Fermi conceived of, and employed, this type of experiment to investigate the possibility of achieving a self-sustaining chain reaction (A1). In principle, the experiment is quite simple, consisting essentially of observing the neutron flux distribution in a volume of the material of interest when one face of the volume is bombarded by neutrons. The significance of such experiments stems from the fact that important quantities – in particular, the material buckling – are quite easily obtained in this way.

Today many other quantities are measured in exponential experiments in addition to macroscopic flux distributions, and the uses of such experiments have similarly ramified. The present state of theoretical reactor physics makes it necessary to rely to some degree on either critical or exponential experiments for a sufficiently accurate prediction of the details of reactor criticality. Moreover, a variety of empirical data may be obtained in exponential assemblies which can serve as the necessary checks of, and stimuli for, theoretical developments.

Integral multiplication experiments are a possible alternative to exponential experiments and have been widely used to investigate various multiplying assemblies. This was the technique primarily employed by the Germans in their early research (H1) and has been used quite recently by Persson (P1). Such experiments involve the study of the multiplication of neutrons from some source as a function of the amount of the materials of interest near the source. Except in rather unusual circumstances, however, integral experiments yield a smaller amount of, and less accurate, information than do exponential experiments (P1), (W1).

Although pulsed neutron methods are becoming more widely used to investigate macroscopic lattice properties, such techniques are as yet not as productive as exponential experiments (S1), (D1). It is to be expected, however, that pulsed neutron measurements

will become complimentary to exponential experiments, particularly with regard to a multigroup, theoretical formulation of such experiments. For, although there is great flexibility in an exponential type experiment to study microscopic lattice properties, the pulsed method entails the potential for studying the dynamics of the neutron slowing-down process in lattices.

Critical experiments involve both advantages and disadvantages when compared to exponential experiments. Among the advantages is that in a critical system, one can measure reactivity effects quite directly, and that the critical, geometric (as well as the material) buckling can be measured. Some measurements which can be performed in both types of experiments are simplified by the higher fluxes generally available in critical systems. The major disadvantages of critical experiments are that they require greater amounts of material, as well as greater safety precautions.

It has been suggested by some investigators that a fundamental difference exists between bucklings measured in a critical facility and those determined in exponential experiments (W9). One of the difficulties involved in evaluating the validity of such an effect is that there is no published account of complete exponential and critical measurements being made in the same facility. Although no convincing theoretical justification for the suggested effect has been proposed, a number of laboratories are beginning to use critical experiments to calibrate their exponential facilities (I1).

A primary objective of the exponential experiment in general and, in particular, of the exponential experiments being performed at MIT, is the measurement of the material buckling, B_m^2, of subcritical assemblies. A theoretical definition of the material buckling is given in section 4.1, but it can be considered as that quantity that must be maximized to produce a nuclear reactor of minimum size out of given materials. The maximization is with respect to the various possible configurations of the materials. Similarly, it may be considered as the single measurable parameter which describes the over-all multiplicative properties of a chain reacting system.

Furthermore, in the usual theoretical description of reactors, the leakage of neutrons is described in terms of the buckling.

1.3 THE MIT LATTICE EXPERIMENTS

The lattice experimental program at MIT is designed to study the physics of slightly enriched uranium-D_2O lattices. In order to provide comparisons with other experiments and to add to them where possible, the first lattices studied were of natural uranium. They consisted of single rods, one inch in diameter, spaced in various configurations as described in Chapter VII.

In addition to the measurements of the buckling, three other aspects of the first lattices were examined in detail. These were the microscopic thermal neutron distribution, to be reported by Brown (B1); the fast fissions in U^{238} as reported by Wolberg (W10); and the resonance capture in U^{238} as reported by Weitzberg (W11). These three measurements provide the basis for the derivation of the factors, f (thermal utilization), ϵ (the fast fission factor), and p (the resonance escape probability), respectively. The infinite multiplication factor, k_∞, may then be derived from the product of these factors and a value for the neutron regeneration factor, η.

CHAPTER II
PEDESTAL EXPERIMENTS

2.1 INTRODUCTION

Neutrons from the MIT Reactor diffuse to the experimental area through the reactor thermal column. The latter is a graphite stack, 63 inches square and 37-1/2 inches long. In order to direct the generally horizontal beam from the thermal column upward to the experimental tank, a four-walled graphite cavity, or "hohlraum", is used. The physical configuration of the system is shown in Fig. 6.1. The design and performance of the cavity has been described by Madell (M1). Above the cavity, an aluminum platform, approximately 7 feet square, supports whatever pedestal is required for flux-shaping beneath the experimental tank. The tank is supported from above, leaving approximately 16 inches between the platform and the tank bottom for the pedestal. Other aspects of the facility are described in section 6.1, and diagrams of the facility are shown in Figs. 6.1 and 6.2.

2.2 GENERAL CONSIDERATIONS

In the design of the pedestal, two criteria had to be considered. The first of these was the requirement of a favorable over-all spatial distribution of the flux. The second was a neutron flux of sufficient magnitude to permit accurate experiments to be carried out.

The first criterion was imposed by the measurement of the material buckling of the lattices. The accurate determination of the axial buckling requires that through a considerable vertical distance, only the fundamental harmonic exist. In the present case of a cylindrical tank, this means that the radial distribution of the flux should be describable by a single J_o Bessel function (see Chapter IV). To the extent that the source distribution at the bottom of the tank

does not correspond to a pure J_o (of the correct argument), higher harmonics will exist in the tank. If the source distribution resembles the correct J_o to a sufficient extent, the harmonic contribution will be small and will become negligible in the bottom region of the lattice (see Chapter IV).

The second criterion, that of magnitude, is effectively imposed by the measurement of the microscopic properties of the lattices. In general, such measurements are insensitive to over-all flux distributions. It is true that in the measurement of the thermal utilization, an intracell flux plot must be corrected for the macroscopic flux distribution. However, the measurement can be made high enough in the lattice so that a simple J_o distribution is known to exist. (It need not exist over any considerable distance, as in the buckling measurement.) The most critical of the measurements with respect to magnitude are those related to the determination of resonance capture. One such experiment involves the activation of dilute (about one per cent) uranium in aluminum foils in the moderator and requires exposures of the order of 24 hours at a flux of 10^9 n/cm^2 sec. Flux levels of much less than 10^9 n/cm^2 sec would make such experiments impractical. (The flux required for accurate macroscopic measurements is about 10^7 n/cm^2 sec.) It was therefore required that as little diminution in flux as possible occur between the thermal column and the tank bottom.

Since the two criteria of shape and intensity tend to conflict with one another, their resolution provided an interesting and informative series of experiments.

The material decided upon for the pedestal was graphite. If water had been used, the attenuation through the pedestal would have been excessive. For example, in a H_2O pedestal, 46 inches on a side, the intensity of the fundamental harmonic would decrease by a factor of 10 in 3 inches. A pedestal of D_2O would produce approximately the same attenuation of harmonics as one of graphite because, with the large diffusion lengths characteristic of these materials, side leakage is the chief cause of the attenuation. Graphite, however,

has the distinct and obvious advantage of being more easily manageable and adaptable to various configurations.

2.3 EXPERIMENTAL METHODS

Flux distribution measurements were made both in the pedestals and in a "pseudotank", a 50 in. × 50 in. × 8 in. stack of graphite placed on top of the pedestal to simulate the experimental tank. In all the experiments, both the pedestal and pseudotank were wrapped in cadmium. Copper foils, one inch in diameter and 0.020 inch thick, were used to make flux traverses in a direction parallel to the thermal column face (the north-south direction) and in a direction perpendicular to the thermal column face (the east-west direction). In all the runs, foils were located four inches from the top of the pseudotank. They were placed in holes milled in the (4 in. × 4 in. × 50 in.) stringers which formed the bottom of the pseudotank. In some runs, foils were also distributed in the pedestal itself.

The beta activity of the foils was counted either with a Nuclear-Chicago proportional flow counter and automatic sample changer, or with a Baird-Atomic G-M flow counter and changer. In all cases, errors due to statistics of counting were less than one per cent.

To obviate repetition of runs, several internal checks were made in the taking and processing of experimental data. Only the flux distribution in the east-west direction was asymmetric and, thus, was of primary concern with respect to flux-shaping. Because of the symmetry of the north-south distribution, two simultaneous measurements of the east-west distribution could be made by taking one traverse 6 inches to the north and one 6 inches to the south of the east-west centerline. Normally, each set of foils was counted at least three times. The usual corrections (for decay before and during counting, and for variation in foil weight) were applied independently each time a set of foils was counted. In this way, the flux distribution was calculated from at least three sets of foil activities at various times after irradiation. Whenever a set of foils was counted, a standard foil was also counted, to check the constancy of the counter sensitivity.

All irradiations were made for 30 minutes at a reactor power of 40 kw. The flux entering the cavity was monitored by placing two foils at the bottom of the vertical thermal column, thus allowing intercalibration of runs.

2.4 RESULTS

A total of seven steps (Runs P1 through P7) was taken in approaching the final pedestal configuration. The salient points of difference between the various configurations are shown in Fig. 2.1.

Madell had used a 72 in. × 72 in. × 16 in. pedestal during most of his cavity experiments. Run P1 was made with the same pedestal with the 50 in. × 50 in. × 8 in. pseudotank added (see Fig. 2.1a). The east-west flux distribution as a function of distance up into the pedestal and pseudotank is shown in Fig. 2.2. The distribution near the top of the pedestal was satisfactory neither as far as shape was concerned (too flat) nor in terms of magnitude (too low).

In order to produce a flux shape nearer to that required in the tank, a pedestal 50 in. × 50 in. × 16 in. was tried next. The flux distribution in the pseudotank obtained in this run (P2) is compared to that of P1 and subsequent runs in Fig. 2.3. The flux values plotted are corrected to a reactor power of 1 Mw. The calibration from copper foil activity to flux was obtained by exposing a cobalt foil and copper foil simultaneously at the face of the thermal column. The absolute disintegration rate of the cobalt foil (and thus the flux) was obtained by means of a coincidence technique, while the copper foil was counted in the same arrangement as the experimental foils.

Although the distribution obtained in Run P2 seemed satisfactory as far as shape was concerned, the intensity was too low. Two steps were taken to increase the intensity. First, in Run P3, a pedestal was made with outside dimensions 72 inches but with a 48 in. × 50 in. hole in the center, as shown in Fig. 2.1c. The magnitude of the flux was indeed increased, as can be seen from Fig. 2.3. The shift in the distribution toward the west indicated that a significant fraction of the flux in the pseudotank was due to

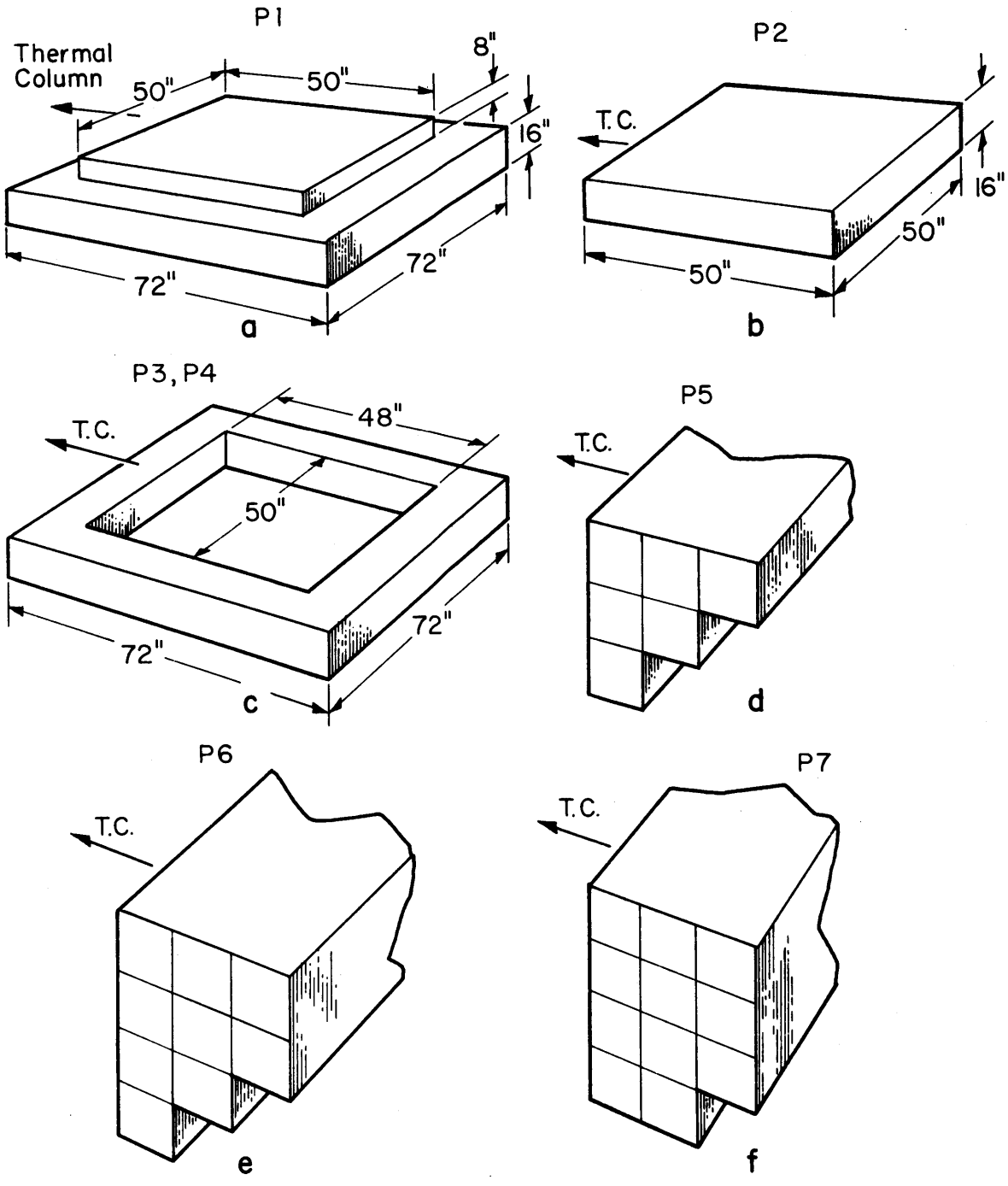

FIG. 2-1 TRIAL CONFIGURATIONS OF THE GRAPHITE PEDESTAL

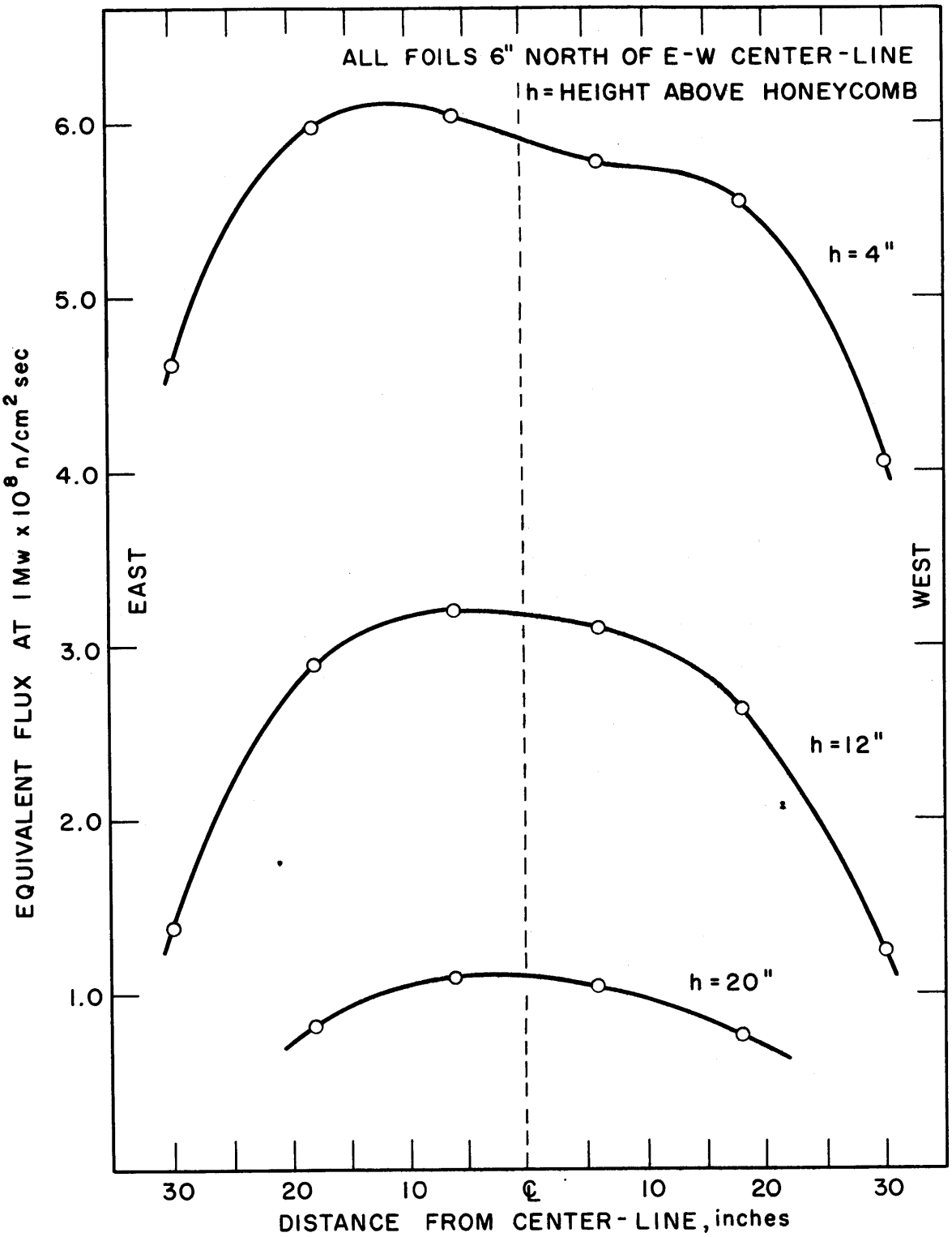

FIG. 2.2 EAST-WEST FLUX DISTRIBUTION AS A FUNCTION OF HEIGHT IN 72 INCH PEDESTAL

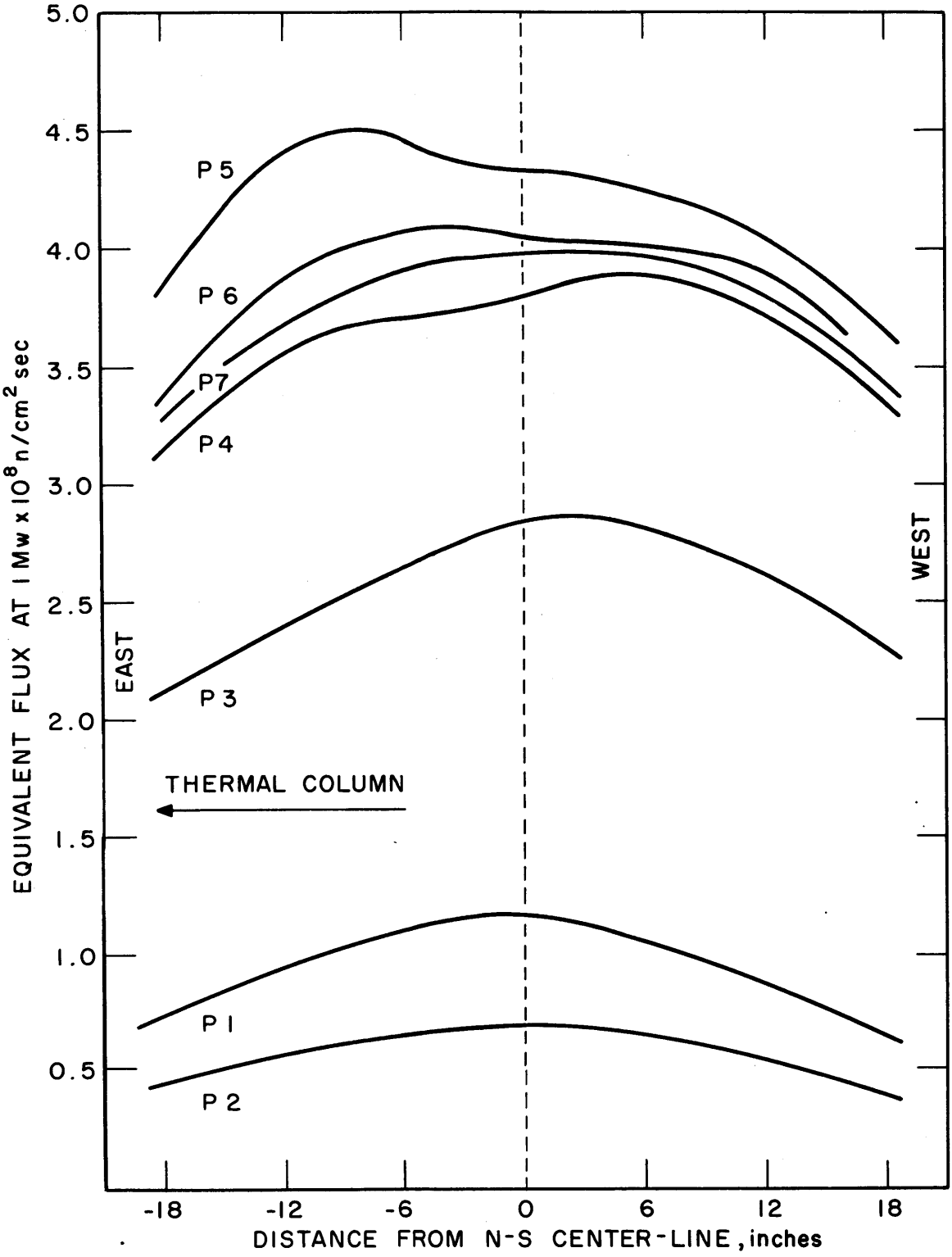

FIG. 2.3 FLUX DISTRIBUTIONS 4 INCHES INTO PSEUDO TANK TAKEN 6 INCHES FROM EAST-WEST CENTER-LINE FOR REACTOR POWER OF 1 Mw

neutrons which came directly from the thermal column face. The removal of the central portion of the pedestal gave the rear of the pseudotank a better view of that neutron source. The second step to increase the flux magnitude (in Run P4) was the removal of a group of graphite stringers forming a saw tooth arrangement at the top of the space between the thermal column and the cavity. The flux distribution shown as P4 in Fig. 2.3 was then obtained. In order to get a more detailed picture of the flux distribution, more foils were used in this and subsequent runs than in Runs P1 to P3. In the earlier runs, foils were placed at -18, -6, +6 and +18 inches; foils at +12 and -12 inches were added for Run P4. Thus, the slightly double-humped effect in Run P4 may have existed, but not have been detected in the earlier experiments. The hump toward the west again suggests the importance of the direct view of the thermal column face afforded the western part of the pseudotank.

To shift the distribution toward the east and, at the same time, increase somewhat the magnitude of the flux, the number of stringers forming the east side of the pedestal was varied. In Runs P1-P4, this section of the pedestal consisted of a stack of 4-inch-square stringers (50 inches long), four stringers high and three wide. In Run P5, six stringers were removed to allow the east part of the pseudotank a view of the thermal column face. The configuration of the stringers remaining and the resultant flux distribution are shown in Figs. 2.1d and 2.3, respectively. The attempt to shift the distribution was evidently too successful. In Runs P6 and P7, two other arrangements of the east section of the pedestal were tried, as shown in Fig. 2.1, e and f, and resulted in flux distributions, again shown in Fig. 2.3.

The pedestal configuration finally chosen was basically that of Run P6. The slight asymmetry toward the east was considered advantageous for the following reason. As is discussed above, it was found that a significant contribution to the flux at the top of the pedestal arose from neutrons coming directly from the thermal column. Because of the angle of incidence of these neutrons, they

provide a non-isotropic contribution to the flux distribution. Hence, the distribution would be expected to shift somewhat toward the west as it entered the bottom of the tank. The only other changes in the pedestal were, first, the removal of some graphite in the south-west corner (to allow space for piping) and, second, the insertion of graphite pieces in the inside corners to approximate more closely a circular hole. The resultant pedestal configuration is shown in Fig. 2.4. The side and upper graphite surfaces were covered with cadmium.

The distribution obtained in Run P6 can be roughly approximated by

$$\phi = A \cos \frac{\pi x}{110} \cos \frac{\pi y}{110} \qquad (2.1)$$

where x and y are distances (inches) in the east-west and north-south direction. The adequacy of this approximation may be seen in Fig. 2.5 where it is compared to the measured fluxes. A rough estimate of the relative contribution of higher harmonics to the fundamental, in the tank, may be made in the following way. The 48-inch diameter tank is approximated by a tank in the form of a parallelepiped, with sides of 46 inches (extrapolated dimension); such a substitution allows for equal radial buckling in the two cases. Then the empirical flux distribution given by Equation (2.1) is expanded in characteristic functions of the square tank $\left(\cos \frac{n\pi x}{46} \cos \frac{m\pi y}{46}\right)$ and the decay constants for each mode determined from the equation,

$$\gamma_{mn}^2 = -B_m^2 + \left(\frac{n\pi}{46}\right)^2 + \left(\frac{m\pi}{46}\right)^2, \qquad (2.2)$$

where B_m^2 is the material buckling. A representative value of $8m^{-2}$ is taken for B_m^2. In this way, it is found that the contribution of the higher harmonics is about one per cent at a height of 60 cm. in the tank, and 0.1 per cent at a height of 104 cm. As preliminary results, these estimates were considered adequate until flux distributions could be measured in the lattices, themselves.

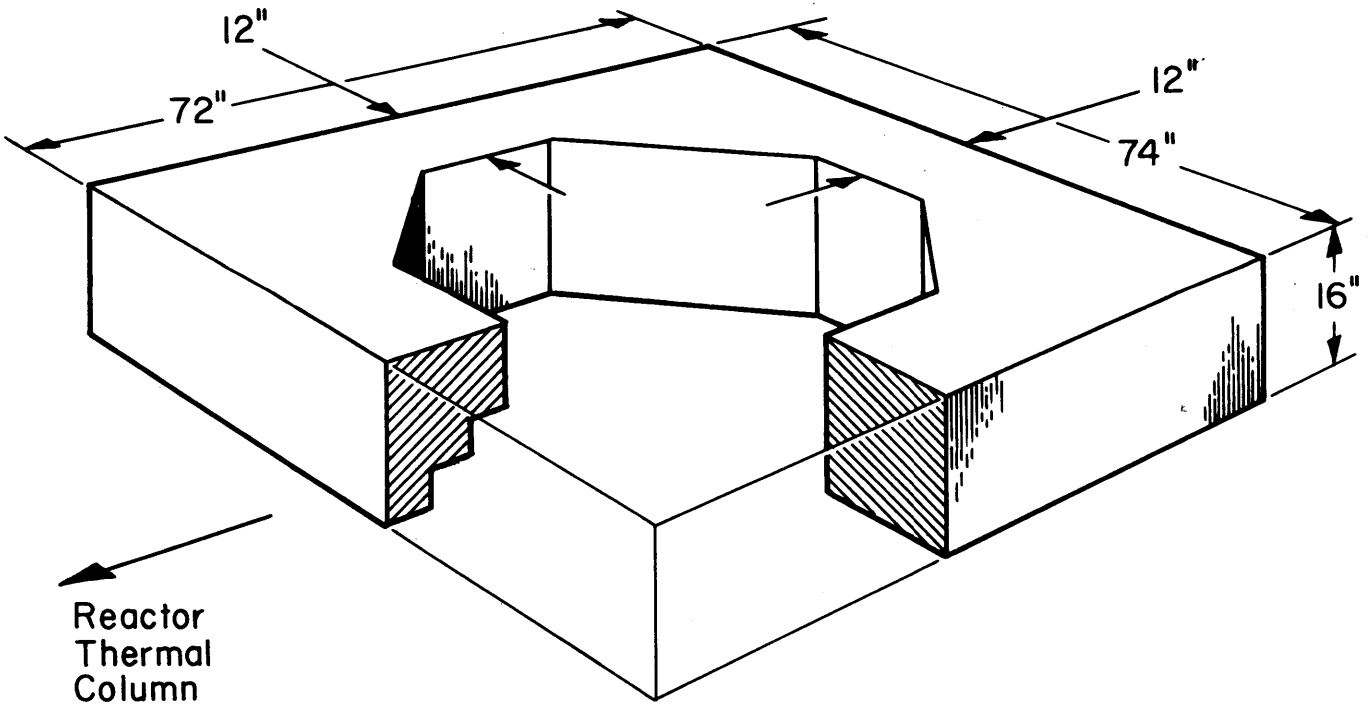

FIG. 2·4 FINAL CONFIGURATION OF GRAPHITE PEDESTAL BENEATH EXPONENTIAL TANK

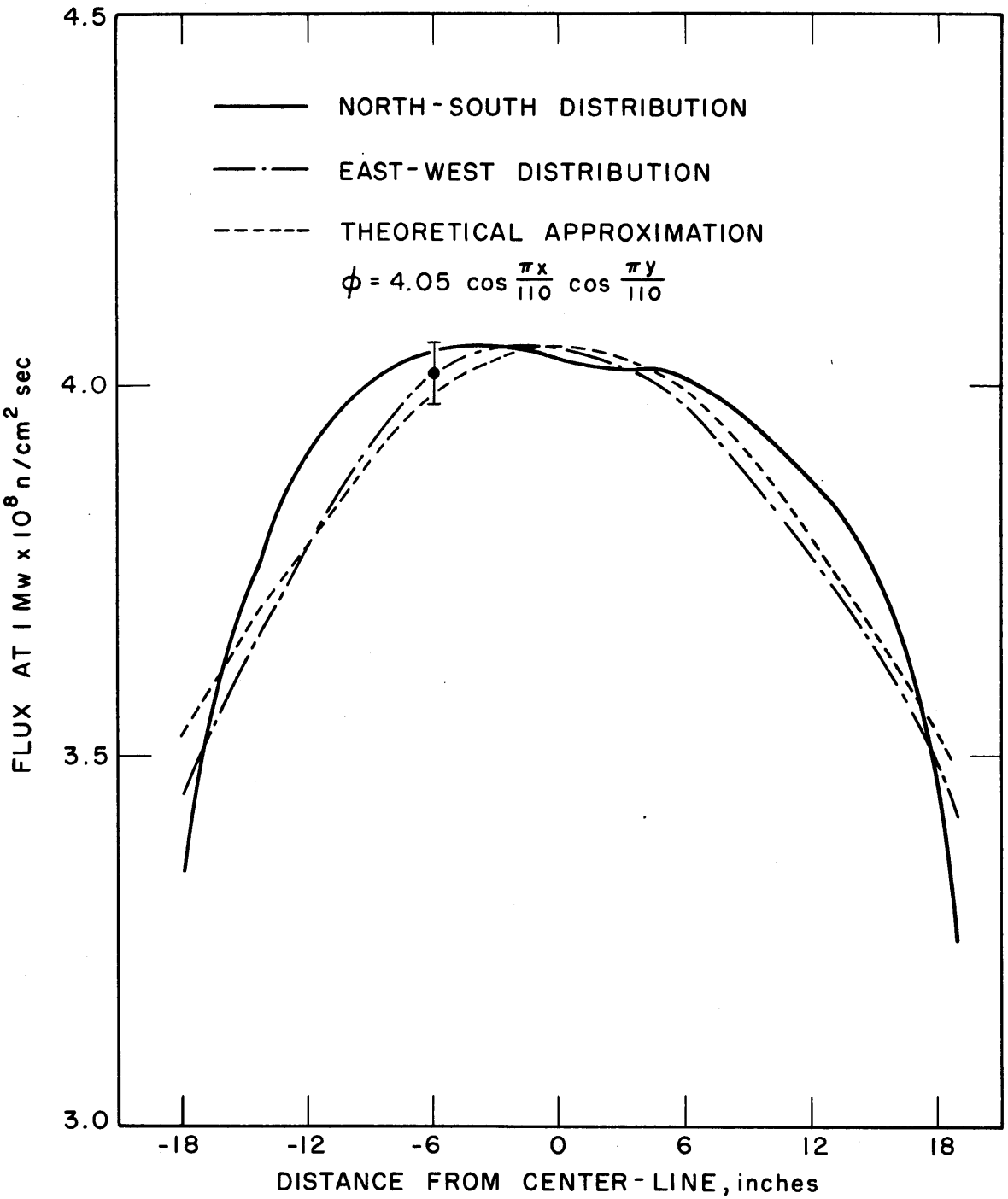

FIG. 2.5 FLUX DISTRIBUTIONS IN PSEUDO TANK AND THE THEORETICAL APPROXIMATION

CHAPTER III
MODERATOR EXPERIMENTS

3.1 INTRODUCTION

The first series of experiments that was performed in the completed facility was designed to study the flux distribution in the exponential tank filled with D_2O. The experiments connected with the design of the graphite pedestal were described in Chapter II. The pedestal experiments were performed between May and August, 1960. At that time, since the exponential tank was not in place, the adequacy of the flux distribution entering the tank could be established only crudely. By June, 1961, the facility was completed to the extent that experiments could be performed in the exponential tank filled with D_2O.

The moderator experiments, performed during June and July, 1961, were designed to serve three purposes:

1) The fundamental intent of the experiments was to examine the adequacy of the spatial distribution of the thermal flux entering the exponential tank. The criteria of adequacy have been discussed in section 2.2, and the main requirement is that the flux be characterized by a single J_o Bessel function over a considerable vertical distance in the tank. No attempt was made to obtain highly precise flux plots in these experiments. Rather, they were designed to point up any large flux irregularity before experiments in the lattices were begun.

2) The experiments were used as a comparing and testing ground for experimental and analytical techniques. During the investigation of the spatial distribution of the flux, several experimental methods were employed. The experience gained in trying various methods was used to establish the techniques to be used to make flux plots in the lattices.

3) A further purpose of the experiments was the investigation of one source of background neutrons - the epithermal component of the flux entering the tank. As is discussed in Chapter IV, it is necessary to assure that energy harmonics have died out at the points where the experiments are performed in the lattices. Such harmonics may be due in part to the fact that the source thermal spectrum is characterized by a temperature different from that characterizing the lattice thermal spectrum. This effect can, of course, be studied only in the lattice, itself. However, the effect may also result from epithermal neutrons entering with the source thermal neutrons, a phenomenon which can be studied in the pure moderator.

3.2 EXPERIMENTAL PROCEDURES

Many of the experimental and analytical procedures used during the moderator experiments were the same as those used in the lattice runs. Since these experimental techniques are described in detail in Chapter VI, they will not be discussed here. Other techniques employed in the moderator experiments will be described in this section, particularly with regard to the choice of methods to be used in the lattices. There are four criteria that must be met by a fully successful method of flux mapping. First, the flux measuring device must be sufficiently sensitive to the neutrons of interest. Second, the device must not distort unduly the flux that is being measured. Third, the location of the flux measuring device must be known accurately; and finally, the whole operation must be relatively simple and efficient.

Many of the criteria are well satisfied by a remote-operated, traveling neutron scanner. However, such a device is usually limited to one plane of the experimental tank. (A scanner designed to operate in the lattices is described in section 6.3.3.) Various methods of flux plotting with foils and wires were, therefore, tried. With these, there is no difficulty of sensitivity, and flux perturbation need only occur at the point of detection. The main difficulty of using

foils or wires in the experiments described here was in their accurate positioning. This difficulty is due to the fact that, during the experiments, access to the tank is gained through the glove box in the rotating tank lid (see section 6.2).

Many of the radial flux plots in the moderator were obtained with the aid of an aluminum frame built to fit into the exponential tank. The frame was made of 1/8 in. × 1/8 in. × 1 in. type 6063 aluminum angle. The bottom element of the frame remained fixed across a diameter of the tank at the tank bottom. The upright members could be located and "locked" to the bottom member from the top of the tank, through the glove box. Figure 3.1 shows one corner of the frame, in the locked position. The uprights were also clipped to a double beam located on the tank top, below the lid.

The upright elements contained holes and adjustment screws for the fixing and stretching of wires or strings. A duplicate bottom member was located in the set-up area so that the wires or foil-carrying strings could be set up outside of the tank. Three different ways of using the frame were tried. In the first, thin (0.020 inch diameter) copper wire was stretched between the uprights to obtain flux plots. The wire was counted in a wire scanner adapted from a chromatogram scanner. A second method entailed the use of thin nylon string from which aluminum foil holders were suspended. Foils suspended in this way are shown in Fig. 3.1. In the third method, pure aluminum wire replaced the string.

Although all three methods of making radial traverses proved manageable, each had disadvantages. In general, it was found difficult to be sure that the positions of the wires or foils set up outside the tank were exactly maintained in the tank. To reduce sagging of the string or wire, considerable tension had to be applied. It was difficult to insure that the same amount of tension was applied in the tank, under water, as existed in the setting up of the frame outside. The difficulties of handling and positioning the copper wires, combined with inaccuracies in their counting, were sufficient to discourage their use in the remainder of the experiments.

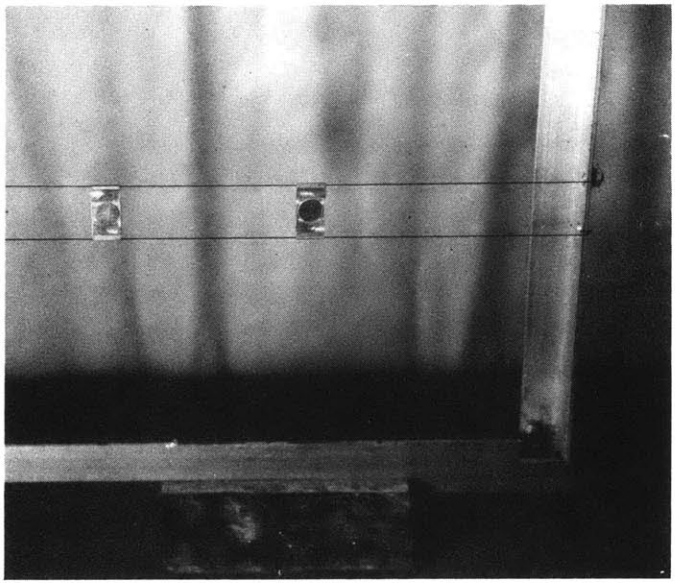

FIG. 3.1 LOWER CORNER OF EXPERIMENTAL FRAME SHOWING STRING-SUSPENDED FOIL HOLDERS. (FOILS ARE 1/2 INCH IN DIAMETER)

Another method of making radial traverses was used, in which the foils were placed on an aluminum foil holder. These could be suspended from the double beam resting on top of the tank. With this method, the relative positions of the foils are accurately established by placing them in depressions milled in the holder.

The axial traverses presented a simpler problem of foil location. Strings of foils could be inserted through the glove box fairly easily. In this case, three methods were used to space the foils. In the first, the foils were placed on small, individual, aluminum foil holders, these being spaced along a nylon string. In the second method, the foil holders were spaced by means of aluminum bead chain; and in the third, the foils were taped to the aluminum foil holder used for the radial traverses. The three different types of suspension are shown in the photograph of Fig. 3.2.

The foils used throughout the moderator experiment were of gold, 0.010 inches thick and 0.5 inches in diameter. Their induced activity was counted in an automatic sample changer, as described in Chapter VI.

During these experiments, the MITR operated at a power level of 1 Mw. Under these conditions, the irradiations of bare gold foils were usually 30 minutes long. The irradiations of cadmium-covered foils were at least 4 hours in duration, the length of irradiation depending on the other experiments being performed.

3.3 THERMAL NEUTRON DISTRIBUTION

3.3.1 Axial Distribution

As will be shown below, the epithermal activation of the gold foils irradiated in these experiments is very small, compared with the thermal activation. Hence, the flux distributions reported here are obtained from bare foil data.

Axial flux plots were made to examine roughly the harmonic contributions to the flux in the tank. Of primary interest was the height in the tank at which the flux could be said to behave in an

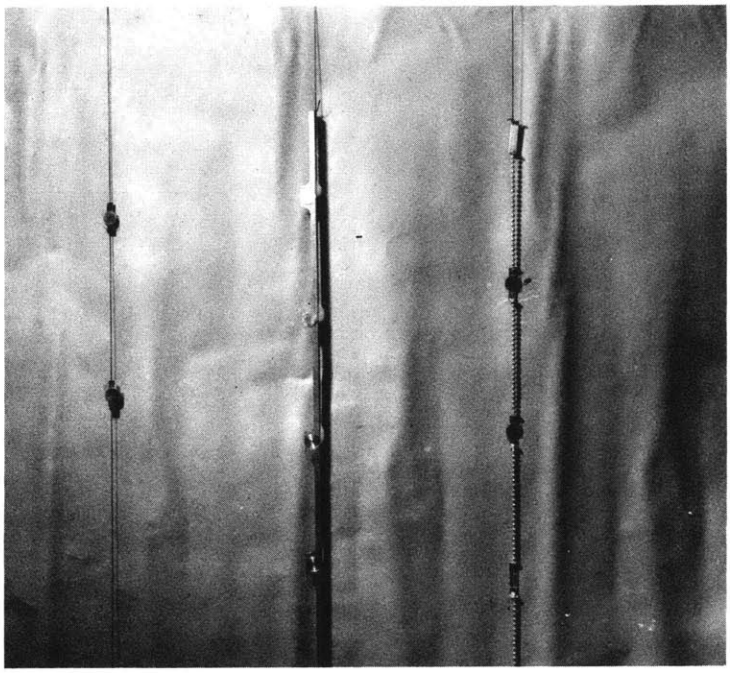

FIG. 3.2 METHOD OF SUSPENDING FOILS FOR AXIAL TRAVERSES. FOILS SHOWN ARE 1/2 INCH IN DIAMETER

exponential manner. A secondary purpose of the axial flux plots was to ascertain whether the type of foil holder had any effect on the measured relaxation length.

Figure 3.3 represents data from two separate axial traverses. The curve is an exponential fit (by eye) to the points. It is clear from these data that at least above a height of 55 cm in the tank, the flux can be considered exponential in nature.

In Run No. 2, the foils were suspended with the string foil holder shown in Fig. 3.2, whereas the solid aluminum foil holder was used in Run 11. As is apparent from Fig. 3.3, the relaxation lengths derived from the two runs are equal within the experimental uncertainties.

3.3.2 Radial Distribution

The radial flux distribution in the tank was studied in two ways, with the measured fluxes being fitted by a single J_o function and by fitting a sum of J_o harmonics.

Figure 3.4 represents the data from three separate radial distribution measurements made at three different heights. Data taken on two sides of the central axis are represented on the plot (i.e., the data are "folded" to one side). The plotted Bessel function curve is the theoretical distribution fitted by least-squares to the data of Run 1. It is clear from the plot that the data of the three runs are in agreement within the accuracy of the experiments and that the data are well represented by the fitted Bessel function.

In the experiments, it was not always easy to determine accurately the absolute position of the foils in the tank or, in other words, the position of the center of the tank with respect to the center of the string of foils. It was of interest, therefore, to determine the effect on a measured radial buckling of an uncertainty in the center of the distribution. The data from one of the runs were analyzed three times, with the foil positions being shifted 0.5 cm, first in one direction and then in the other. Table 3.1 shows the result of this analysis.

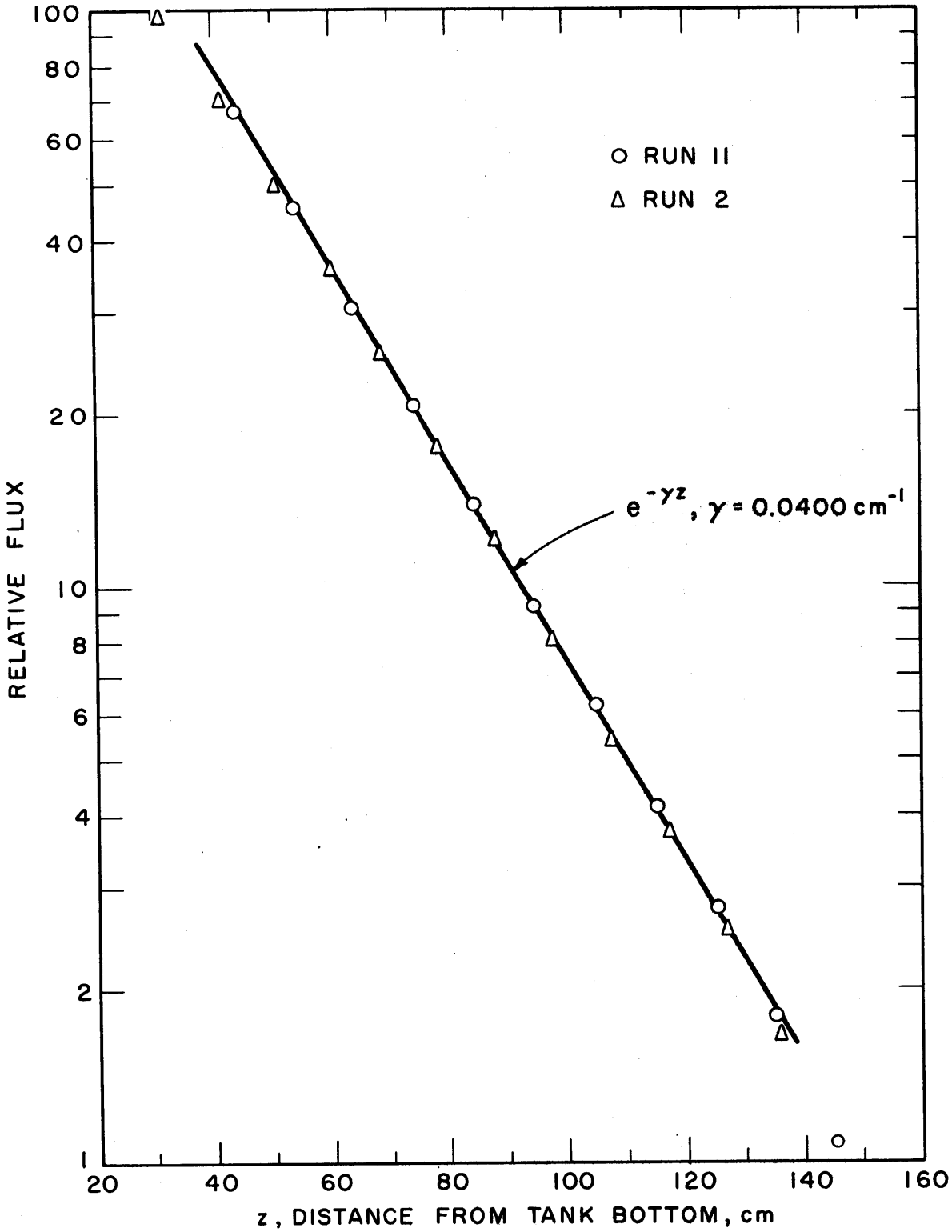

FIG. 3.3 AXIAL DISTRIBUTION IN MODERATOR RUNS 2 AND 11

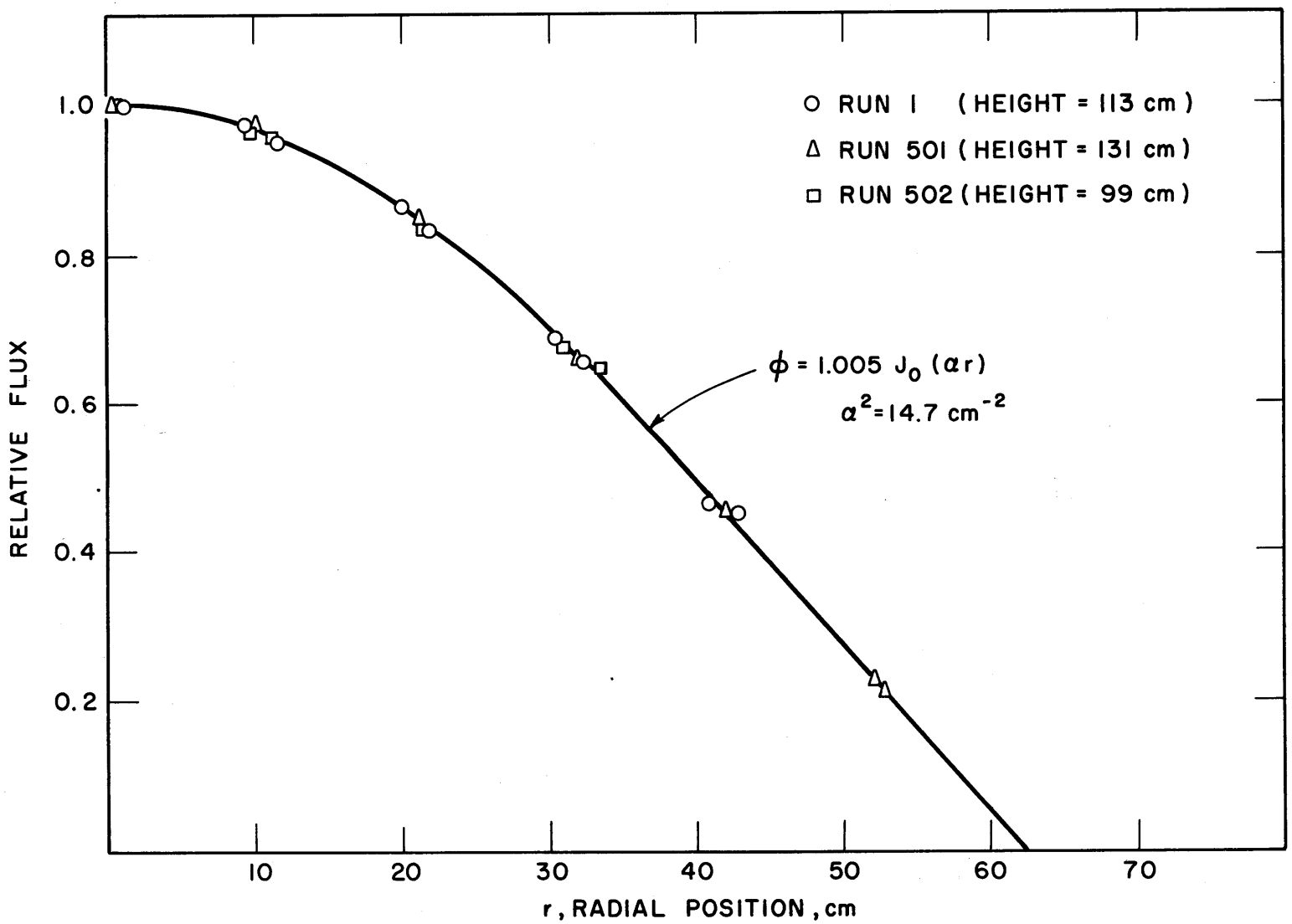

FIG. 3.4 RADIAL TRAVERSES IN MODERATOR

TABLE 3.1 EFFECT OF FOIL POSITION SHIFT ON A MEASURED BUCKLING

Run	Amount of shift	Buckling
101	0.0 cm	14.70 m^{-2}
105	0.5 cm	14.71 m^{-2}
106	1.0 cm	14.70 m^{-2}

Since the foils are positioned symmetrically about the center, a total shift of one centimeter is seen to have an insignificant effect on the measured buckling. The Bessel function is sufficiently linear over a distance of one centimeter in this situation, so that the shifting of the foils on opposite sides of the center balance one another.

As is described in section 6.4, it is possible to fit a measured flux distribution to a function of the form:

$$\phi(r) = A_1 J_o(\alpha_1 r) + A_2 J_o(\alpha_2 r) + A_3 J_o(\alpha_3 r) , \qquad (3.1)$$

where

$$\alpha_1 = \frac{2.4048}{R'} , \quad \alpha_2 = \frac{5.5201}{R'} , \quad \text{and} \quad \alpha_3 = \frac{8.654}{R'} , \quad \text{and}$$

R' = the extrapolated radius.

In Run 5, flux distributions were determined at three heights. These were fitted to single J_o functions to obtain a value of the appropriate extrapolated radius, R'; and, with that value of R', the data were analyzed to determine the coefficients of Equation (3.1). Table 3.2 shows the results of this analysis.

TABLE 3.2 RESULTS OF HARMONIC ANALYSIS IN MODERATOR

Run	Height of traverse	A_1	A_2	A_3
504	131 cm	1.005	0.004	-0.006
505	99 cm	0.995	-0.005	0.008
506	57 cm	1.006	0.008	-0.013

The main conclusion to be drawn from these results is that very

little, if any, higher harmonic contribution can be observed in the data. It is doubtful whether an analyzed contribution of less than one per cent is meaningful, in view of the small number of experimental points involved (11 points in each run). This conclusion is supported by the inconsistency of the signs of the coefficients in Table 3.2. The fact that the signs of A_2 and A_3 are always complementary (and that A_2 and A_3 are of the same order of magnitude) indicates that there is no large flux flattening or peaking, as compared to a simple J_o Bessel function.

3.3.3 Azimuthal Distribution

Although the radial distribution experiments showed the flux to be quite symmetric, all the radial experiments were performed in the same plane. To examine the azimuthal distribution, six strings of foils were irradiated. The strings were located in such a way that, at each of three levels, six foils were spaced equally around a circle 4 feet in diameter.

Figure 3.5 represents the azimuthal flux distribution as measured at the three heights. The distribution is seen to be symmetric except for a bulge in the south-west side. This asymmetry was not explained until the multiplication experiment on the first lattice was performed. At that time, it was found that certain pieces of shielding (for neutrons) had not been in place during the moderator runs. Thus, neutrons had been entering the tank through the ionization chamber port, which is located about half way up the tank on the south-west side. That this was really the cause of the asymmetry is supported by the fact that the greatest perturbation in the flux occurs part way up into the tank and not at the bottom. Furthermore, because of the symmetrical arrangement of the components below the tank, a perturbation caused by the incoming flux should be symmetric about a direction toward and away from the reactor.

On the basis of the experiments and analyses discussed above, it was concluded that the flux distribution entering the tank would probably be adequate for the buckling measurements in the lattice.

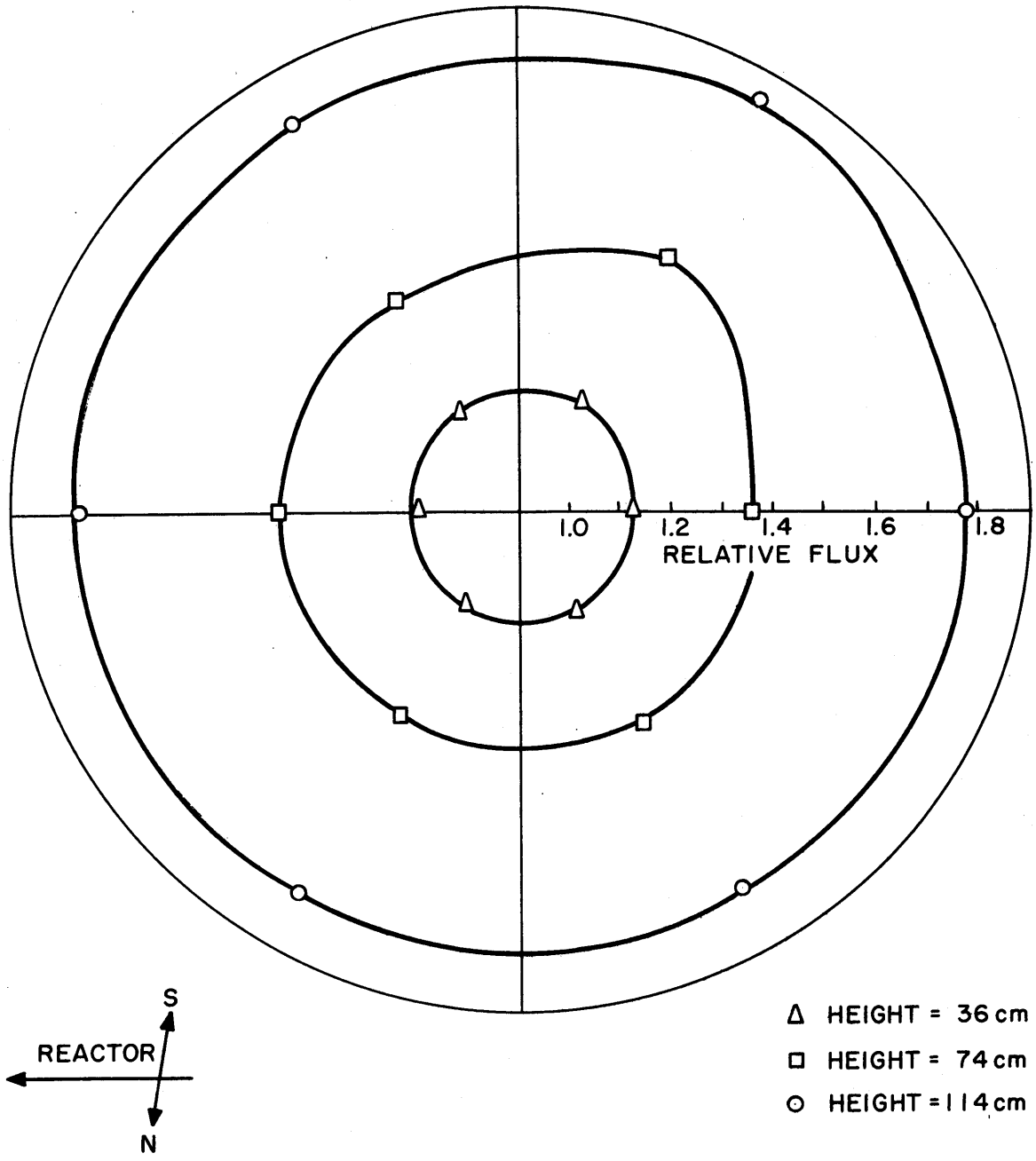

FIG. 3.5 AZIMUTHAL FLUX DISTRIBUTION IN EXPONENTIAL TANK

Further checks on the flux distributions were, of course, made in the lattices, themselves, and these are reported in Chapter VII.

3.4 EPITHERMAL NEUTRON DISTRIBUTION

The epithermal component of the flux in the tank was studied by making traverses with 1/2 inch diameter gold foils covered with 0.020 inch cadmium.

Figures 3.6 and 3.7 show the results of an axial and a radial cadmium-covered traverse. The unexpected shape of Fig. 3.7 indicates that a significant fraction of the epicadmium component of the flux enters the tank from the side, from the direction of the reactor. (It is possible that these neutrons result from photoneutron interactions caused by gamma rays from the reactor.) This phenomenon also explains the rather long relaxation length indicated by the curve of Fig. 3.6.

In Figs. 3.8 and 3.9, the bare and cadmium-covered foil data are combined to give plots of the cadmium ratio as a function of radial and axial position. The plots were made from the curves fitted to the data of Figs. 3.6 and 3.7 and the thermal distributions discussed above. From these curves, it can be seen that the cadmium ratios in the tank are generally around 1000 to 3000. In the lattice experiments, cadmium ratios of 5 to 10 are characteristic. Hence, as would be expected from the source configuration, it was concluded that the epicadmium component of the source, or background, would not be a serious concern in the lattice experiments.

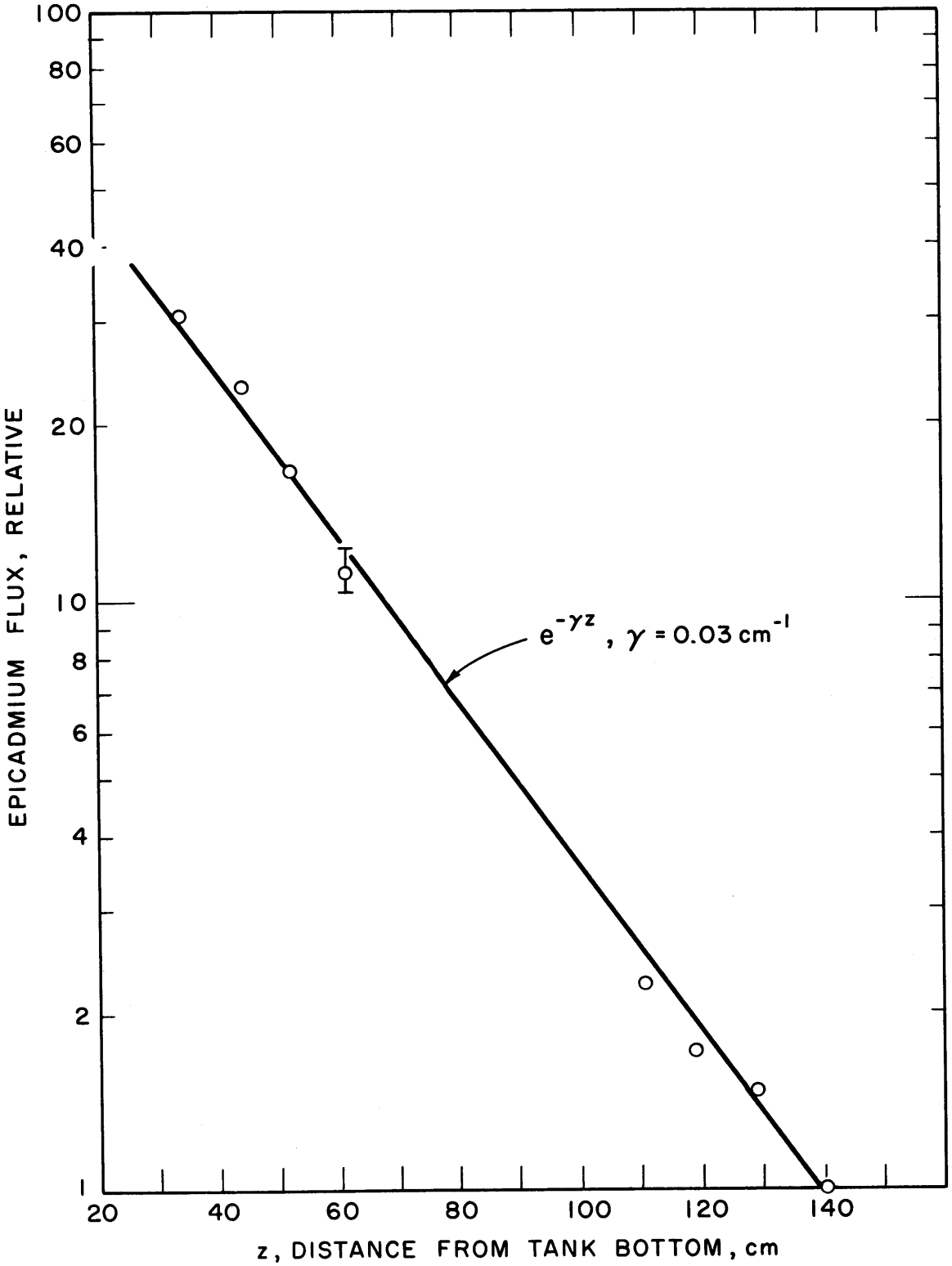

FIG. 3.6 AXIAL DISTRIBUTION OF EPICADMIUM FLUX IN MODERATOR

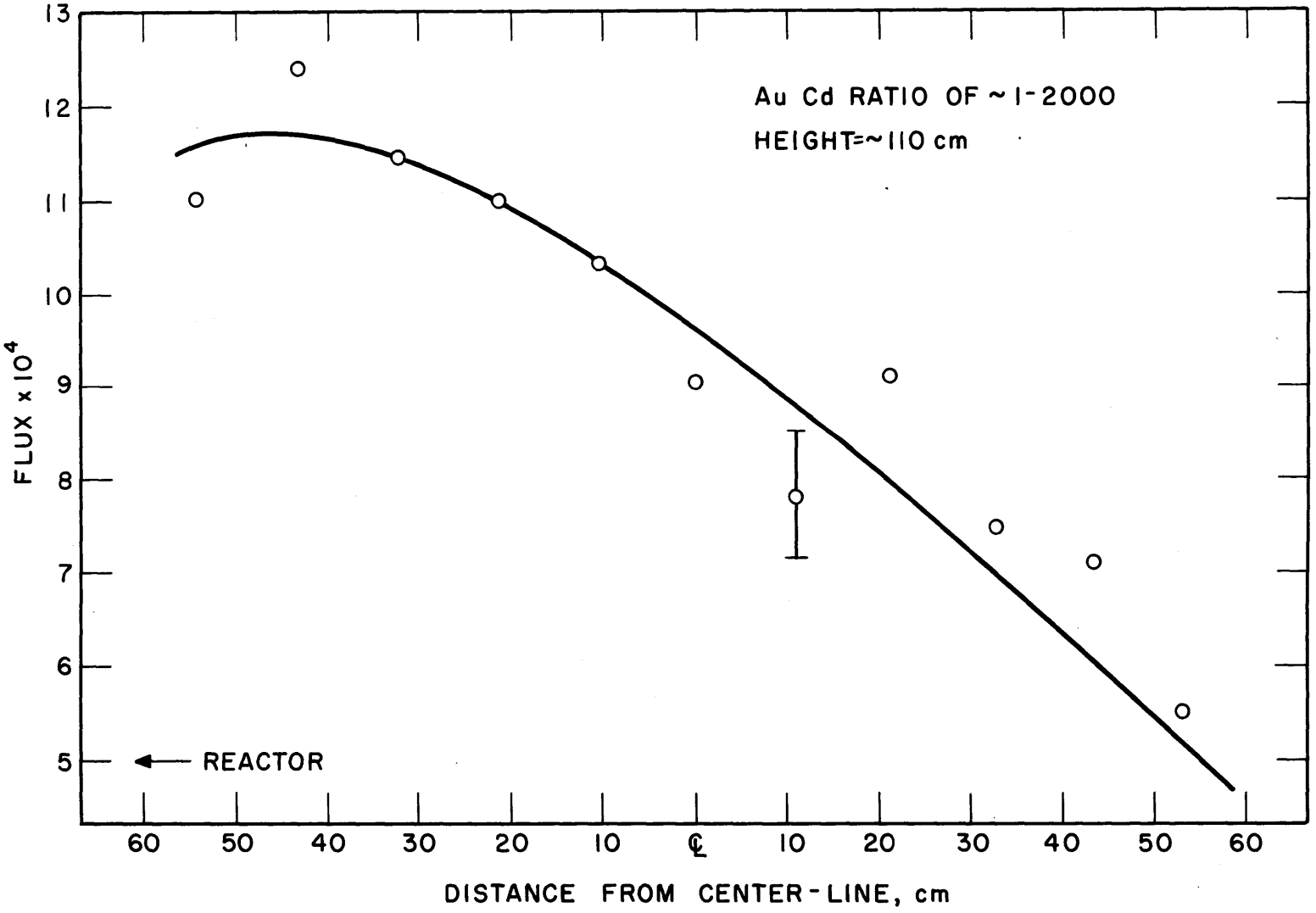

FIG. 3.7 EPICADMIUM FLUX IN D_2O AS A FUNCTION OF RADIAL POSITION

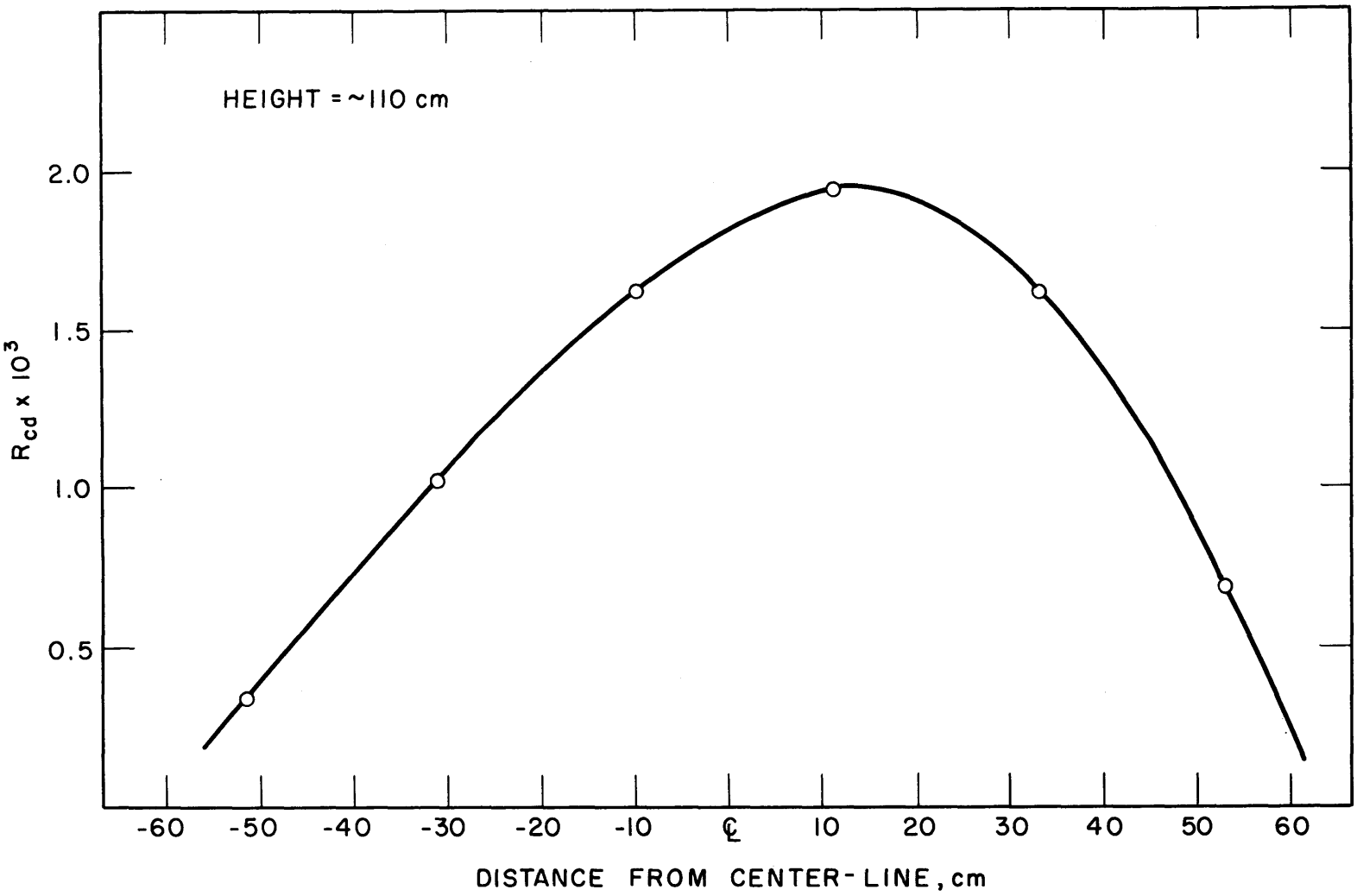

FIG. 3.8 GOLD CADMIUM RATIO IN D_2O AS A FUNCTION OF RADIAL POSITION BASED ON RUNS # 5 AND 7

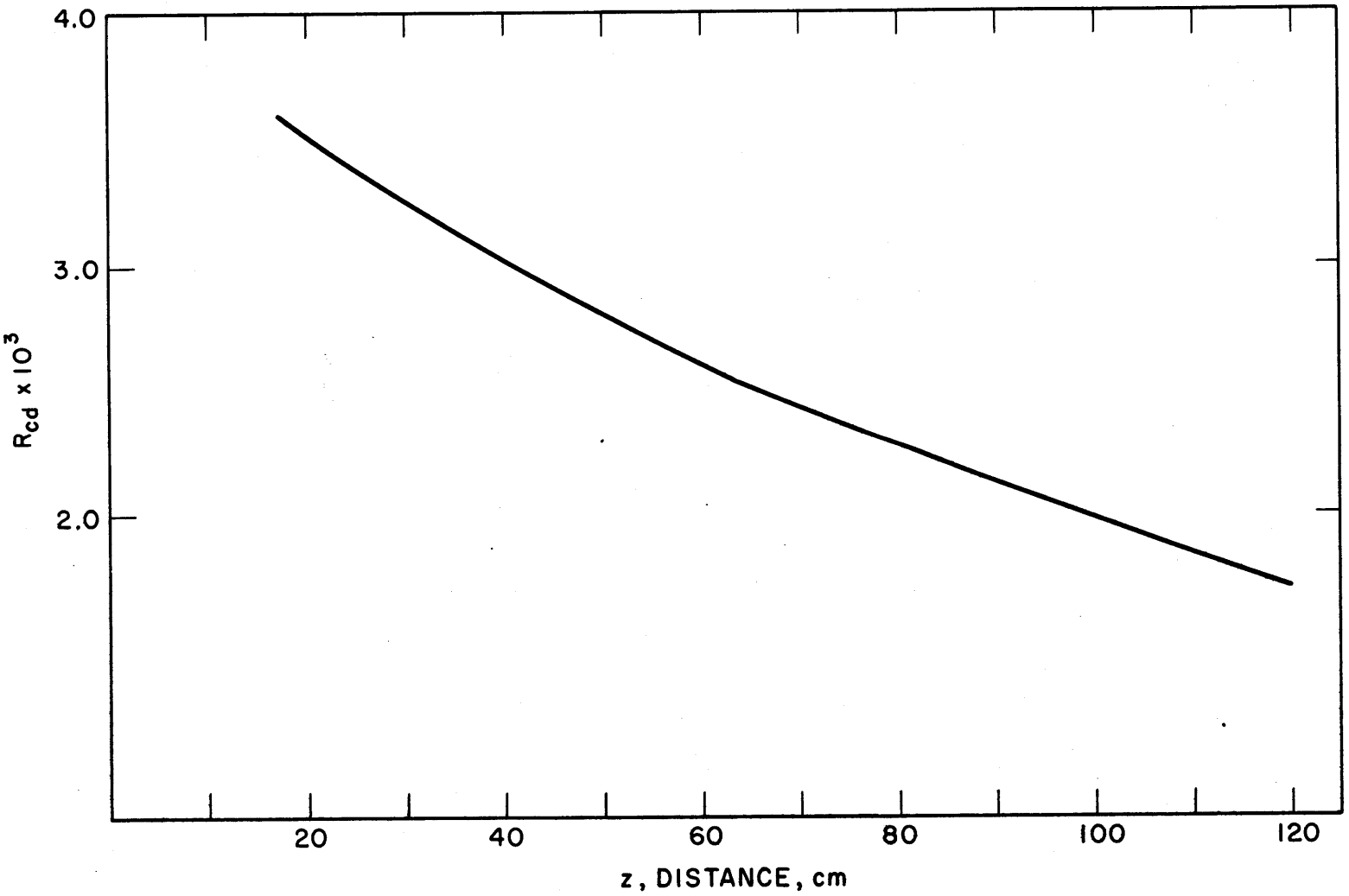

FIG. 3.9 GOLD CADMIUM RATIO AS A FUNCTION OF AXIAL DISTANCE INTO EXPONENTIAL TANK (RUNS 1 AND 3)

CHAPTER IV
THEORETICAL BASIS OF BUCKLING MEASUREMENTS

4.1 THE HOMOGENEOUS, ONE GROUP THEORY

The material buckling, B_m^2, may be defined as the lowest eigen-value of some critical equation for a bare, homogeneous reactor. In a one neutron velocity description, the critical equation may be written (as by Weinberg and Wigner (W2)):

$$-L^2B_m^2 - 1 + k_\infty \mathcal{K}(B_m) = 0 \ , \tag{4.1}$$

where $\mathcal{K}(B_m)$ is the Fourier transform of the slowing-down kernel, and L^2 is the thermal diffusion area. The most commonly used approximation to Equation (4.1) is the age-diffusion equation as given, for example, by Glasstone and Edlund (G1):

$$k_\infty e^{-B_m^2\tau} \left(1+L^2B_m^2\right)^{-1} = 1 \tag{4.2}$$

Implied in Equations (4.1) and (4.2), and allowed by the qualification that the system be bare and homogeneous, is the assumption that far from sources and boundaries, the neutron distribution satisfies the Helmholtz equation:

$$\nabla^2\phi(\vec{r}) + B_m^2\phi(\vec{r}) = 0 \tag{4.3}$$

The measurement of the buckling consists of measuring the flux distribution implied by Equation (4.3). The basis of the measurements to be discussed here is the one velocity analysis assumed above. Higher energy neutrons were considered to determine the region of the facility in which Equation (4.3) was valid (see sections 4.2 and 6.4).

The experiments were performed in a cylindrical assembly.

Thus, the form of Equation (4.3) of interest is that in cylindrical coordinates, or

$$\frac{1}{r}\frac{\partial}{\partial r}\left(r\frac{\partial\phi}{\partial r}\right)+\frac{1}{r^2}\frac{\partial^2\phi}{\partial\theta^2}+\frac{\partial^2\phi}{\partial z^2}+B_m^2=0\,, \tag{4.4}$$

where

$$\phi=\phi(\vec{r})=\phi(r,\theta,z)\,.$$

With the boundary conditions that the flux is finite everywhere inside the experimental tank, and that the flux vanishes at some extrapolated height, h', the solution to Equation (4.4) may be written:

$$\phi(r,\theta,z)=\sum_{\nu k}\left[A_{\nu k}\sin\nu\theta+F_{\nu k}\cos\nu\theta\right]J_\nu(\alpha_{\nu k}r)\,\frac{\sinh\gamma_{\nu k}(h'-z)}{\sinh\gamma_{\nu k}h'} \tag{4.5}$$

$$k=1,2,3,\ldots \qquad\qquad \nu=0,2,2,\ldots$$

where, for each set of values of k and ν, a value of B_m^2 is given by

$$B_{m_{\nu k}}^2=\alpha_{\nu k}^2-\gamma_{\nu k}^2 \tag{4.6}$$

Another boundary condition to be satisfied is that the flux vanish at $r=R'$, the extrapolated radius. Thus, $\alpha_{\nu k}$ must be such that $J_\nu(\alpha_{\nu k}R')=0$. The $A_{\nu k}$ and $F_{\nu k}$ are constants, the relative magnitude of which can be adjusted to match any azimuthal flux dependence (at the plane, $z=0$).

Equation (4.5) must be simplified considerably before determining B_m^2 from experiment. Each step in the simplification must be justified, however, either theoretically or experimentally, in each particular experimental arrangement. The first simplification to be considered is the elimination of the θ-dependent terms. Normally, azimuthal independence is tacitly assumed, but it may be readily checked experimentally (see section 3.3.3). If azimuthal independence is valid, then Equation (4.5) may be written:

$$\phi(r,z)=\sum_{n=1}^{\infty}A_nJ_o(\alpha_nr)\sinh\gamma_n(h'-z)\,, \tag{4.7}$$

where A now contains all the constants of Equation (4.5). Since

$$\sinh \gamma_n(h'-z) = Ce^{-\gamma_n z}\left[1-e^{-2\gamma_n(h'-z)}\right], \qquad (4.8)$$

it can be seen that, since $\gamma_n > \gamma_{n-1} > \ldots > \gamma_o$, the higher harmonics will die out spatially more rapidly than the fundamental. For the sake of experimental accuracy and analytical convenience, it is customary to make measurements in the region where higher spatial modes are not significant (W3). This assumption and the limitation to a one neutron velocity theory will be examined in section 6.4. However, the equation which will provide the basis for analysis may be written:

$$\phi = AJ_o(\alpha r) \sinh \gamma(h'-z) \qquad (4.9)$$

In some interpretations, for the sake of analytical ease, the hyperbolic sine term is replaced by an exponential, and a correction factor corresponding to the second factor on the right of Equation (4.8) is used (K1).

4.2 ASSUMPTIONS OF SEPARABILITY

Two fundamental assumptions are usually made (explicitly or tacitly) when the foregoing theory is applied to actual measurements; it is assumed that the over-all flux distribution is separable from the cell distribution and that the spatial distribution is separable from the energy distribution.

The assumption of the separability of the two spatial components arises from the way in which the theory evolved. The theory was originally derived for, and is strictly applicable only to, homogeneous systems. When the theory is applied to heterogeneous systems, it is assumed that the radial flux distribution may be expressed:

$$\phi(r) = AJ_o(\alpha r) \cdot f_\infty(\vec{r}) \qquad (4.10)$$

where $f_\infty(\vec{r})$ represents the flux distribution in one cell of an infinite array of cells. This assumption is basic to the use of an effective

multiplication factor made up of the product of k_∞ and terms to account for the leakage. Measurements of the "four factors" of k_∞ in a lattice assume that only the value of $f_\infty(\vec{r})$ need be considered, at the particular energy involved. The separability assumption is implied, for example, whenever a value of the thermal utilization measured in the central cell of a lattice is considered to apply to every cell in the lattice (the "measurement" of the thermal utilization consists of determining $f_\infty(\vec{r})$ for thermal neutrons). In terms of the measurement of the buckling, the assumption takes the form operationally of assuming that one need only make measurements of the macroscopic flux distribution at equivalent points in lattice cells.

Despite the fundamental nature of the assumption of spatial separability (or perhaps because of it), it is mentioned only rarely (B2). Its analysis in terms of diffusion or related theories is difficult (W4), with attempts having been made only in greatly simplified systems, such as semi-infinite slab lattices (D2), (G2). Small source theory, as developed by Teller (T4) and Horning (H7) in this country and Feinberg (F1) and Galanin (G5) in the USSR, would seem to be better suited to such an analysis (L1).

An experimental approach to the question may be made in basically two ways. Either one may study the effect of the fine structure on the measurement of the macroscopic distribution or the effect of the macroscopic distribution on measurements of the cell flux distribution. The former method would involve examining the macroscopic distribution, using points at various positions in the cells. The latter alternative was chosen by Cohen when he investigated the cell thermal flux distribution in two points in a lattice (C1). The microscopic flux distribution was measured in a cell 6.7 inches from the tank wall in a 4-foot diameter tank and in a cell at the center. The lattice was composed of 1-inch diameter, enriched uranium rods in D_2O, with a square lattice spacing of 4.9 inches. Each measured value of the flux was divided by the appropriate value of the J_o term describing the macroscopic distri-

bution. The resulting microscopic distribution measured in the outer cell was "only slightly distorted from" that measured in the central cell.

On the other hand, recent attempts to observe non-separability by examining the effect of the cell distribution on macroscopic measurements have indicated a positive effect. Such experiments have recently been reported by Wood for graphite lattices (W8) and have also been performed in Sweden on uranium-D_2O lattices (W14).

The other fundamental assumption which has been made in the foregoing theoretical development is that the stationary neutron distribution is separable in space and energy. Although the "First Fundamental Theorem of Reactor Theory" (W5) maintains that this is the case in a critical bare reactor, it is also held to be true in an exponential experimental not too far from critical at distances far from the source (W6). This assumption, of course, can and should be tested experimentally by making flux plots with detectors sensitive to neutrons of different energies (K2), (B3). Energy-space separability must obtain if the use of detectors sensitive over a range of energies is to be valid (unless the detector has a 1/v sensitivity). Gross energy harmonics are expected to exist at the bottom of the tank, due to the high ratio of source (thermal) neutrons to lattice-born (fast and thermal) neutrons. Even if only the thermal group is considered, the source thermal distribution may have a characteristic temperature different from that characterizing the lattice flux. In the experiments under consideration here, energy transients are expected to exist at the bottom of the tank since the source neutrons are well thermalized, with a very small epithermal component. Experiments must therefore be used to determine the height in the system at which the spectrum has become characteristic of the lattice under study.

CHAPTER V

CONTEMPORARY APPROACHES TO THE MEASUREMENT OF BUCKLING

5.1 THE GENERAL APPROACH

The actual experimental determination of material bucklings admits of variation in detail but not in basic approach. This section will deal with the various techniques that have been used in studying the bucklings of subcritical systems. Although the buckling of a critical system can be determined by measuring its physical dimensions, bucklings of subcritical assemblies must be determined by measuring the distribution of the flux in at least one dimension. The most common method of determining B_m^2 in cylindrical systems is to make measurements of the flux in both the radial and the axial directions, fitting these to an expression such as Equation (4.9). In the fitting process, α and γ are determined, and B_m^2 then obtained as:

$$B_m^2 = \alpha^2 - \gamma^2 \tag{5.1}$$

In some cases, the measurement of the radial buckling, α^2, is not repeated with, say, change of lattice spacing, but assumed constant, and only the axial distribution, and γ, determined.

Of course, data may be fitted to more refined theoretical expressions for particular purposes. For example, the azimuthal flux distribution was investigated during the preliminary testing of the North American exponential assembly. The four Po - Be neutron sources used to feed the assembly might reasonably have given rise to azimuthal harmonics. In this case, the measured neutron flux was fitted to the Fourier-Bessel expansion of the flux at a particular height, as given by the equation,

$$\phi(r,\theta) = \frac{1}{2} b_o(r) + \sum_{n=1}^{\infty} \{a_n(r) \sin n\theta + b_n(r) \cos n\theta\} \tag{5.2}$$

The fitted coefficients, $a_n(r)$ and $b_n(r)$, could be expressed as series of Bessel functions:

$$a_n(r) = \sum_k A_{nk} J_n(\alpha_{nk} r) \ , \tag{5.3}$$

and

$$b_n(r) = \sum_k B_{nk} J_n(\alpha_{nk} r) \ . \tag{5.4}$$

The analysis validated the assumption of azimuthal independence.

The experimental facilities in use for exponential experiments are usually quite similar. A three- to five-foot diameter tank is normally situated on a graphite pedestal three to five feet thick. The pedestal may be part of a reactor thermal column, or it may contain neutron sources. The tank is usually covered around the outside with cadmium. The Swedish experiments are distinguished by the use of a small diameter tank (1 m diameter) and a borated plastic coating around the tank (P3).

5.2 DETECTORS

A great variety of methods has been used recently to obtain flux distributions in lattice experiments. Probably the most common method makes use of foils, the most popular foil material being indium (C1), (K3). Gold foils are used primarily for detailed measurements, while the use of both lindium (75 per cent indium, 25 per cent lead) (E1) and manganese foils (H2) has been reported.

In the axial direction, the foils may be placed as close as possible to each other, consistent with avoiding interaction (flux depression) between them; placement of foils as close as 3 cm apart has been reported (R1). In the radial direction, however, it is usual to take one point per cell. The points are typically the centers of the cells, but measurements may be made in any point in the cell, including in the fuel rods, themselves (K3). For the sake of experimental accuracy, placement of the foils in cell flux gradients should be avoided if possible.

In some types of experiments, it is necessary to correct for the flux depression in and around the detecting foils. The correction factors are, however, functions only of the properties of the foil and the diffusion properties of the surrounding medium (T1), (B4). Thus, in measurements of relative flux distributions, such corrections are unnecessary. It is possible to use wires for flux scanning although they have been used, so far, mostly in operating reactors or critical facilities (P2). The use of cobalt wire has been troubled by manganese impurity, but an alloy of indium and magnesium has been used successfully (K4). Pure manganese wire has been used in Canada for microscopic flux distribution measurements (H2), while Tuttle has used an alloy of manganese, copper and nickel for measurements of macroscopic distributions (T2), (T3).

The fuel rods of a lattice have, themselves, served as a means of determining the flux shape, the induced fission product activity being measured (B3). Although this is a fairly straightforward process in the case of axial traverses where only one fuel rod is used, radial traverses with such a technique involve problems of normalization, etc.

The use of a large detector, such as a large section of a fuel rod or an ionization chamber, has been justified theoretically by Harris (H3). In a proof similar to that of the second fundamental theorem by Weinberg and Wigner, he shows that, if the flux is distributed as a single eigen-function of the wave equation, the center of a symmetric detector may be regarded as a point detector in the mapping of the flux. The agreement found by Brown between flux distributions measured with foils and fuel rods lends credence to the theory (H3).

In some situations, it is convenient to use a travelling chamber of some sort inside the lattice. A small travelling BF_3 counter has been used by Uhrig (U1), and a gamma compensated ion chamber has been employed at Savannah River (B5), (J1). Persson has used a BF_3 detector, 1 cm in diameter and 3 cm in effective length (P1). The placement of the detectors may be such

as to reduce the efforts of harmonics (P3), or the size of the detectors may accomplish this. For example, Persson has also used a BF_3 proportional counter with an effective length of 35 cm and oriented horizontally, to measure axial distributions (P4). The higher radial harmonics are suppressed by the integrating effect of such long detectors. In this case, the counter is moved continuously and the integrated intensity over 5-15 cm is recorded. However, a discontinuous motion of the counter could be employed to yield greater accuracy. Current reading (ionization) chambers are particularly appropriate in source fed subcritical assemblies where flux levels are too low for either pulse counting or foil activation (A2), but pulse operation is preferable where possible.

5.3 DATA ANALYSIS

There are a number of methods of analyzing the flux distribution data after they have been collected. All methods aim at extracting from a theoretical distribution such as (4.9) a value of the axial and/or radial buckling. This may be done by expanding the expected distribution, say a J_o, in a power series for ease of analysis (P1). Various functions may be defined to provide an iteration scheme to approach more and more accurate values of the bucklings (K2), (K3), (C1). A common technique with the axial distribution is to fit to an exponential and treat the sinh behavior as a correction factor (K3). If a computer of some kind is available, however, there is no reason why a least-squares fitting process cannot be applied directly to the J_o Bessel function and to the sinh distributions.

An unusual method of determining the axial buckling has been suggested by Uhrig. In this technique, the data from two measurements of the radial buckling at two levels in the lattice are used to obtain the axial buckling (U1), (U2). This method would seem to be inferior to the more straightforward methods, however, because of the greater difficulties involved in measuring the radial than the axial distribution. In the axial direction, one may usually take as many points as are useful. In the radial direction, on the other hand, it is

usual to take only one point per cell, resulting in less than ten points along a diameter in some cases (e.g., where heavy water is the moderator).

Another factor should be mentioned pertaining to the relative accuracies of axial and radial bucklings. As shown by Equation (5.1), the final answer is given by the difference between the two measured quantities. In the first lattice measurements in the MIT exponential facility, the radial buckling, α^2, will be approximately twice as great as the axial buckling, γ^2. Thus, if the percentage probable errors of α^2 and γ^2 are comparable, the probable error of B_m^2 will be influenced most strongly by that of α^2.

Nevertheless, it should be noted that there is one type of situation in which the method suggested by Uhrig would be useful. In order to measure the axial buckling accurately by axial flux plotting, the flux distribution must be characterized by only the fundamental harmonic over a considerable axial distance (see Chapter II). If, for some reason, this is experimentally unattainable, Uhrig's method could be used.

In a least-squares fit to the axial distribution, the experimental quantities to which the fit is to be made may have a range of magnitudes of two or three decades. Unless some weighting scheme is used, the points of higher magnitude, i.e., those near the source, will be favored in the fitting process. According to Seren and Tsakarissianos (S2), during the fitting process, the points should be weighted inversely proportional to the square of the magnitude of the flux at that point. Their conclusion was arrived at by critically testing various weighting schemes. This conclusion can also be arrived at on the basis of a statistical analysis. For the minimum error in the final value of γ^2, the experimental points should be given weights inversely proportional to the square of their standard deviations (W13). If the fractional errors of all the points are the same, the standard deviations are proportional to the magnitudes of the flux. Hence, a weighting inversely proportional to the square of the flux is the appropriate one in this case.

Several different approaches have been taken to the problem of

handling the radial distribution data as far as the outer points are concerned. Two questions are involved: whether energy-space separability exists, and whether a simple J_o distribution exists. For example, during the experiments on H_2O-U lattices at Brookhaven, two criteria were considered to determine how many of the outer points of a radial traverse could be used to obtain the radial buckling. First, the fitting process was made with fewer and fewer outer points until the resultant buckling was no longer altered. Second, both thermal and epi-cadmium traverses were considered, points again being dropped until the two derived bucklings were in agreement (W12). On this basis, it was decided to reject from the analysis all points within three lattice units of the edge of the core (K3). In most of these experiments, however, there was a reflector of considerable thickness between the core and the containing tank.

Brown suggests a seemingly effective procedure for handling the outer points of radial distribution data (B3). First, a J_o fit is made to those points which do not appear to be affected by the boundary. The fitting process yields the buckling and the deviation of each measured point from the best fit. The latter compose the residuals, the sum of whose squares is minimized in the fitting process. The J_o function is then subtracted from those points near the boundary not used in the fitting process and residuals are obtained. It has been found in light water lattices that these residuals may be fitted by an exponential function (which is to be expected if the function describing the flux near the boundary is a sum of a J_o and an I_o Bessel function). A least-squares fit is made to these residuals and the curve obtained is extrapolated back to the central points. The extrapolated values can be used either as correction factors or as a basis for the rejection of points. In these experiments, energy-space separability was assumed in the asymptotic region, flux plots being made with foils (of uranium) sensitive to neutrons of various energies. It should be noted that the reflector effect in a D_2O lattice is, in general, not as great as in a H_2O lattice. However, the fewer cells characteristic of D_2O lattices

provide fewer points for any fitting process. In the Canadian experiments on heavy water lattices, spectrum considerations were employed to decide which points could be used in the fitting process. On the basis of cadmium ratio distributions, it was decided to exclude all points 1.5 migration lengths from the lattice boundaries (H2).

Some experimenters have considered it appropriate to make two radial traverses to obtain a "bare" and a "Cd-covered" value of the buckling, from which a "thermal buckling" is obtained (K2). However, if there is a difference between these two bucklings, it is due to a reflector effect and points have been used in the "bare" buckling which do not correspond to a simple J_o. It would seem preferable to use only those points which give the same value of the buckling for the bare and Cd-covered traverses.

5.4 CORRECTIONS

In the measurement of the material buckling of lattices, various kinds of correction factors to the basic data must be considered.

One type of correction factor is that which must be applied, owing to the disturbance of the flux distribution to be measured by the measuring instruments. For example, in some experiments, there is a vertical foil holder in the center of the lattice during the axial traverses which is not present during the radial traverses. In this case, the flux distribution during the axial traverse will not be given by Equation (4.9) but rather by

$$\phi = A[J_o(\alpha' r) + Y_o(\alpha' r)] \sinh \gamma'(h' - z) \qquad (5.5)$$

where B_m^2 is given by $\alpha'^2 - \gamma'^2$. However, it is α (of Equation (4.9) and γ' which are measured. Under the assumption that the effective (extrapolated) radius of the tank is the same in both cases, it can be shown that

$$\alpha = \alpha' \left(1 + 0.409 \frac{S}{4D}\right) \qquad (5.6)$$

where S is the absorption cross section per unit length of the foil

holder, and D is the diffusion coefficient of the moderator (K2).

Another type of correction that must be considered is that for neutrons other than those of experimental interest. In most cases, the neutrons of interest are those in the fundamental mode. As has been discussed in section 4.1, the consideration of higher modes may be eliminated by only using points described by the fundamental mode. Three other undesired types of neutrons are: a) epithermal neutrons from the neutron source, b) distributed neutrons due to γ's from the neutron source or other regions, and the γ-n reaction in D_2O, and c) neutrons which originate from fast neutrons leaking from the facility and being reflected back into the tank.

The first source of neutrons is usually assumed to have the form of an additional sinh (K5) or exponential (K6) distribution. Interference by this type of neutron source or the γ-n source can be obviated by taking experimental points only at locations with constant cadmium ratios (K7). A standard background measurement, covering the source with a cadmium- or boron-containing sheet, may also be used to evaluate the intensity of these two extraneous sources of neutrons. When a cadmium sheet is used in experiments involving heavy water, it should be realized that a new, extraneous, neutron source is being introduced. Neutron capture gamma rays from the cadmium will produce photoneutrons in the D_2O. Unless this effect can be proved negligible in a particular situation, it would be preferable to make the background measurement, using a boron-containing sheet. In the MIT experiments, this problem is not serious because of the unusual configuration of the lattice facility. As is shown in Fig. 6.1, the cadmium shutter is located far enough from the experimental tank so that it is not a source of gamma rays in the tank.

The third extraneous neutron source, reflected fast neutrons, is more difficult to evaluate. In the radial direction, it may be considered as a reflector effect to be handled in the fitting process, as discussed above. Persson has determined theoretically the effect of these neutrons on the measurement of the axial relaxation length (P3). He analyzes the axial distribution, assuming it has the form:

$$\phi = A e^{-\gamma z} + C\psi(z) \qquad (5.7)$$

where $\psi(z)$ is the contribution of the background.

The final type of correction to be considered is that which allows for intercomparison between experiments made under slightly different conditions. The most common correction of this sort is that for differences in D_2O purity. The method of correction depends on the calculation scheme used to analyze the particular experimental results but usually consists of the evaluation of the various parameters such as p, L^2, τ and f at different D_2O purities in a two-group analysis (B6), (B7), (G3). It would be useful to check these calculations by using a standard lattice at various stages of H_2O contamination. Dessauer has reported a comparison between experimental and theoretical results with respect to this correction (D3).

It is sometimes also necessary to correct for different claddings used in various experiments. Such corrections have been discussed by Andrews and Dastur (A2).

5.5 VARIATIONS ON THE CONVENTIONAL APPROACH

There are a number of interesting variants of the normal buckling measurement which should be mentioned briefly.

The first is the so-called "substitution method". It consists of replacing one or more fuel elements at the center of a measured lattice and deriving the buckling that would be obtained in a complete lattice of the substituted type of element. At the Brookhaven National Laboratory, this type of experiment was carried out as a critical experiment employing two-region, one-group perturbation theory (D4). The theory was checked by using in the substitution, rods which had been employed in a full scale experiment. Critoph has outlined the calculational methods to be used in this approach when one rod is substituted (C2), while Persson has described the theory pertaining to the substitution of a varying number of rods or clusters (P5), (P6). Anderson and Aspedlund have also reported on such experiments (A3). By increasing the size of the central foreign zone in steps, they found it possible to obtain the buckling of the substituted

rods by extrapolation. At the Savannah River Laboratory, critical substitution experiments are used extensively to obtain bucklings. The two-group, two-region theory used to evaluate these experiments has been reported by Dessauer (D3) and Carmichael (C3). The type of experiments performed at the Physical Constants Testing Reactor (PCTR) at Hanford is closely related to the substitution type of measurement (H9). The unusual features of the PCTR experiments include the attempt to make null type measurements, and the use of a "buffer" region around the test region to shift the spectrum of the feed distribution to that characteristic of the test area.

Perhaps the ultimate simplification of the exponential experiment is represented by measurements on a single fuel rod in a moderating material (E2), (E3). Such experiments are based on heterogeneous reactor theory as developed by Feinberg and Galanin (G4). The experiments consist primarily of observing the flux distribution around the single element or cluster and have been described by Zink and Rodeback (Z1).

An interesting minor variation on the usual exponential experiment is found in the possibility of investigating xenon poisoning with buckling measurements. Copper foils of various thicknesses can be placed between the uranium slugs of a fuel rod to simulate xenon absorption and the normal type of experiment is then performed (K8).

CHAPTER VI
EXPERIMENTAL AND ANALYTICAL METHODS

6.1 INTRODUCTION

This chapter and Chapter VII deal with the measurements made in the lattices of 1.010-inch diameter natural uranium rods. The experimental techniques and the methods of analysis that were used are described in the current chapter, while the results of the measurements are given in Chapter VII.

The experimental and analytical methods to be described were designed to be applicable, not only to the particular lattices studied, but also to the various types of lattices which will be investigated in the future by the MIT Lattice Project. These methods were also designed to analyze various details of the macroscopic flux distribution, other than those usually studied in the measurement of the buckling.

6.2 THE FACILITY

The lattice facility has been described in a previous report (H6). The aspects of the facility germane to the buckling measurements are shown in Figs. 6.1 and 6.2.

The neutron source for the experiments is the thermal column of the MIT reactor. The MITR is a highly enriched uranium, D_2O moderated reactor which operated at power levels up to 1.8 Mw during the experiments reported here. A graphite-lined cavity serves to reflect neutrons from the thermal column up to the bottom of the experimental tank. The graphite pedestal, located directly beneath the exponential tank, has been described in Chapter II. The flux at a height of two feet in the tank, with all shutters open and the MITR operating at 1.8 Mw, is about 10^9 n/cm^2 sec and is about 10^{10} at the tank bottom. The steel shielding doors shown in Fig. 6.1 have boral

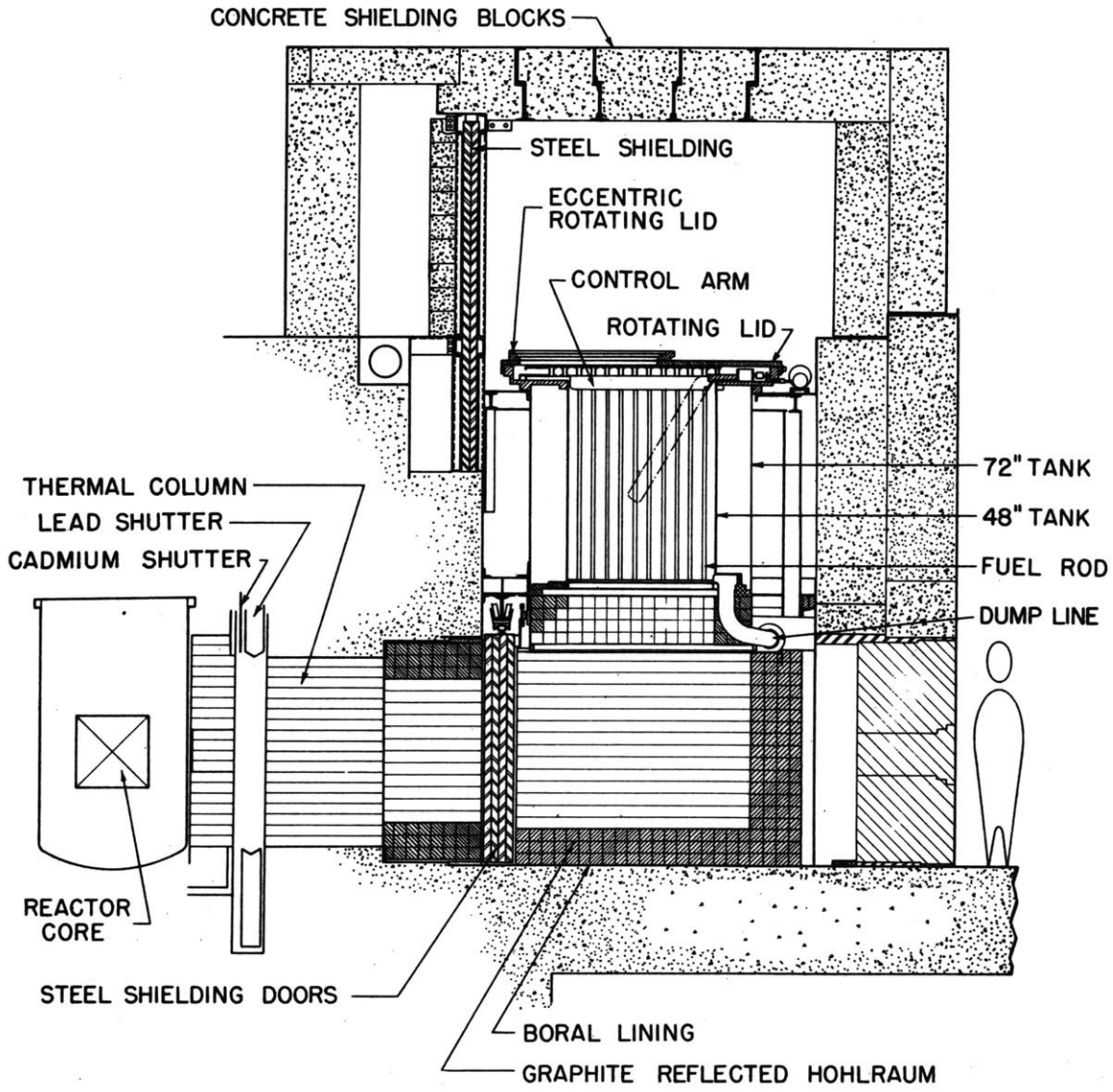

FIG. 6.1 VERTICAL SECTION OF THE SUBCRITICAL ASSEMBLY

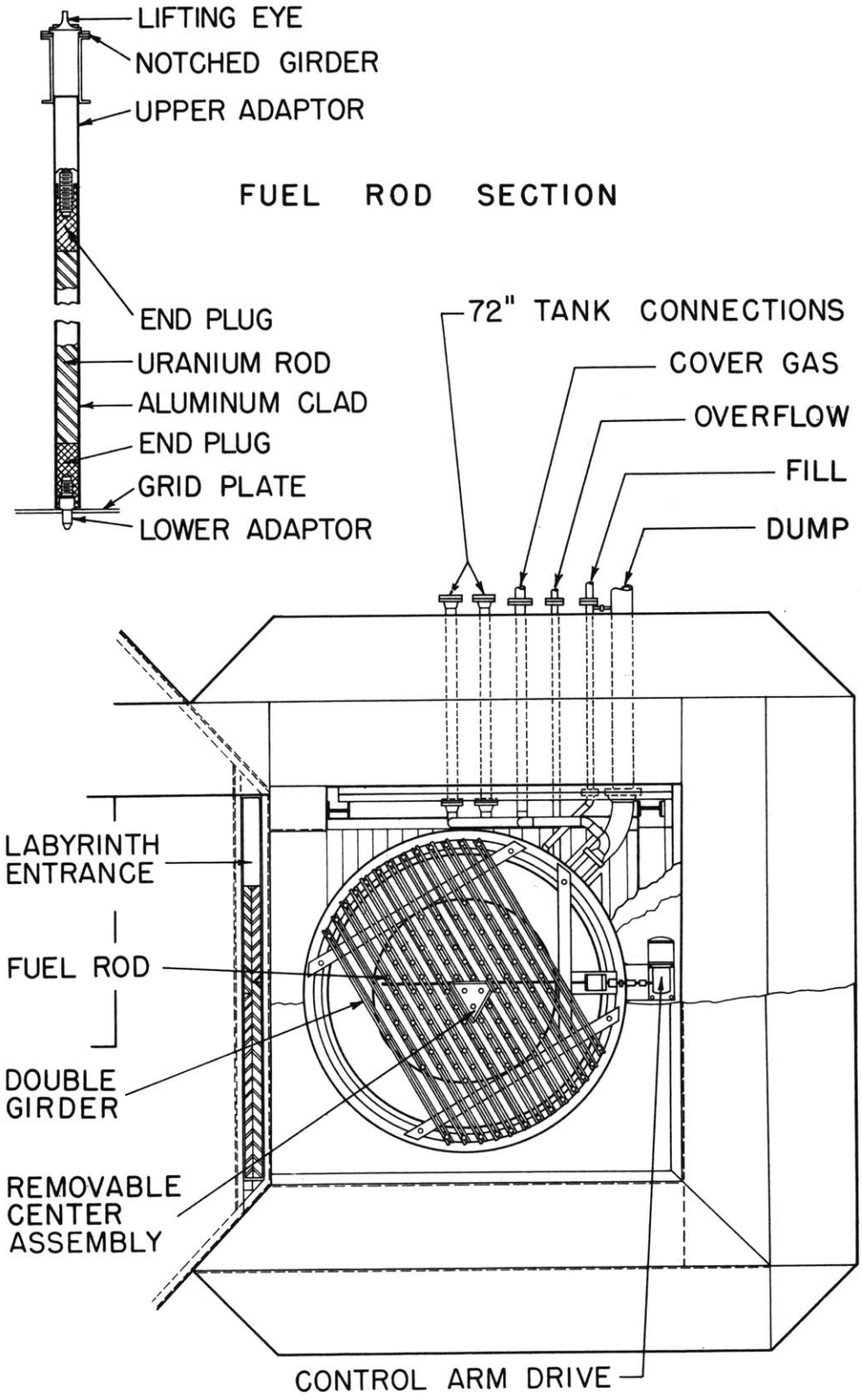

FIG. 6.2 PLAN VIEW OF THE SUBCRITICAL ASSEMBLY

on the surface toward the reactor, and their closing reduces the neutron flux in the facility by at least a factor of 10^3. The opening and closing of the shield doors, or of the cadmium thermal column shutter, was used to start and terminate runs.

As is shown in Fig. 6.2, the fuel rods are suspended from double girders at the tank top. The spacing of the fuel rods is established by the relative spacing of the girders and by notches in spacing bars at the top of the girders. Tabs in the fuel rod upper adapters fit into the spacing bar notches. In addition, a grid-plate near the tank bottom contains locating holes for the lower adapters of the fuel rods. Three central rods are attached together to provide a removable central assembly.

Normally, the lattices are assembled on the floor of the reactor building and then loaded in their entirety into the experimental tank. Figure 6.3 shows the 4-1/2-inch spacing, 1.010-inch natural uranium rod lattice ready for insertion in the tank. Note that the central cell has not been put in place. A photograph of the top of the 5-inch spacing lattice in the tank is shown in Fig. 6.4. The fuel rod spacing arrangements are clearly shown in this photograph, which also shows the relative location of the vertical drive motor of the traveling neutron counter.

The aluminum subcritical assembly tank in which the experiments to be reported here were performed is 48 inches in diameter and 67-1/4 inches high. It is surrounded by a sheet of cadmium 0.020 inches thick. A concentric, outer tank, 72 inches in diameter, surrounds the experimental tank. The concrete shielding around the facility, as shown in Figs. 6.1 and 6.2, is at distances of 1 to 3 feet from the outer tank.

The facilities described above were designed to be adaptable to various types of experiments and experimental conditions. When the experimental situation was required to approximate, as closely as possible, bare - i.e., unreflected - assemblies, several alternatives existed. One of the major considerations in this case was to preclude to as great a degree as possible the scattering back of neutrons from

FIG. 6.3 $4\frac{1}{2}$ INCH SPACING LATTICE
BEFORE INSERTION INTO TANK

FIG. 6.4 TOP CORNER OF $4\frac{1}{2}$ INCH SPACING LATTICE

the surrounding shielding. One alternative to the current approach of encasing the inner tank with cadmium, and leaving the outer tank empty, consisted of filling the outer tank with a solution of B_2O_3 in H_2O. A theoretical investigation of such a configuration (made on a two-group, two-region basis) showed that very high concentrations of boron in the water (about 90 gm/liter) were required before the thermal reflector effect was eliminated. The solubility at 100° C is only 157 gm/liter and is 11 gm/liter at 0° C. Furthermore, because of the efficient reflection of fast neutrons by the waters, even at very high boron concentrations, the resultant thermal buckling does not correspond to the buckling of a bare system. A summary of the calculations which were originally performed by Mr. F. Becker, and their results, are reported in Appendix A2.

The tank lid is normally supported on a gasket which provides a seal for the nitrogen cover-gas. Alternatively, it can be supported by a ring of ball bearings which permits the rotation of the lid. A smaller eccentrically located lid makes up part of the larger, and includes a shutter and removable glove box. With this arrangement, any location on the lattice top is accessible through the glove box by the proper rotation of the two lids. The configuration of the lids is indicated in Fig. 6.1.

Most of the experimental apparatus that had to be inserted for short periods in the exponential tank was designed so that it could be introduced through the glove box. With the D_2O out of the tank and the tank dried, the lid could be removed in order to insert other types of apparatus. The central cell can be inserted through the glove box, and small pieces of equipment can be introduced with it. Permanent pieces of apparatus can, of course, be attached to the lattice before it is introduced into the tank.

6.3 EXPERIMENTAL TECHNIQUES

6.3.1 Foil Preparation and Irradiation Techniques

Because of the great experimental flexibility which it allowed,

the method of foil activation was used in all the macroscopic flux measurements to be reported. Gold was chosen as the foil material because it combines the following four advantages:

1. The metal is readily available in pure form and is easily handled.
2. There is only one stable isotope, Au^{197}, to undergo activation.
3. The activation cross section of 96 barns is conveniently high so that irradiation times can be low.
4. The activity produced is of conveniently long half-life, 2.7 days, so that the foils need not be counted hastily after irradiation.

One of the disadvantages of using foils, as opposed to some sort of movable counter to map flux distributions, is that of assuring that all foils used have the same neutron sensitivity (or the necessity of knowing the relative sensitivity of each foil). Variations in sensitivity may arise from variations in foil purity, thickness, or surface area. The first hazard is avoided by using foils of very pure (99.9 per cent) gold. The difficulties of foil weight, or thickness, were handled in the following way. First, it was decided to count the beta activity of the irradiated foils. An experiment was performed to study the effect of foil thickness on foil activity as observed in the counting arrangement to be used in the later experiments. A set of 1/2-inch diameter gold foils of varying thickness was irradiated on a wheel turning in the flux over the graphite cavity mentioned above. The foil wheel arrangement is a standard method of assuring that all the foils of a set are exposed to the same flux for the same length of time. The beta activity of each foil was then counted, all the activities being corrected back to some common time.

Figure 6.5 presents the results of this experiment. As would be expected, for very thin foils, the induced activity is approximately proportional to the thickness of the foil. For thicker foils, owing to absorption of beta particles in the foil, the activity becomes

insensitive to foil thickness. Flux depression by the foil and self-absorption would also tend to flatten the curve of Fig. 6.5. On the basis of this experiment, it was decided to use foils 0.010 inch thick. Furthermore, all foils used were punched from the same sheet of material. As a further precaution, all the foils used were weighted and placed in groups, each group containing foils with no more than 1 per cent variation in weight. In any one experiment, the foils of one group (or, in some cases, two adjacent groups) were used.

In Chapter III, various methods of making radial and axial flux plots were described. On the basis of the experiments described there, the following techniques were decided upon for the lattice experiments.

Radial Traverses:

All the radial traverses were made with gold foils, usually 1/4-inch in diameter, attached to thin 6063-type aluminum foil holders. Since we are concerned only with relative flux values (or relative foil activities), any flux depression caused by the aluminum foil holder should not affect the final results. Furthermore, with the very light holders used, such depression would not be significant, compared to that caused by the foils, themselves. At various times during the experiments, traverses were made with foils supported by string which could be compared to runs made with an aluminum holder. No systematic difference was ever observable in these cases. (See, for example, Fig. 3.3 and Table 7.10.) The locations of the foils along the foil holders were determined by depressions milled in the aluminum at the required positions. A description of the three lattices studied is given in Chapter VII. They were all hexagonal arrays of nominally 1-inch diameter rods, with a fuel rod situated at the tank center. Since all "radial" traverses were taken in the moderator, they could not pass through the center of the tank, or fuel rod array, but were rather taken along

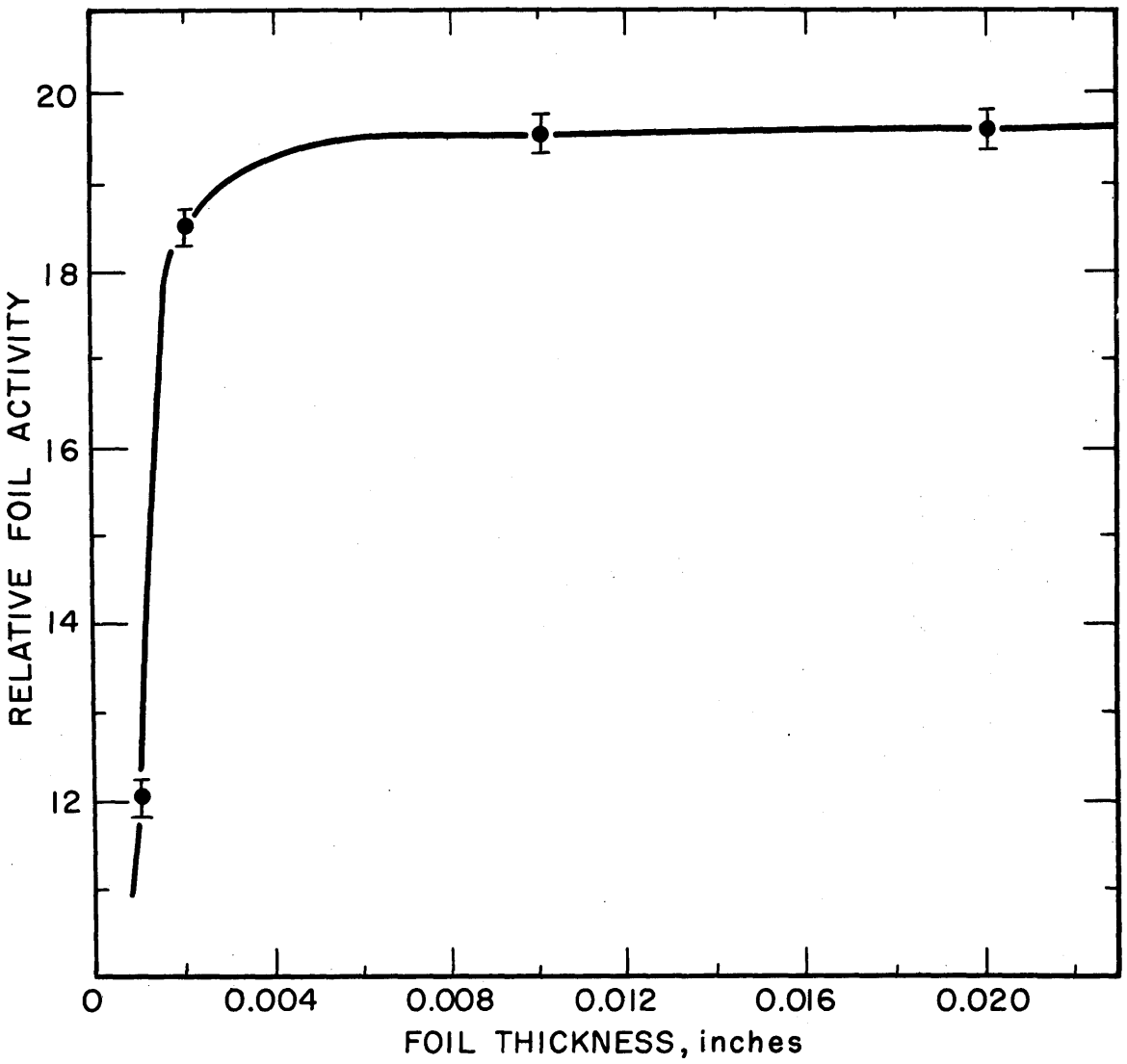

FIG. 6.5 ACTIVITY OF 1/2 INCH DIAMETER Au FOILS COUNTED IN A G-M COUNTER AS A FUNCTION OF FOIL THICKNESS

a chord. The analysis of these traverses, however, was made in terms of the radial positions of foils. In the first lattice, in which the rod spacing was 4-1/2 inches, the radial foil holder was supported by two aluminum pieces, each being attached between two adjacent rods at the outer edge of the lattice. The location of these supports is shown in Fig. 7.1.

In the 5-inch and 5-3/4-inch spacing lattice, a more versatile scheme for suspending the radial foil holders was developed and used. The holder was suspended with aluminum bead chain at each end from the top of the lattice. Its position relative to the fuel rods was fixed by adjustable arms at the ends of the holder. One end of such a holder is shown in Fig. 6.6.

Axial Traverses:

The axial traverses were made with all three types of foil holders described in section 3.3.1 and shown in the photograph of Fig. 3.2. The most convenient and most accurate technique involved the use of a solid foil holder such as the one shown in Fig. 3.2, but milled to accommodate 1/4-inch foils at a minimum separation of 1-1/8 inch.

6.3.2 Foil Counting

In most of the experiments, 0.010-inch thick, gold foils of either 1/4-inch or 1/2-inch diameter were irradiated, and their beta activity was then counted. A Geiger-Müller gas-flow counter was used in connection with a Baird-Atomic automatic sample changer. Several checks on the constancy of the counter sensitivity were made over the course of the experimentation; whenever the activity of a set of foils was counted, the activity of a standard source was also counted. Furthermore, each set of foils was counted at least three times, with a background count being taken each time. The activity of each foil was then corrected back to a standard time for each of the times it was counted. These corrected activities were then compared for consistency before averaging.

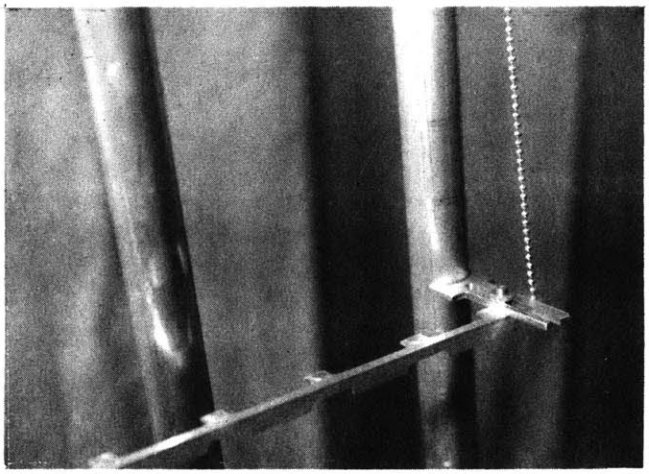

FIG. 6.6 METHOD OF MAKING RADIAL TRAVERSES IN LATTICES. FOILS ARE 1/4 INCH IN DIAMETER, FUEL RODS ARE 1.08 INCHES IN DIAMETER

In some cases, when other types of foils were used, a NaI scintillator was used for foil counting. The scintillator was part of a system including a Nuclear-Chicago automatic sample changer and a single-channel pulse height analyzer.

The foils were always washed with acetone and wiped clean before counting, as well as before being weighed or being irradiated. Normal care was taken not to damage the foil surfaces or edge.

6.3.3 The Automatic Flux Scanner

Although only foil activation techniques were used to obtain the results reported in the next chapter, an automatic flux scanner has been designed and built to operate in the facility. The scanner, developed primarily by Mr. M. Quinteiro (Q1), is designed to operate in one plane of the lattice. One corner of the scanner frame, in the 5-inch spacing lattice, is shown in Fig. 6.4. It can be programmed to move either continuously or discontinuously in any pattern in that plane, involving any combination of axial and radial traverses. When it is operated discontinuously, the count rate from the miniature fission chamber (1/4-inch diameter) prints out automatically at the control station. A fixed monitor counter determines the length of each counting time.

Foil activation was a versatile technique for the various types of flux distribution measurements made in the first lattices. However, it is expected that in future routine measurements of the buckling, the flux scanner will be an adequate and convenient instrument.

6.4 ANALYTICAL TECHNIQUES

6.4.1 Analysis of Radial Measurements

The theoretical basis of the experiments, and thus of their analysis, has been given in Chapter IV. The analytical treatment of the experimental data was made efficient, complete, and rapid by the development of a set of codes for an IBM 709 computer. The

computer used was that of the MIT Computation Center.

The codes were written with primarily two ideas in mind. The first and basic purpose was the derivation of a value of the material buckling of a lattice from measured axial and radial flux distributions. Secondarily, the codes were designed to examine some of the assumptions and approximations mentioned in Chapter IV. The details of the theoretical basis and the operation of the codes, along with Fortran listings, are presented in Appendix A2. Only their analytical structure will be reported in this section.

The basic code for the radial distribution performs the following steps:

1. Experimental values of the flux at various radial positions are calculated from measured foil activities by correcting for a) decay during and before counting, b) the measured counter background, c) the counter dead-time measured as a function of count rate, and d) the perpendicular distance of the chord along which the measurements are made from the lattice center.

2. The values of the corrected foil activities for each radial position are printed out for comparison and then averaged to obtain a flux at that point. A multiplicative correction factor may then be applied to any points to correct for foil weight, microscopic distributions, etc. The fluxes are normalized, the flux nearest the center being set equal to 1.0.

3. The measured values of the flux are fitted, according to the least-square criterion, to the theoretical distribution given by

$$\phi = AJ_o[\alpha(r-c)] \ , \qquad (6.1)$$

where the "best" values of A, the normalization factor, and α^2, the radial buckling, are determined in the fitting process. Since the equation is not linear in α, an iterational scheme must be used for the solution. The value of c, the center of the distribution, is preset.

4. The fitted and experimental fluxes at each point are printed out, along with the fitted values of α^2, A and their probable errors.

5. The fitting process is repeated for all experimental points

except the outermost until some preset number of points has been used in the fit.

6. The process is repeated for other values of c.

The fitting process can be performed with any point-weighting desired, and the iteration can be accelerated or decelerated. The details of these variations are described in Appendix A1. Usually, in the radial analysis, all points were given unit weight. Although this tends to accentuate the center points in the fitting process, the variation in the magnitude of the foil activities along an experimental chord was usually only a factor of 5. Furthermore, the central points would be expected to be somewhat "better" than the outer ones, since the latter would be subject to reflector effects, etc., if such exist. Other weighting schemes were used for analytical purposes, as described in section 7.3.1. It is shown there that the final value of the radial buckling obtained is insensitive to the weighting used. It can be seen that, although this code is designed primarily to extract values of α^2 from radial flux distributions, it can be used to examine edge effects (by refitting with points dropped), gross distribution shifts (refitting with various c's), microscopic effects (by employing periodic correction factors), etc.

As is discussed in Chapter IV, the theoretical analysis used in the measurement of the buckling depends on the assumption that the radial flux distribution is describable by a single J_o Bessel function over a certain vertical distance in the tank. The simple J_o flux shape may be distorted through two effects: higher harmonic contributions may be present (due, perhaps, to the inadequate attenuation of the harmonics in the source distribution), or there may be a reflector effect. The latter may arise from incomplete filling of the tank by the lattice, or the back-scattering of epicadmium neutrons.

Thus, one code is designed to analyze a measured radial distribution for the presence of higher harmonics. The data reduction portion is identical to that included in the J_o code (steps 1 and 2); but in this case, the experimental flux is fitted by least-squares to the equation

$$\phi(r) = A_1 J_o(\alpha_1 r) + A_2 J_o(\alpha_2 r) + A_3 J_o(\alpha_3 r) , \qquad (6.2)$$

where

$$\alpha_1 = \frac{2.4048}{R'} , \quad \alpha_2 = \frac{5.5201}{R'} , \quad \alpha_3 = \frac{8.654}{R'} ,$$

and

R' = the extrapolated radius.

In this case, R' is an input quantity and may be determined by use of the J_o code. The code solves for the "best" values of A_1, A_2, and A_3 and prints them out, along with values of the experimental and fitted fluxes at the experimental points.

The third code used to analyze radial flux distributions is designed to look for reflector effects. Again, the same data reduction portion is included; and, in this case, the measured flux is fitted to the formula,

$$\phi(r) = A_1 J_o(\alpha_1 r) + A_2 I_o(\alpha_2 r) , \qquad (6.3)$$

where the quantities A_1, A_2, α_1 and α_2 are determined in the iterative, least-squares fitting process.

As will be shown in the next chapter, no observable reflector effect existed in the lattices studied, nor were there higher harmonic contributions except at the bottom of the lattices. However, a note of caution should be entered here concerning the use of the codes described above to analyze a flux distribution that possibly involves both reflector and harmonic effects. Each code takes into account one of the effects and assumes that the other does not exist. Let us consider how one could use the codes if both effects were extant. First of all, the codes could be applied to radial traverses taken at various heights in the lattice. The higher harmonic contribution to the fundamental mode should diminish with height while the reflector effect should be constant. Thus, hopefully, the reflector effect as determined by the code should vary with height but approach some asymptotic or constant value. Secondly, the codes could be applied to fewer and fewer points of a radial traverse. The harmonic contribution, as determined by the code, should vary as outer points are dropped only if a reflector

effect is involved. As fewer points are used, the reflector-effect contribution should decrease and the harmonic contribution, as determined by the code, should approach an asymptotic, "true" value.

Of course, other techniques may be used to look at both of these effects. For example, if the radial distribution contains higher harmonic contributions, so does the axial distribution. (See section 4.1.) Thus, the axial distribution can be used for the harmonic analysis if a reflector effect interferes with the radial harmonic analysis. Similarly, alternative methods for looking for a reflector effect may be used, such as refitting the measured distribution to a J_o with successively fewer points and observing the trend in the fitted radial buckling. (See section 7.3.1.)

While the set of computer codes was used to check the spatial "purity" of the fitted J_o flux distributions, the requisite energy-space separability was checked in two other ways. The bare gold foils used in the experiments have a relatively high response (particularly at the 4.9 ev resonance) to epithermal neutrons. If the neutron energy spectrum shifts appreciably near the edge of the lattice, different values of the measured buckling should be obtained as fewer points are used in the fit. A second, and more sensitive, test of energy-space separability in the radial direction can be made by measuring the flux distribution with cadmium-covered foils. If separability holds, the value of α^2, determined by fitting the cadmium-covered foil data, should be the same as that derived from the bare-foil data. This effect can be studied with greater accuracy by examining the cadmium ratio as a function of radial position. A region of constant cadmium ratio indicates a region of energy-space separability.

6.4.2 Analysis of Axial Measurements

As is described in section 4.1, the axial flux distribution in the lattices is expected ideally to have the form

$$\phi(z) = A \sinh \gamma(h' - z), \tag{6.4}$$

where γ^2 is the required axial buckling and h' is the extrapolated height. The experimentally measured distribution is expected to deviate from the distribution of Equation (6.4) for various reasons in different regions. The situation is represented in Fig. 6.7, where four distinct regions are distinguished. The solid line represents the distribution given by Equation (6.4), while the circles represent fictitious values of the flux as might be determined by the activation of bare gold foils. The various effects, which are exaggerated in the figure for the sake of clarity, are as follows.

Region I

Near the bottom of the tank, it is expected that higher spatial harmonics will be evident. This is due to the fact that the source distribution is not a perfect J_o. Since the higher harmonics have shorter relaxation lengths than the fundamental (see section 4.1), a more rapid decrease in the flux would be expected than that given by Equation (6.4).

Region II

The source neutron energy distribution contains practically no epithermal component (see section 3.4). As the source neutrons enter the lattice, the epithermal component of the lattice flux gradually builds up. In Region II, the ratio of epithermal to thermal neutrons is still lower than the ratio characteristic of the lattice spectrum. Thus, gold foils sensitive to both kinds of neutrons exhibit an activity lower than the theoretical curve. Although Regions I and II are distinguished in this discussion for the sake of clarity, the phenomena characteristic of the two regions do, of course, occur simultaneously. Which phenomenon determines the lower limit of Region III will depend upon the particular experimental situation involved.

Region III

Throughout this region, the spectrum is that characteristic of

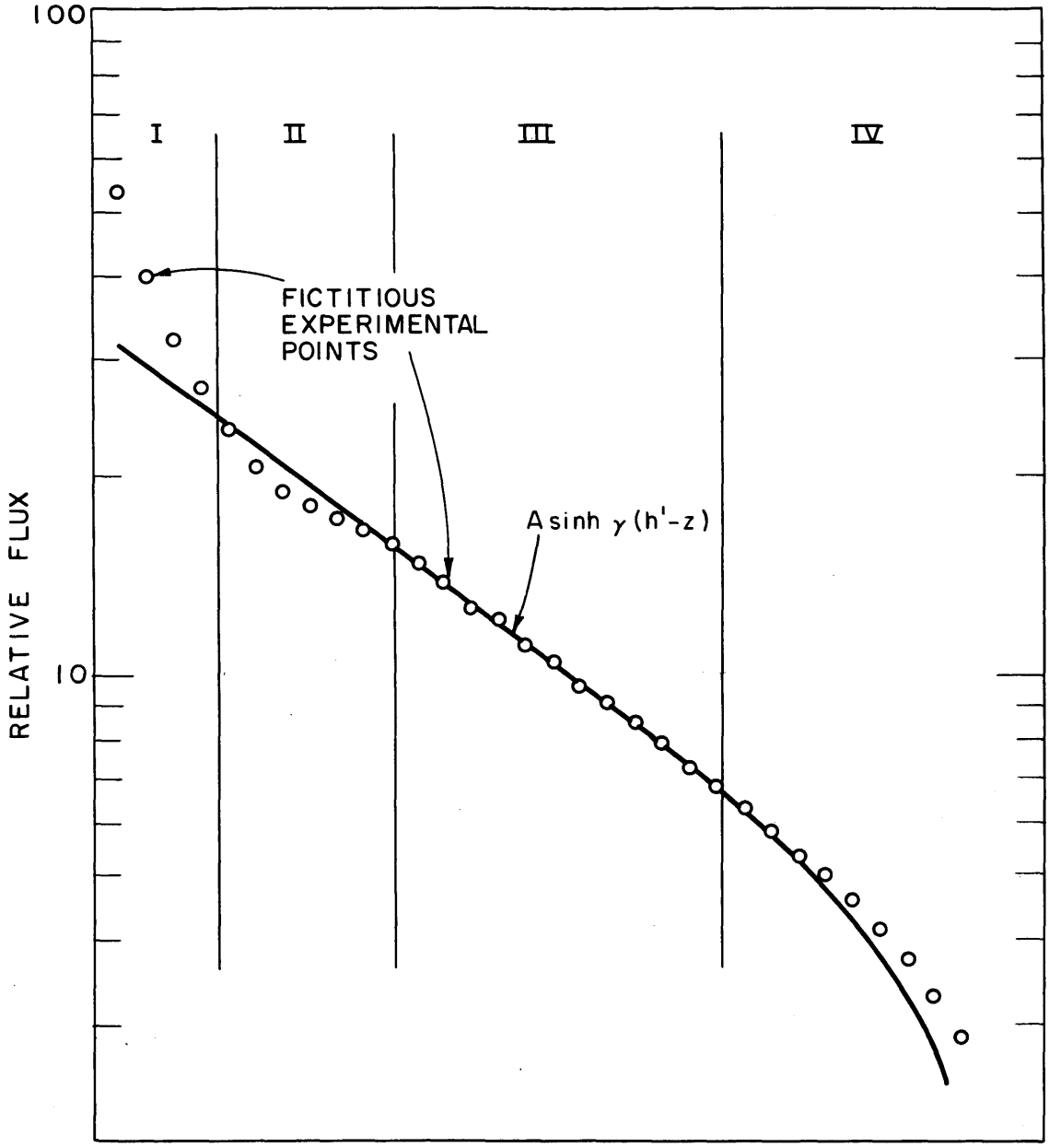

FIG. 6.7 COMPARISON OF IDEAL SINH BEHAVIOR OF AXIAL FLUX AND POSSIBLE EXPERIMENTAL POINTS

the lattice, energy and space separability holds; and the experimental points conform to the theoretical distribution.

Region IV

At the top of the lattices, neutrons of different energies may respond differently to the upper boundary conditions, and may again cause a discrepancy between the measured points and the theoretical distribution. Equation (6.4) assumes that neutron fluxes of all energies go to zero at an extrapolated height, h'. However, the upper boundary of the tank is not as clearly defined as the radial boundary (defined by the cadmium sheet). Both fast and thermal neutrons are expected to be scattered back to the top of the lattice by the aluminum (fuel rod upper adapters, support beams, etc.) above the nominal lattice top. The neutrons scattered back will augment the lattice flux and cause the experimental points to fall above the ideal curve.

Before the measurement of γ can be made, the extent of Region III must be determined; only points from this region are then used in the analysis for γ. The region can be specified experimentally by examining the gold-cadmium ratio as a function of height in the lattice. In Region III, this ratio should be constant. In other regions, the ratio should vary from that in Region III for the following reasons. In Regions I and II, the epithermal component of the flux is small, compared to that in Region III, thus producing a higher cadmium ratio. In Region IV, the spectrum of the excess neutrons will be determined by the energy dependence of the scattering and return effects above the tank. It is to be expected that the spectrum of the returning neutrons would be quite different from the spectrum characteristic of the lattice, thus producing a shift in cadmium ratio in Region IV.

Another, independent, method may be used to determine the extent of Region III: a hyperbolic sine function can be fitted to all the experimental points of a run. The residuals of the experimental points and the fitted curve can be examined for the systematic variations that would appear because of the effects occurring in Regions I, II, and IV. The points whose residuals show no systematic variation

can then be used to make the final fit to determine γ.

As in the case of radial traverses, a code was written to analyze the axial distributions. The axial code performs the following steps:

1. The raw input data of either neutron-counter output or foil activities are reduced to normalized flux values. The same operations specified under steps 1 and 2 of the J_o code description are performed. The flux values are normalized, with the first input point set equal to 1.0.

2. A value of h′ is chosen and the experimental points are fitted by least-squares to a function of the form of Equation (6.4). The "best" values of A and γ are determined and are printed out along with their probable errors. At each experimental point, the experimental and fitted fluxes and the residual are printed out. Again, an iterational approach must be used in the analysis.

3. Other values of h′ are tried and step 2, repeated. The best value of h′ can be deduced by comparing the value of the probable errors of γ for various h′ and by considering the axial distribution of the residuals.

4. End points are dropped successively and steps 2 and 3 repeated. In this way, the number of points used in the fitting process is reduced to those corresponding to the theoretical distribution, i.e., corresponding to Region III of Fig. 6.7. Points are dropped by the code, starting with the last point read in as data, until some specified number of points has been used in the fit. Since, in this process, only one end of a traverse is examined, the code must be run twice if points of both ends of the traverse are in doubt. When one end of the distribution is being examined, any points on the other end that may not correspond to the theoretical distribution should not be included in the analysis.

The fitting process may be performed with any weighting scheme desired. Usually, the experimental points were weighted inversely proportional to the square of the magnitude of the flux for reasons

discussed in section 5.3. Other weighting schemes were used for specific analytical purposes (see section 7.3.3).

The details of the theoretical basis and of the operation of the axial code are presented in section A1.5 of Appendix A1.

In describing the experimental results in the next chapter, examples will be given of some of the features of the analysis.

CHAPTER VII
EXPERIMENTAL RESULTS

7.1 INTRODUCTION

In presenting and discussing in this chapter, the results of the lattice experiments, two basic purposes are to be served. It is shown, first of all, that the flux distribution in the lattices is satisfactory for buckling measurements. This step is, then, the final one in the series of design considerations and experiments described in Chapters I, II and III. Second, the material bucklings of three natural uranium lattices in D_2O will be reported. These represent a contribution to the available data on such lattices. A comparison with experimental results obtained at other laboratories provides a test for the theoretical, experimental, and analytical bases of the experiments, described in Chapters IV and VI.

The experimental results of an investigation of the separability of the macroscopic and microscopic components of the radial flux distribution will also be presented.

7.2 DESCRIPTION OF THE LATTICES STUDIED

The experiments to be reported were made on three lattice spacings of natural uranium rods in D_2O.

The cylindrical fuel rods are of natural uranium metal, 1.010 ± 0.005 inches in diameter and 60 inches long. They are canned in Type 1100 aluminum tubes, 0.028 inches thick, with an outside diameter of 1.080 inches. Upper and lower aluminum plugs and adapters bring the total length of the fuel rods to about 71 inches (see Fig. 6.2). Figure 7.1 shows the vertical configuration of a fuel rod with respect to the tank. The top of the lattice is defined by the top of the fuel and the normal height of the D_2O at about 64 inches (163 cm) from the tank bottom.

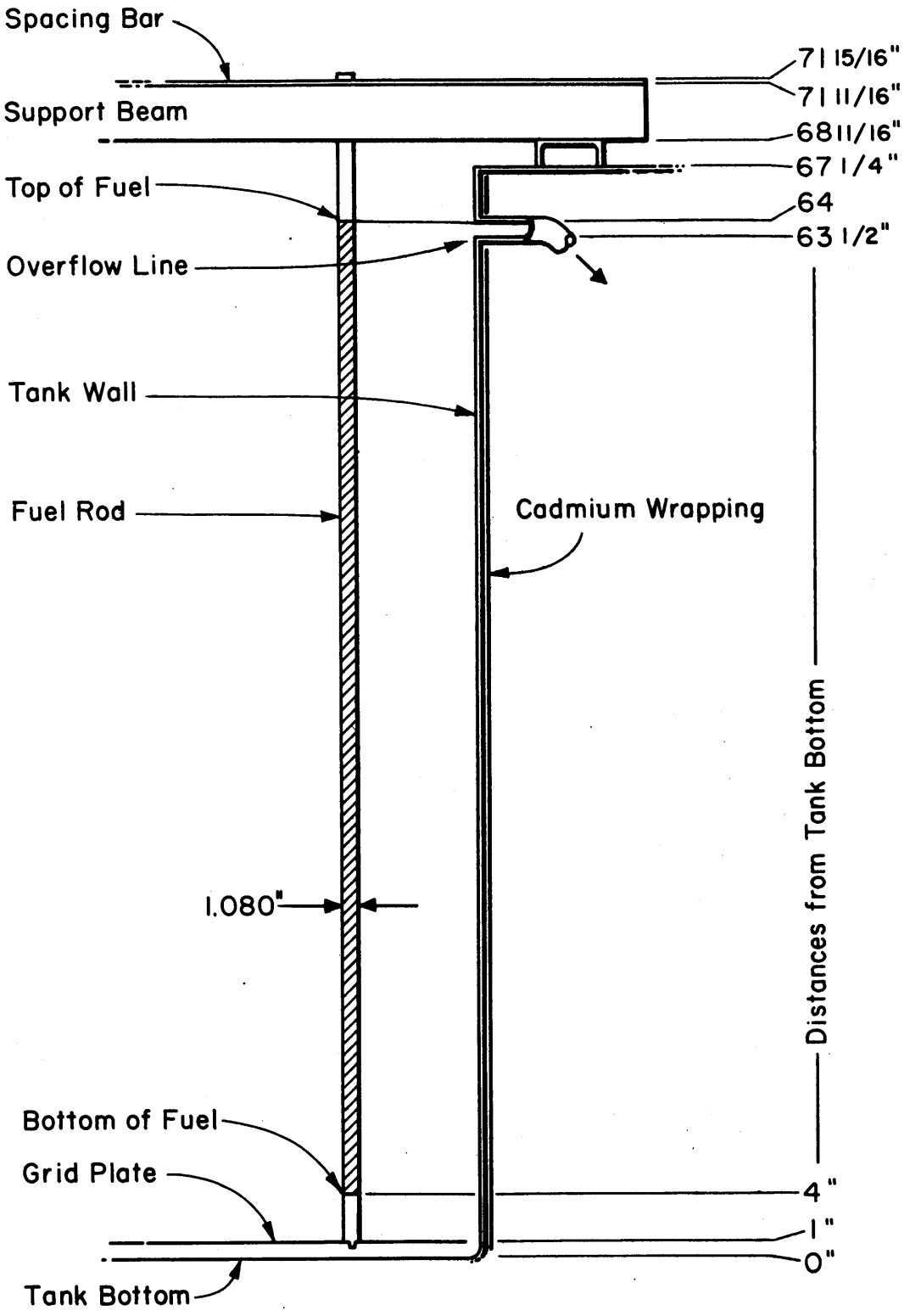

FIG. 7-1 VERTICAL CONFIGURATION OF A FUEL ROD IN THE TANK

In the lattices, the fuel rods were arranged in triangular arrays with rod-to-rod spacings of 4-1/2, 5, and 5-3/4 inches. The three configurations are shown in Figs. 7.2, 7.3, and 7.4.

7.3 FLUX ANALYSIS RESULTS

7.3.1 Radial Flux Distribution

Whenever a radial flux distribution was measured to obtain a value of the radial buckling, the validity of the assumption of a simple J_o distribution was checked. An example of a measured radial distribution is shown in Fig. 7.5. As can be seen, the experimental points are well represented by the fitted J_o distribution, and no reflector effect is apparent. A more sensitive test for a reflector effect can be made by examining the residuals, i.e., the differences between the experimental and the fitted flux, as a function of radial or chordal position. If there is a reflector effect, the residuals, δ, near the outside of the lattice would tend to become more positive. A plot of the residuals from a traverse in the 4-1/2-inch lattice is shown in Fig. 7.6. Points from both sides of the center are included in the plot. The outermost points recorded were taken in the outer cell of the lattice. The random distribution of the residuals attests to the adequacy of a J_o distribution in characterizing the flux.

It was mentioned in section 6.4 that the experimental points could be weighted in any way desired in the fitting process. By varying the weighting in the J_o-fit routine, another test for non-ideal behavior of the radial distribution is provided. With all points receiving unit weight, the points near the center of the lattice are accentuated in the fit. If a weighting inversely proportional to the square of the flux is used, the outer points are weighted much more heavily. If a departure from the J_o distribution occurs, the value of the radial buckling derived in the two cases should differ. Such a test was made with a distribution measured in the 4-1/2-inch lattice. The two bucklings determined by the code were $14.17 \pm .10$ m.$^{-2}$ and $14.18 \pm .09$ m.$^{-2}$, again verifying the J_o distribution.

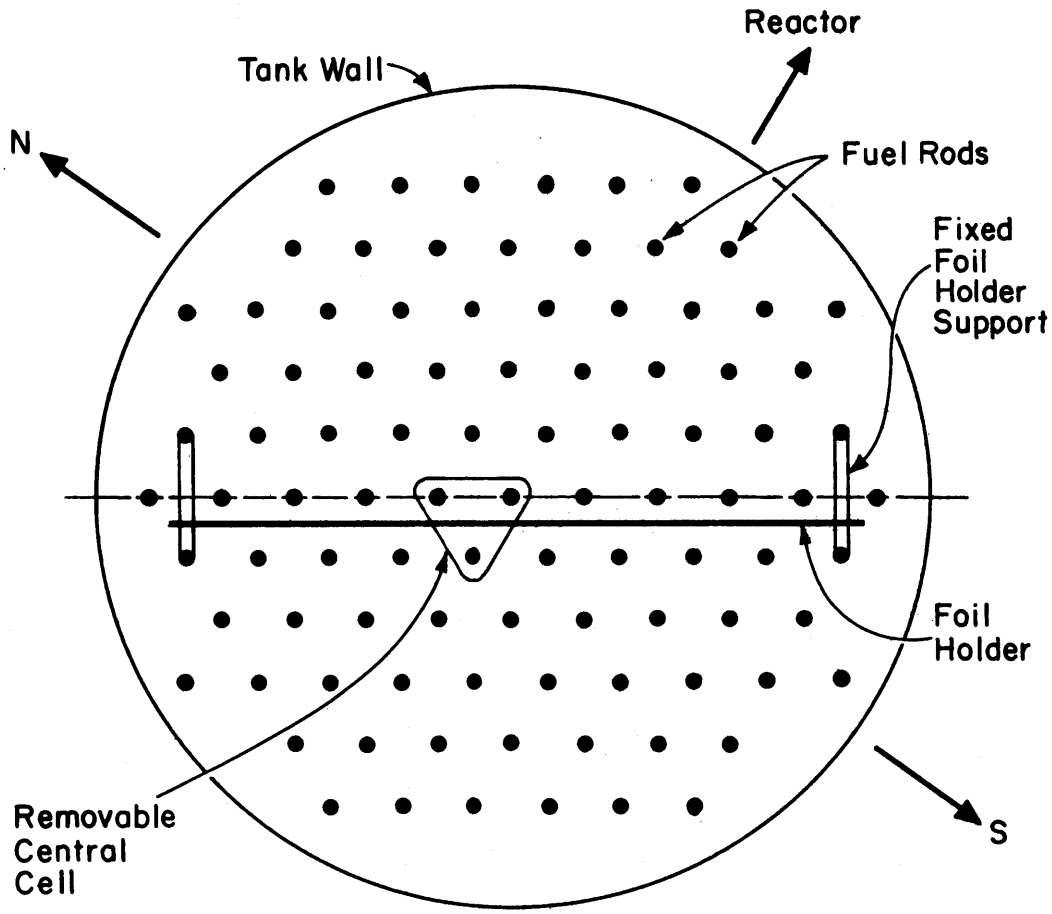

FIG. 7-2 CONFIGURATION OF 4 1/2 INCH SPACING LATTICE

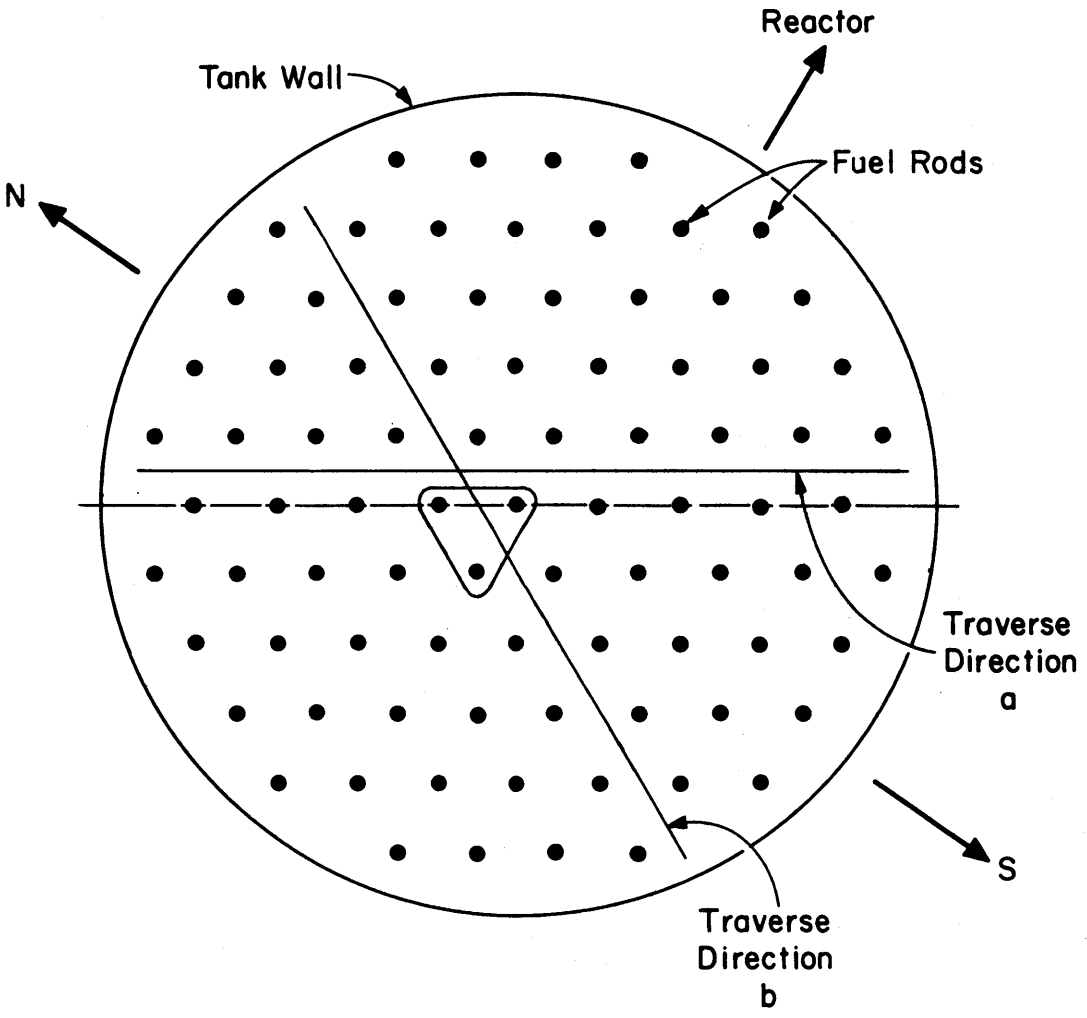

FIG. 7-3 CONFIGURATION OF 5 INCH SPACING LATTICE

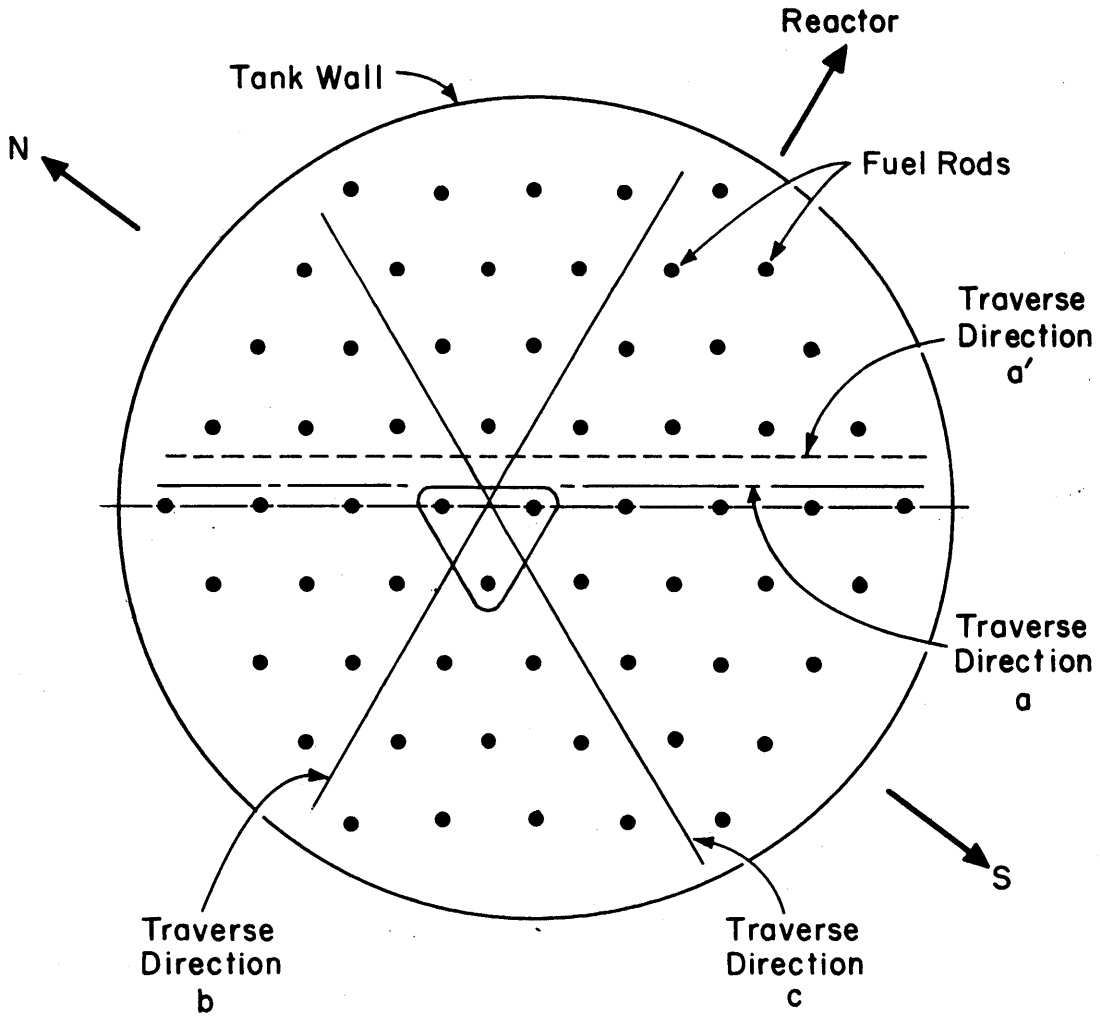

FIG. 7-4 CONFIGURATION OF 5 3/4 INCH SPACING LATTICE

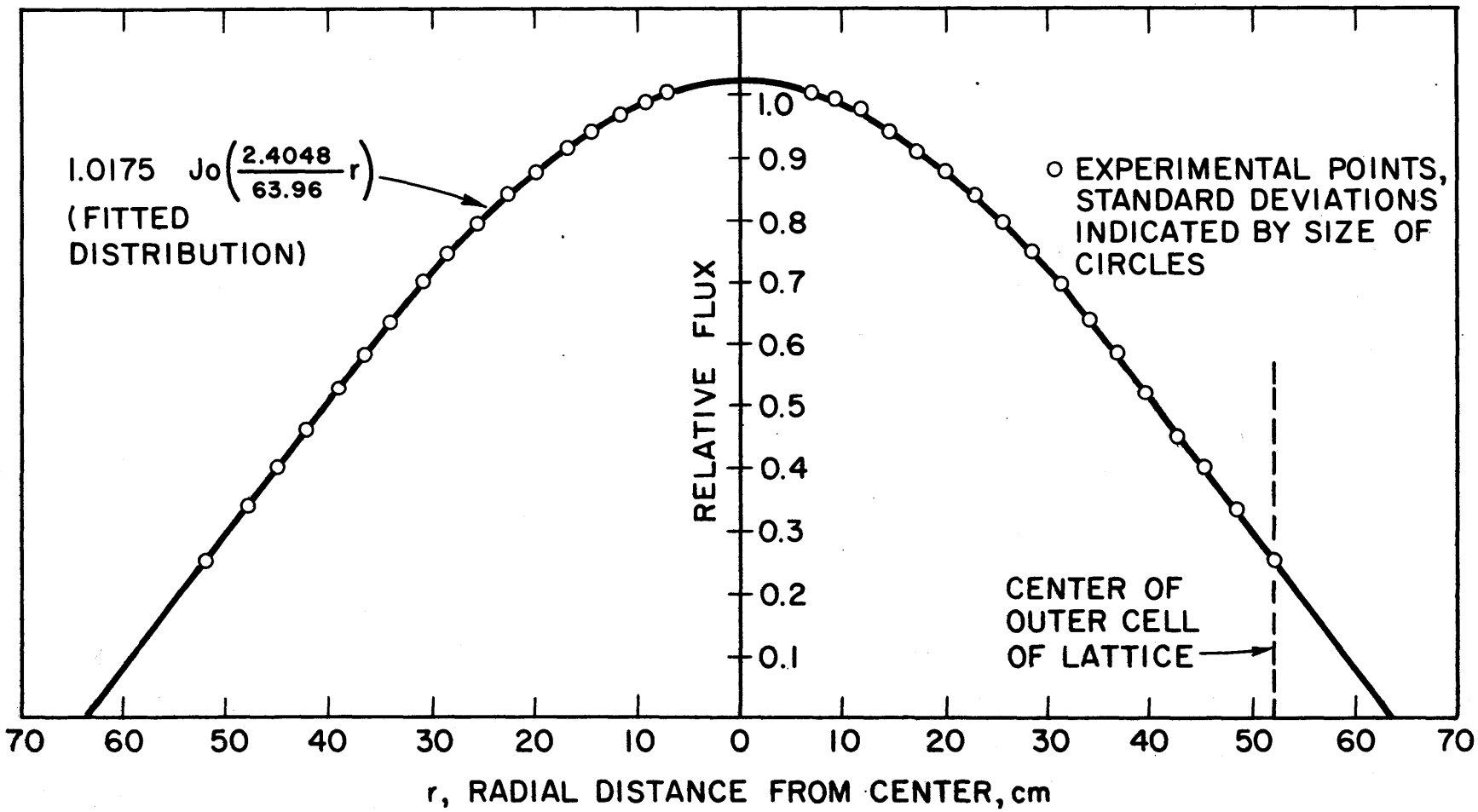

FIG. 7.5 RADIAL FLUX DISTRIBUTION IN $4\frac{1}{2}$ INCH SPACING LATTICE

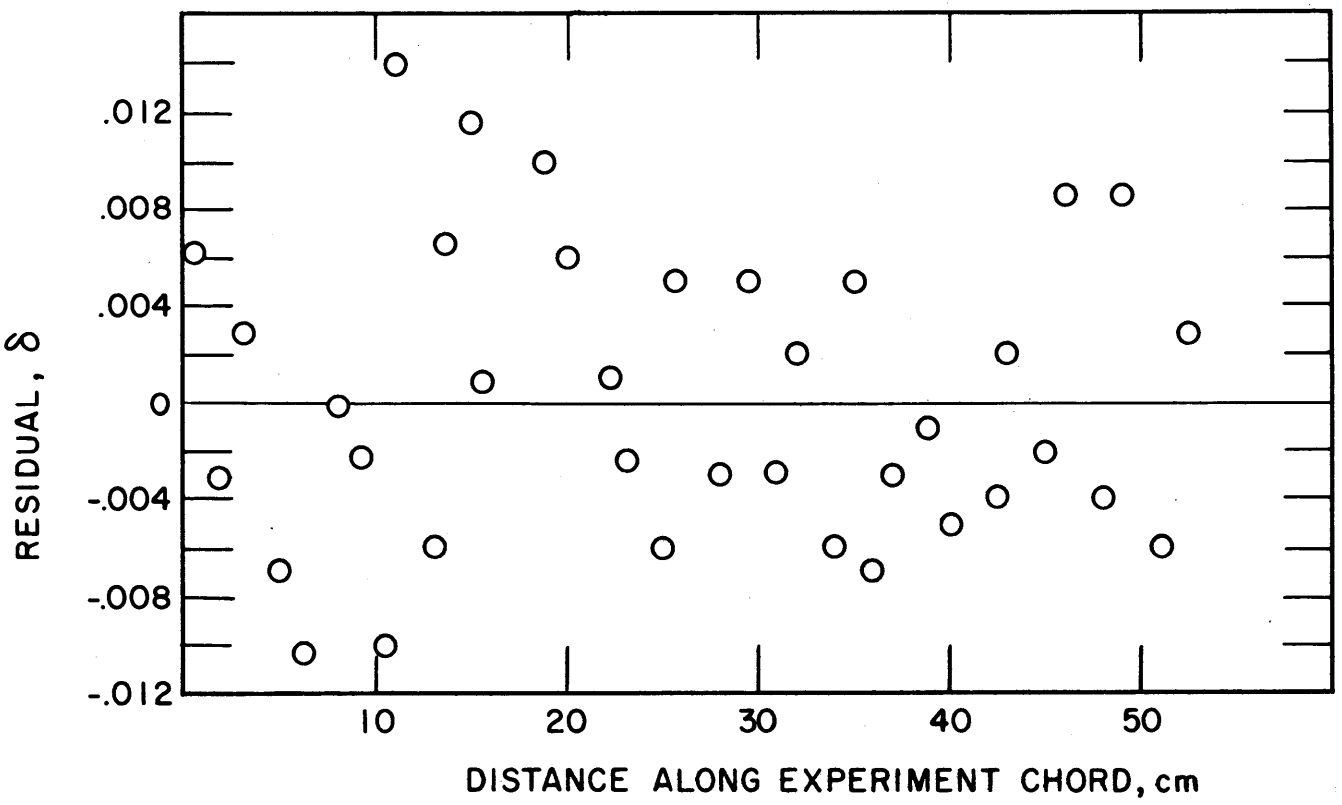

FIG. 7.6 CHORDAL DISTRIBUTION OF RESIDUALS. EXPERIMENTAL FLUX NORMALIZED TO 1.0 AT CHORD CENTER

As was discussed in Chapter VI, a point of concern during the design of the facility was the possibility of the scattering back into the lattices of fast leakage neutrons. Although this phenomenon would lead to a distortion of the J_o distribution, and would probably be detected by the methods discussed above, a more sensitive test can be made by examining the gold-cadmium ratio as a function of radial, or chordal, position. Figure 7.7 shows the result of such an experiment. The cadmium ratios that will be reported in this chapter are defined as

$$R_{cd} = \frac{\text{Activity of bare gold foil}}{\text{Activity of Cd-covered gold foil}} \qquad (7.1)$$

No attempt was made to reduce the cadmium ratios to values at infinite dilution since they were used only relatively, as a spectral indicator. The average value of the cadmium ratios of all the points shown in Fig. 7.7, except the outermost, is 10.5 and the standard deviation of this value is 0.10. Since the cadmium ratio of the outer point, 10.8, is three standard deviations from the average, a statistically significant shift in the cadmium ratio may be indicated. Nevertheless, the effect is small, since a 3 per cent shift in the cadmium ratio indicates a change in the epicadmium flux of about 0.3 per cent.

Correcting for the Cell Distribution

When the radial buckling is determined from an experimental flux distribution, the cell (or microscopic) flux distribution is accounted for in the following way. First, the J_o code is used to obtain a first estimate of the over-all flux distribution. Correction factors are then estimated, by which the experimental points can be corrected for the microscopic effect. This may be done in two ways; either a separate experiment can be performed to analyze the intracell flux distribution, or the residuals (obtained in the fit made to the over-all distribution) can be analyzed. The J_o code is then applied again, to get a corrected value for the buckling. Each method of

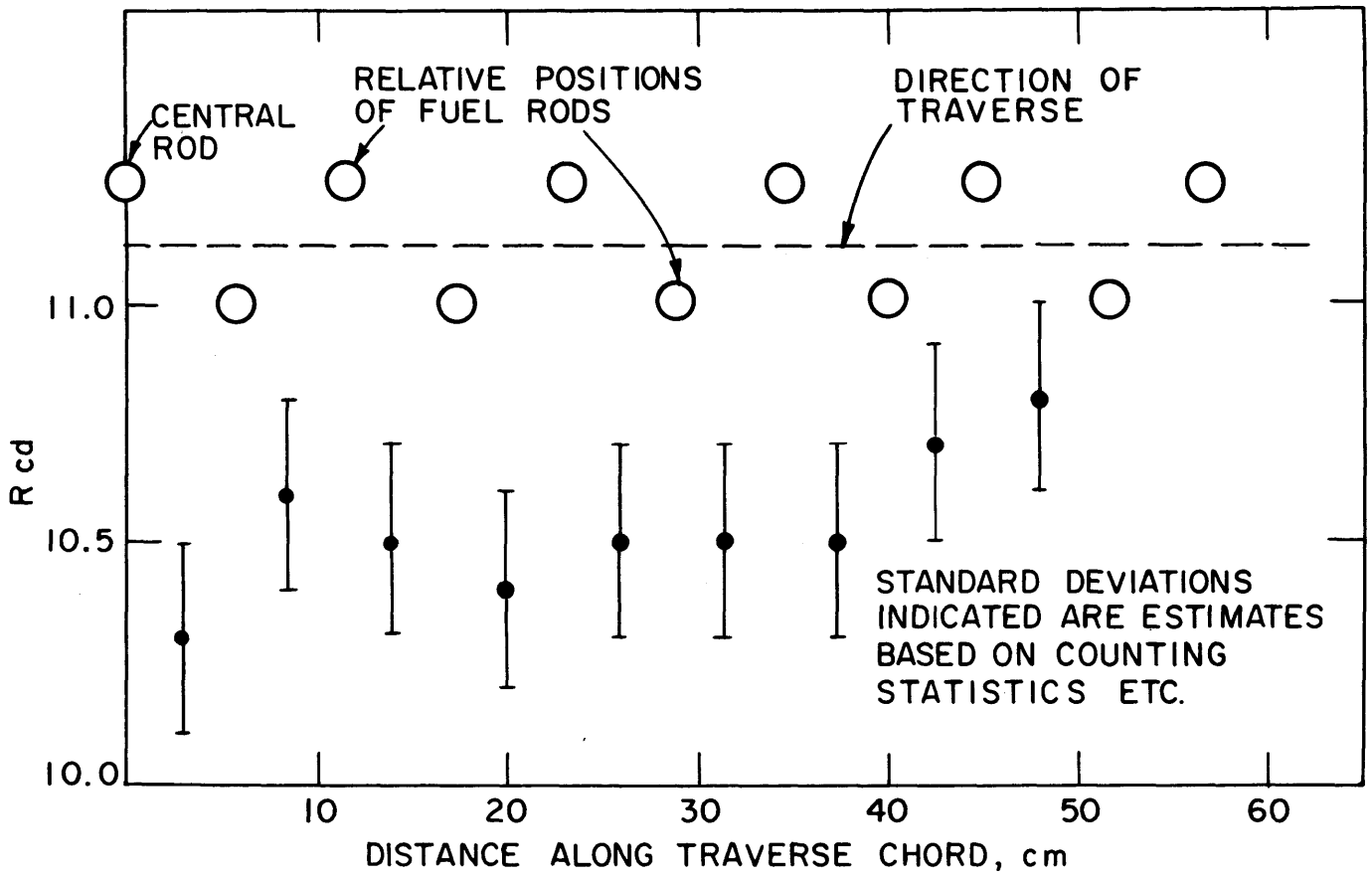

FIG. 7.7 CADMIUM RATIO AS A FUNCTION OF CHORDAL POSITION IN 4 1/2 INCH LATTICE

determining the correction factors will be exemplified by a particular example. These examples will also serve to point out further details of the radial flux distribution.

In the 4-1/2-inch lattice, a separate experiment was used to obtain the correction factors. In order to obtain accurate radial traverses, the foils for the macroscopic measurement were placed along a line midway between the two rows of fuel (see Fig. 7.2). Three points were taken in each cell. These points were used to obtain the first estimate of the over-all flux distribution. A separate experiment was then performed in the central cell of the lattice to measure the cell distribution in the direction used for the macroscopic traverse. A matched set of eight 1/8-inch diameter, 0.005-inch thick gold foils were used and located as shown in Fig. 7.8. Figure 7.8 also shows the measured microscopic distribution. Each point has been corrected for the macroscopic distribution determined in the first experiment and represents the average of two experimental points, one on either side of the cell center. In this case, the microscopic distribution is flat within the accuracy of the experiment, so that no correction factors need be applied to the measured macroscopic flux. A microscopic effect would appear as a periodicity in the macroscopic distribution and in the residuals. No such periodicity is evident, for example, in the uncorrected distribution shown in Fig. 7.5. The neutron flux terrain through which our traverse passes is undoubtedly quite variable, owing to depression of the flux around fuel rods. The position of the traverse is "well chosen", however, in that it follows a path that is relatively level.

For reasons that will be discussed in the next section, the traverses taken in the 5-inch, and 5-3/4-inch lattices were made near rows of fuel rods. In these traverses, correction factors for the cell distribution were obtained by examining the residuals obtained in a J_o fit to the over-all distributions. This process is exemplified in Fig. 7.9, where the residuals obtained from a fit to the uncorrected points of Run 41 (computer Run 4101) are plotted. From the distribution of the residuals, it was estimated that a correction factor of

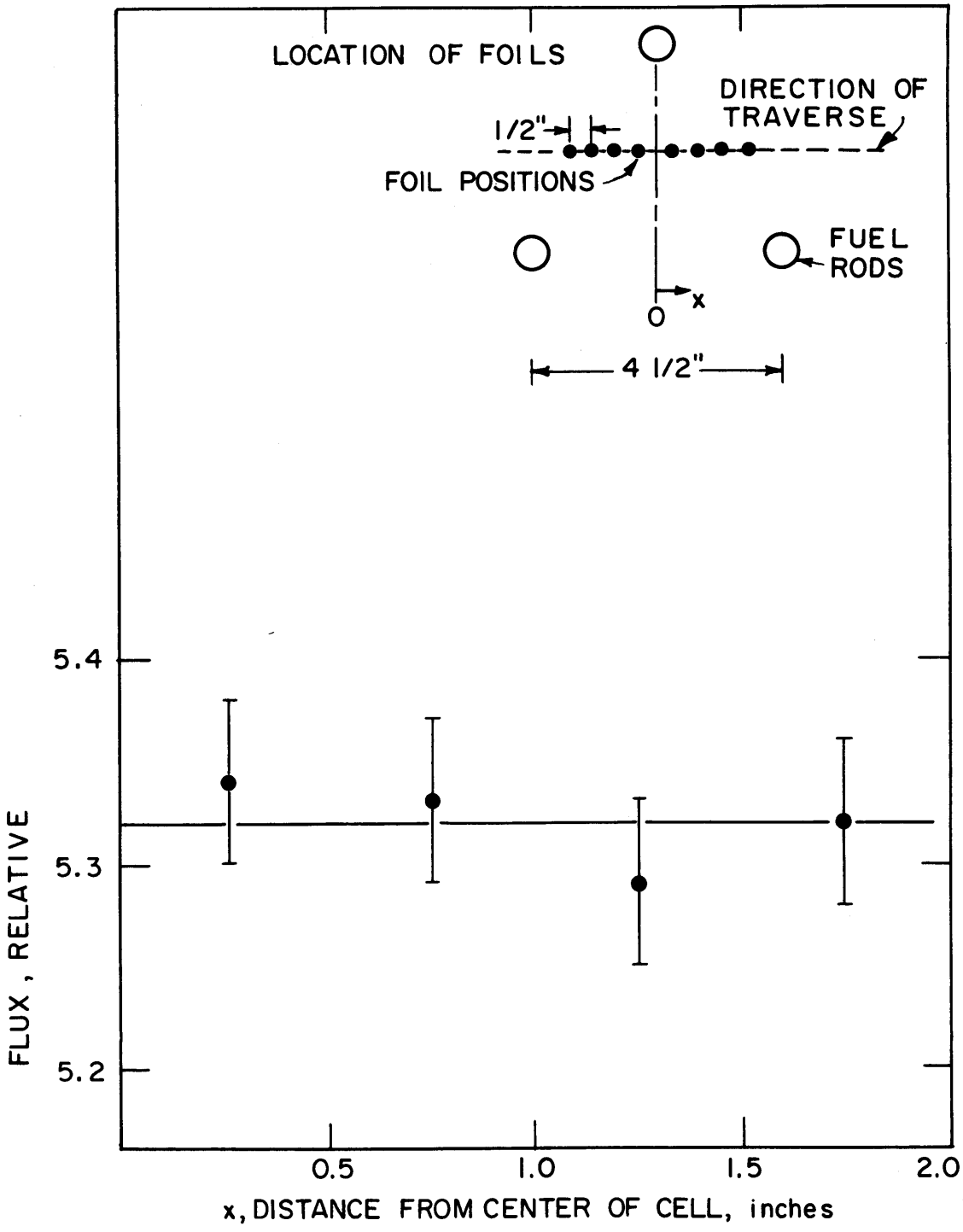

FIG. 7.8 MICROSCOPIC FLUX TRAVERSE IN 4 1/2 INCH-SPACING LATTICE

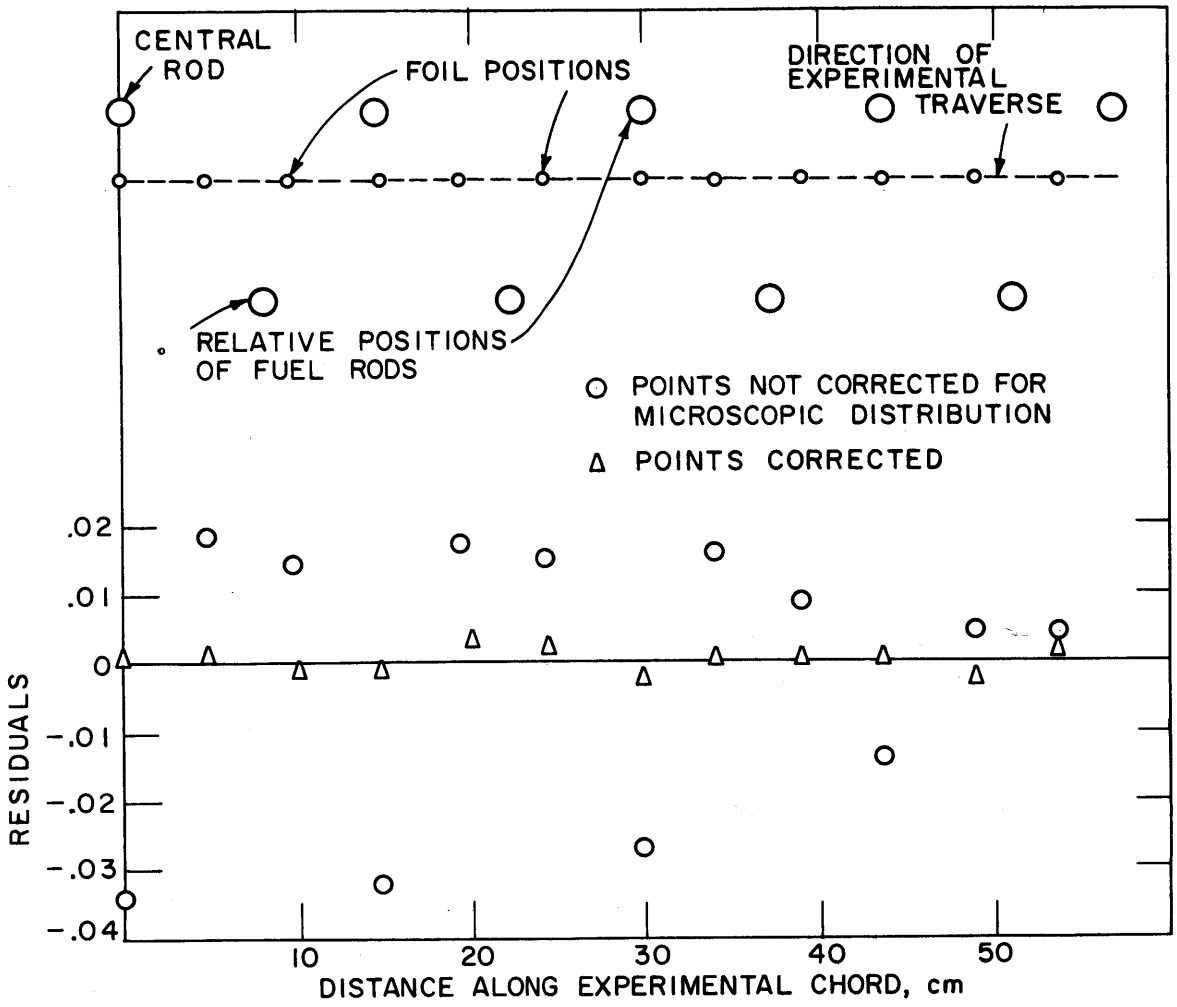

FIG. 7.9 CHORDAL DISTRIBUTION OF RESIDUALS IN 5 3/4 INCH SPACING LATTICE - RUN 41

1.05 should be applied to all points taken near a fuel rod, (i.e., that the value of the flux at points such as (a) in the sketch in Fig. 7.9 should be multiplied by 1.05). The corrected points were then fitted again, by using the J_o code, to obtain a new estimate of the over-all flux distribution and thus of the radial buckling. The Residuals obtained in this analysis are also shown in Fig. 7.9. The periodicity of the residuals has been effectively eliminated by use of the correction factor, 1.05. Hence, the buckling determined in the last J_o analysis is the buckling corrected for the microscopic distribution. If the residuals still show a periodicity after the first-estimated correction factor has been applied, the process can, of course, be repeated until the proper correction factor (or factors) has been found.

Two additional remarks should be made with respect to the residuals for the uncorrected traverse shown in Fig. 7.9. First, it should be observed that the residuals tend to diminish as the chordal distance increases. This is a phenomenon related to the macroscopic-microscopic separability, and will be discussed in the next section. Second, it might be suggested that a trend is indicated by the fact that the inner of each of the pairs of positive residuals is always greater than the outer. This trend is not corroborated by other runs, however, and is not considered to be real.

The Interdependence of Analytical Conditions

As is discussed in Chapters V and VI, a common and useful method of looking for edge effects in fitting a radial distribution is to compare fitted values of the buckling obtained with successively fewer points used in the fit. Such refitting was performed wherever the J_o code was used. The changes in the resulting values of the fitted radial buckling depended on the other analytical conditions, i.e., on whether the traverse was corrected for the cell distribution and on the point weighting used. The interdependence of the various analytical conditions is displayed in Table 7.1. The change in the radial buckling as points are dropped is tabulated for various analytical conditions. Again, experimental Run 41 is considered.

TABLE 7.1 FITTED RADIAL BUCKLING FROM RUN 41 UNDER VARIOUS ANALYTICAL CONDITIONS

Run	Corrected for Micro.?	Weighting Exponent	Points Used in Fit	Radial Buckling, α^2
4101a	No	0	23	14.29 ± .23
b			21	14.31 ± .25
c			19	14.34 ± .28
4102a	No	-2	23	14.22 ± .18
b			21	14.32 ± .21
c			19	14.48 ± .25
4103a	Yes	0	23	14.30 ± .06
b			21	14.31 ± .06
c			19	14.30 ± .06
4104a	Yes	-2	23	14.29 ± .09
b			21	14.34 ± .08
c			19	14.31 ± .08

Several characteristics of the fitting process are evident in the table. First, it can be seen (by comparing Runs 4101a and 4103a) that correcting for the microscopic distribution does not effect the resultant buckling significantly although the probable error is reduced. The probable errors quoted are those calculated by the code and are determined by the scatter in the experimental data. Other experiments indicated that the probable errors determined by the code are somewhat larger than those suggested by the reproducibility of the measurements.

If a weighting exponent of -2 is used, i.e., if the points are weighted inversely proportional to the square of the magnitude of the flux, a slight difference in the resulting value of α^2 is apparent (compare Runs 4102a and 4104a). The effect of dropping points can best be seen where the outer points are emphasized; that is, when a weighting exponent of -2 is used. Thus, it can be noted that a significant shift in the measured value of α^2 occurs between Runs 4102a, b,

and c, where corrections are not made for the microscopic distribution. However, when the microscopic flux is corrected for, as in Run 4104, no significant change in the fitted value of α^2 is observed as points are dropped in the fitting process. The reason for the effect is obvious; as points are dropped, and no microscopic correction has been applied, the relative number of points whose residuals are negative (or positive) changes. Of greatest importance are the points at the edge that remain in the fitting process. As the last three points of Run 41 are dropped in the fitting process, the low experimental point, third from the end, would tend to predominate (see Fig. 7.9). Thus, in Table 7.1, we see that the buckling increases in Runs 4102a, b, and c.

It is of interest to examine the higher harmonic contribution to the radial flux distribution as a function of height in the lattice. Such a study was made in the 5-3/4-inch lattice. The experimental distributions, measured at various heights, were fitted to a distribution given by Equation (6.2), using values of R′ determined by the J_o code. The results of the analysis are shown in Table 7.2.

TABLE 7.2 RADIAL HARMONIC ANALYSIS

Height of Traverse	A_1	A_2	A_3
127 cm	1.027	0.002	-0.005
103 cm	1.021	0.0006	-0.002
61 cm	1.029	0.006	-0.016

Even at a height of 61 cm, the higher harmonic contribution is very small. The contributions at 103 cm and 127 cm are negligible.

Two other aspects of the radial flux distribution were studied, in order to determine whether radial bucklings measured at one particular location in the lattice were characteristic of the lattice as a whole. The first was the azimuthal dependence of the radial distribution. Table 7.3 summarizes three runs made in the 5-3/4-inch

spacing lattice in the three directions indicated in Fig. 7.4.

TABLE 7.3 AZIMUTHAL DEPENDENCE OF RADIAL FLUX DISTRIBUTION

Run	Traverse Direction	Fitted Radial Buckling
40	a	$14.19 \pm .20\ m^{-2}$
41	b	$14.29 \pm .23$
42	c	$14.26 \pm .19$

For this comparison, all points were used in the fitting processes, and given unit weight. No correction was made for the microscopic distribution (for reasons discussed with reference to Table 7.1), a fact which explains the large quoted errors. The three bucklings are all within $\pm\ 0.05\ m^{-2}$ of the average, $14.24\ m^{-2}$, so that there are no significant differences among them.

The other aspect of the radial distribution, which is important in terms of the generality of the measured buckling, is its axial variation. Three runs summarized in Table 7.4 were made to study this effect.

TABLE 7.4 AXIAL DEPENDENCE OF RADIAL FLUX DISTRIBUTION

Run	Height of Traverse	Extrapolated Radius	Fitted Radial Buckling, α^2
60	61 cm	64.0 cm	$14.10 \pm .15\ m^{-2}$
46	103 cm	64.0 cm	$14.14 \pm .11\ m^{-2}$
47	124 cm	64.7 cm	$13.83 \pm .24\ m^{-2}$

All distributions were taken in direction a′ shown in Fig. 7.4. There is certainly no significant difference between the values derived in Runs 60 and 46; however, the difference between these values and that derived in Run 47 is probably meaningful. Two reasons for the

difference are possible. It was observed during the experiments that the radius of the tank slightly increased (about 1/4 inch) with height near the tank top; it can be seen from Table 7.4 that the difference in radius corresponding to the variation in radial buckling is only 0.7 cm. Another possible explanation of the variation in α^2 is the presence of neutrons scattered back from the aluminum above the lattice. Because of the possible presence of these effects, considerable care was taken in fitting the axial distributions. Successively fewer points were used in the axial fit, to assure that points in a region of changing relaxation length (corresponding to a region of changing radial buckling) were not used (see section 7.3.3 below).

7.3.2 Radial Spatial Separability

An examination of the fine structure of the radial flux distribution was prompted by two considerations. When it was decided to take more than one point per cell on the radial traverses, it was recognized that the over-all distribution would have to be corrected for the cell distribution if an accurate buckling was to be obtained (see section 7.3.1). Also, as is discussed in section 4.2, the question of the separability of the microscopic and macroscopic distributions was of interest in itself.

Although results of microscopic investigations, such as those shown in Fig. 7.8, are to be welcomed in terms of the accurate measurement of the buckling, they are hardly adequate in terms of observing a possible interaction between the microscopic and macroscopic flux distributions. In the 5-inch and 5-3/4-inch lattices, traverses were made near rows of fuel rods in order to observe both the over-all distribution and the fine structure. The distribution of residuals shown in Fig. 7.9 is typical of such experiments. The separability effect was studied in the following way. First, the experimental points were corrected for the fitted J_o flux distribution. Then, for each cell, a quantity related to the difference between the flux near the fuel rods and the flux in the moderator was determined. This quantity, Δ, can be expressed as

$$\Delta = \frac{\bar{\delta}_f - \delta_m}{\phi_o} \qquad (7.2)$$

where δ_f is the residual (difference between the experimental and fitted flux) at a point near a fuel rod, e.g., at point (a) in Fig. 7.9, and $\bar{\delta}_m$ is the average of the residuals at adjacent points in the moderator, e.g., at points (b) and (c) in Fig. 7.9. ϕ_o is the flux at the center of the lattice and acts as a normalization factor. If the cell flux distribution is uneffected by the macroscopic lattice distribution, and is thus unaltered across the lattice, the quantity, Δ, should, of course, remain constant throughout the system. If, on the other hand, the microscopic and macroscopic flux distributions are not separable, Δ should vary as a function of position. Figure 7.10 is a plot of Δ as a function of radial position. Each point is an average of six measurements; the six radial directions possible for experimental plots are determined by the first ring of six rods around the central rod of the lattice (see Fig. 7.4). The standard deviations shown are determined from the scatter of the data in the averaging process. The figure clearly indicates that the fluxes are non-separable. The radial variation in the microscopic distribution is apparent in Fig. 7.9 if the uncorrected residuals are examined. It can also be observed in Fig. 7.11, which is a plot of the radial distribution of the cadmium ratio. That the shift in cadmium ratio evident in that figure is not a macroscopic effect, is supported by the plot of Fig. 7.7. In the latter, where microscopic effects are not observable, the trend in the cadmium ratio at the tank edge is upward if anything. In terms of the macroscopic distribution, the effect is small; Fig. 7.10 indicates a shift of about 2 per cent in the microscopic contribution between the central and the outer cell. However, the interest in the effect stems partly from the prevalence of the tacit assumption of the separability of the macroscopic and the microscopic fluxes in the diffusion theory approach to lattice analysis, as discussed in Chapter IV. It is not within the scope of this report to discuss in detail the effect of a result such as that shown

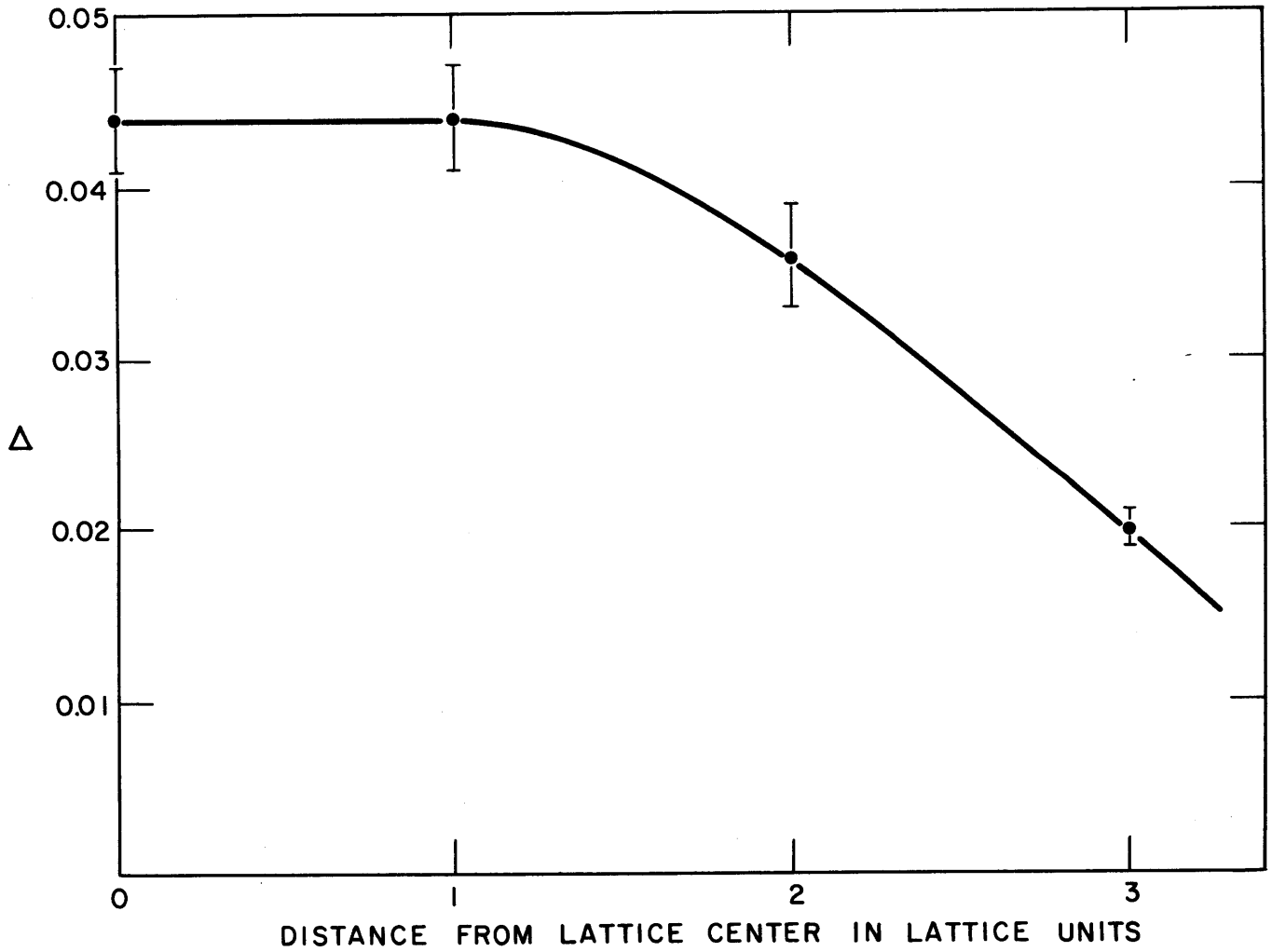

FIG. 7.10 DIFFERENCE BETWEEN FLUX NEAR FUEL ROD AND FLUX IN MODERATOR CORRECTED FOR MACROSCOPIC DISTRIBUTION $5\frac{3}{4}$ INCH SPACING

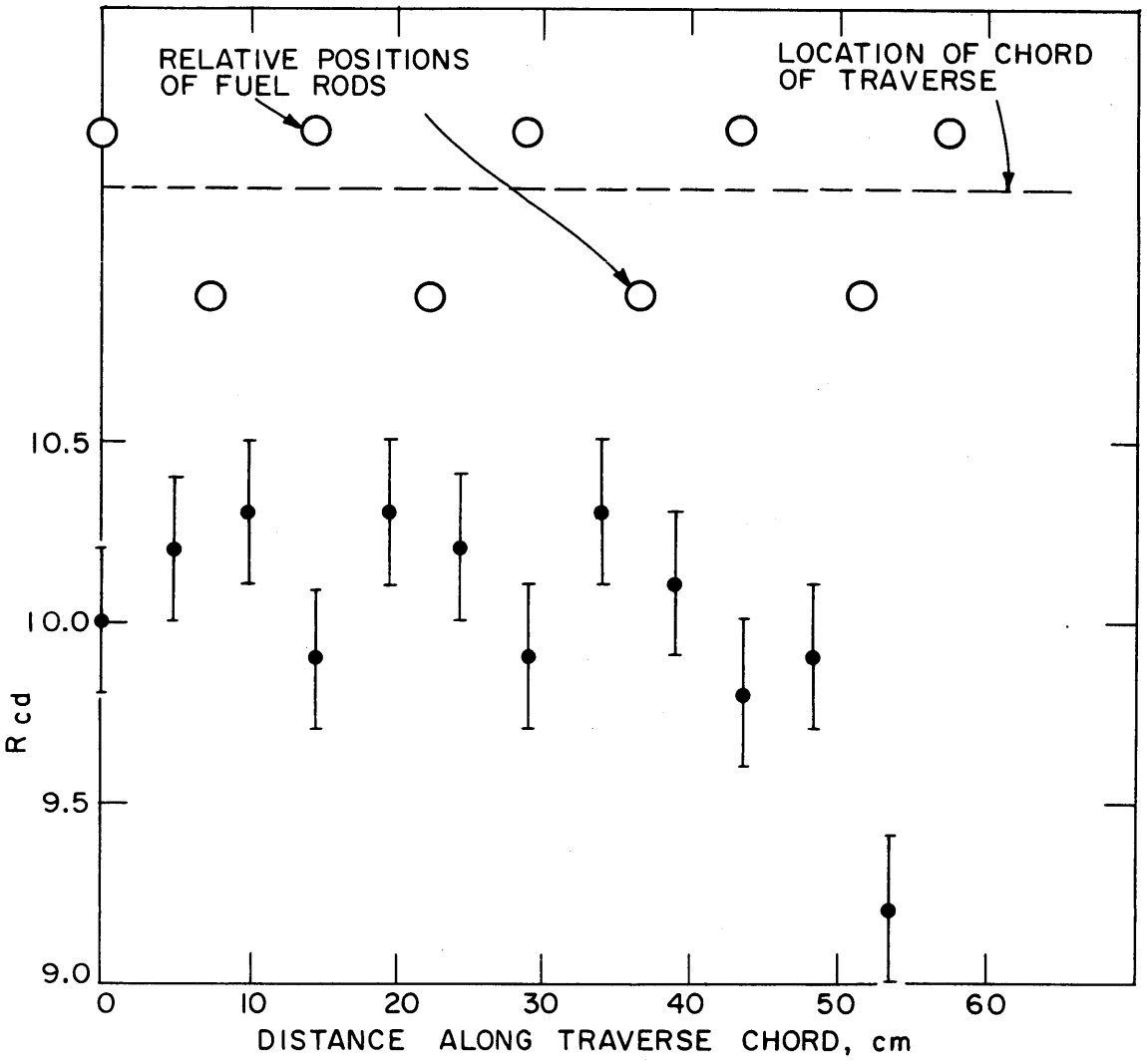

FIG. 7.11 CADMIUM RATIO AS A FUNCTION OF DISTANCE ALONG TRAVERSE CHORD IN 5 3/4 INCH LATTICE

in Fig. 7.10 on the measured microscopic properties of lattices, although some comments will be made in this regard in Chapter VIII.

7.3.3 Axial Flux Distribution

As was the case with the radial distribution, several aspects of the axial distribution were studied in the three lattices. The purpose of these experiments was to establish the region of validity of Equation (6.4) and to use experimental points in that region to determine γ^2, the axial buckling.

As is discussed in section 6.4.2, two methods were used to establish the extent of Region III of Fig. 6.7. The first involved the study of the spectrum as a function of axial position. Axial traverses made with bare and cadmium-covered gold and cadmium-covered uranium foils are shown in Fig. 7.12. The line plotted in the same figure corresponds to a sinh function fitted to the bare gold data. The "uranium" foils used were an alloy of natural uranium in aluminum. The activity counted was that due to resonance absorption in U^{238}; techniques described by A. Weitzberg (W15) were used in the counting process. It can be seen that the three sets of data are in agreement, at least between 40 cm and 120 cm. A similar method would be to examine the cadmium ratio as a function of height. This type of measurement was made in the 5-3/4-inch lattice to study in detail the lower end of the lattice (Regions I, II, and III). The results of this experiment are shown in Fig. 7.13. It should be noted that no substantial region corresponding to Region II of Fig. 6.7 is evident. The constancy of the cadmium ratio between 40 cm and 120 cm attests to the energy-space separability in that region. A similar (though less precise) experiment performed in the 5-inch lattice shows the same behavior at the bottom of the lattice and a decrease in the cadmium ratio above 140 cm.

The second method of establishing the region of validity of Equation (6.4) was refitting the data points of a traverse with successively fewer points. Figure 7.14 exemplifies this technique when applied to the upper region of the lattice. As points are dropped from

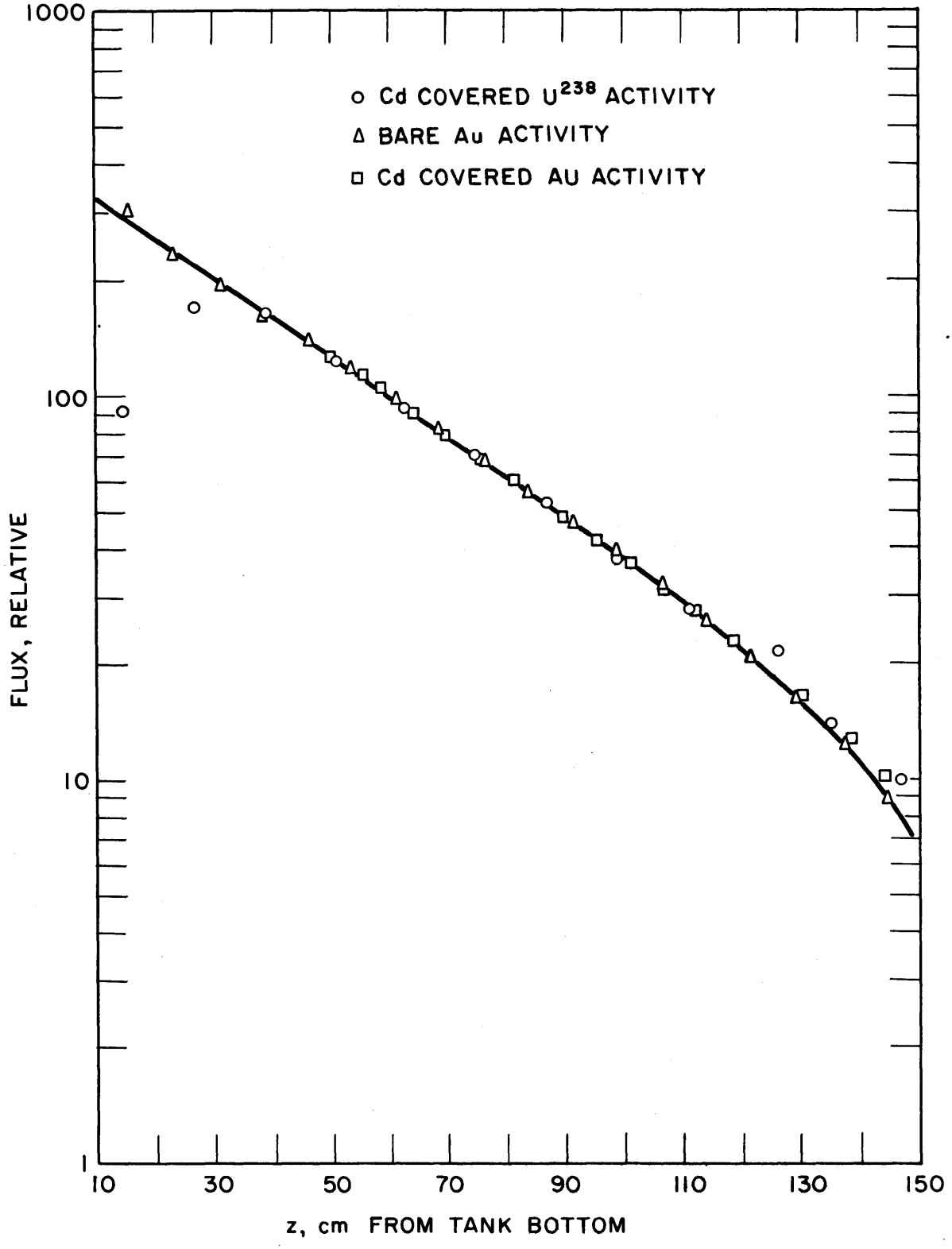

FIG. 7.12 COMPARISON OF AXIAL FLUX DISTRIBUTIONS IN $4\frac{1}{2}$" SPACING LATTICE

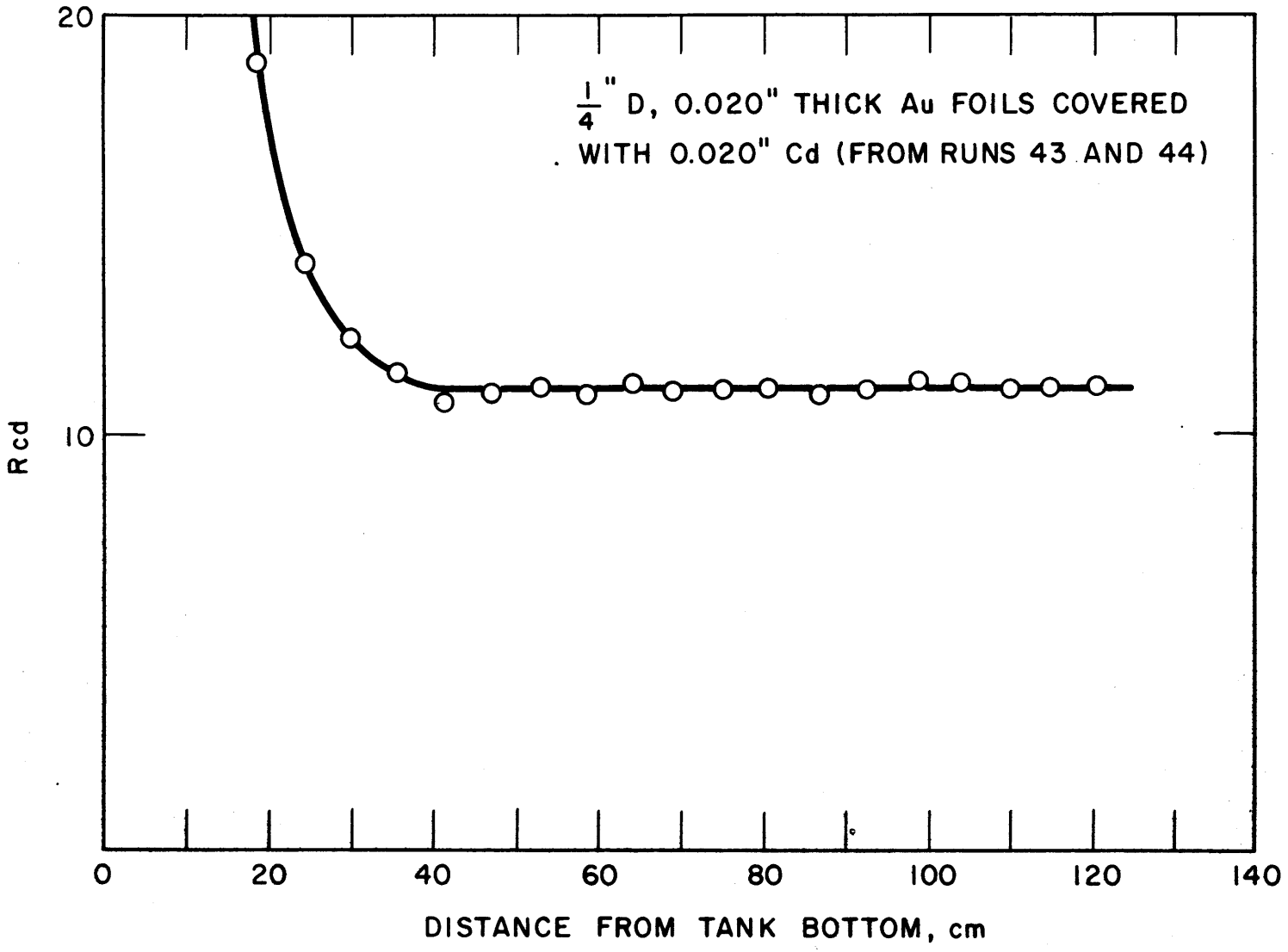

FIG. 7.13 CADMIUM RATIO IN $5\frac{3}{4}$" SPACING LATTICE AS A FUNCTION OF HEIGHT FROM TANK BOTTOM

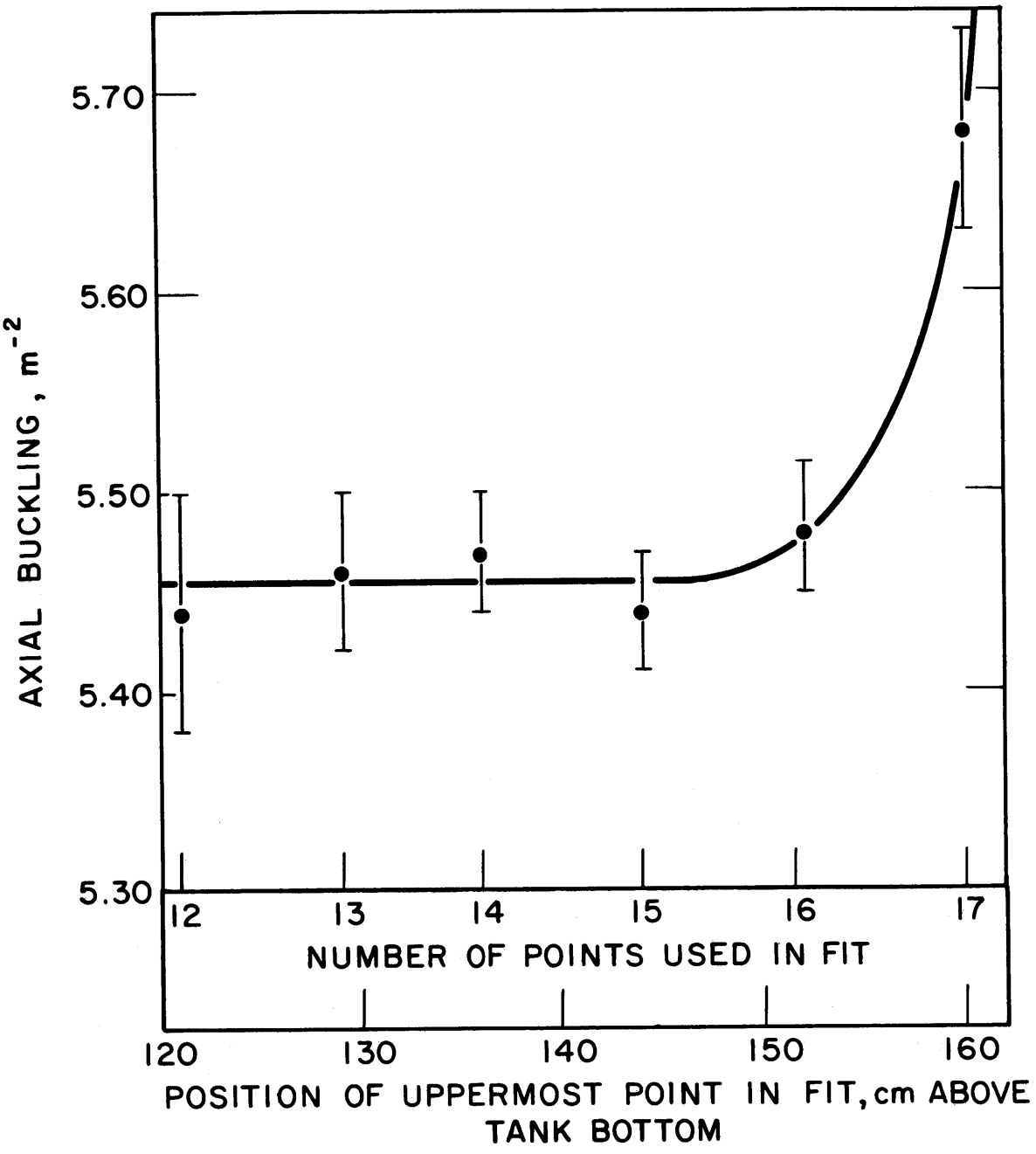

FIG. 7.14 FITTED AXIAL BUCKLING AS A FUNCTION OF THE NUMBER OF POINTS USED IN THE FIT. RUN NO. 21 - $4\frac{1}{2}$ INCH SPACING LATTICE

the fitting process, the fitted value of γ^2 rapidly approaches the asymptotic value - in this case, of 5.46 m^{-2}. The point at which the asymptotic value is attained indicated the point below which the distribution can be considered a sinh function. The results of the particular run shown in Fig. 7.14 indicates that points below 145 cm are acceptable. It is also of interest to examine the variation in the probable error of the fitted buckling as a function of the number of points used in the fit. The first three points at the left side of Fig. 7.14 show the expected trend of decreasing error with increasing number of points used in the fit. This trend is not continued when more points are used. This result also indicates that the upper points are not in agreement with the fitted curve.

By using the two methods discussed above - of examining the spectrum and successively dropping points - the valid points of each run were determined. By collecting evidence from all the runs, there was established a vertical span in the tank corresponding to Region III of Fig. 6.7. This region extends at least from 40 cm from the tank bottom to about 130 cm.

The other question of analytical importance was that of the correct extrapolated height to use in each lattice. Again, this problem was looked at in two ways. One method was to fit a traverse with various values of the extrapolated height, h', and to examine the error in the fitted value of γ^2 as a function of h'. An example of such an analysis is shown in Fig. 7.15, where the fitted values of γ^2 and the probable errors are plotted as a function of h'. Such an analysis indicates clearly the "best" value of γ^2 and h' for a particular run. The other method used to choose between values of the extrapolated height was to examine the distribution of residuals with various trial values of h'. When the correct value of h' is used, the residuals should be randomly distributed (plus and minus) over the length of the traverse. A value of h' that is too large would produce a bunching of negative residuals near the top of the tank and create a preponderance of positive residuals elsewhere. Similarly, a guessed value of h' that is too small would

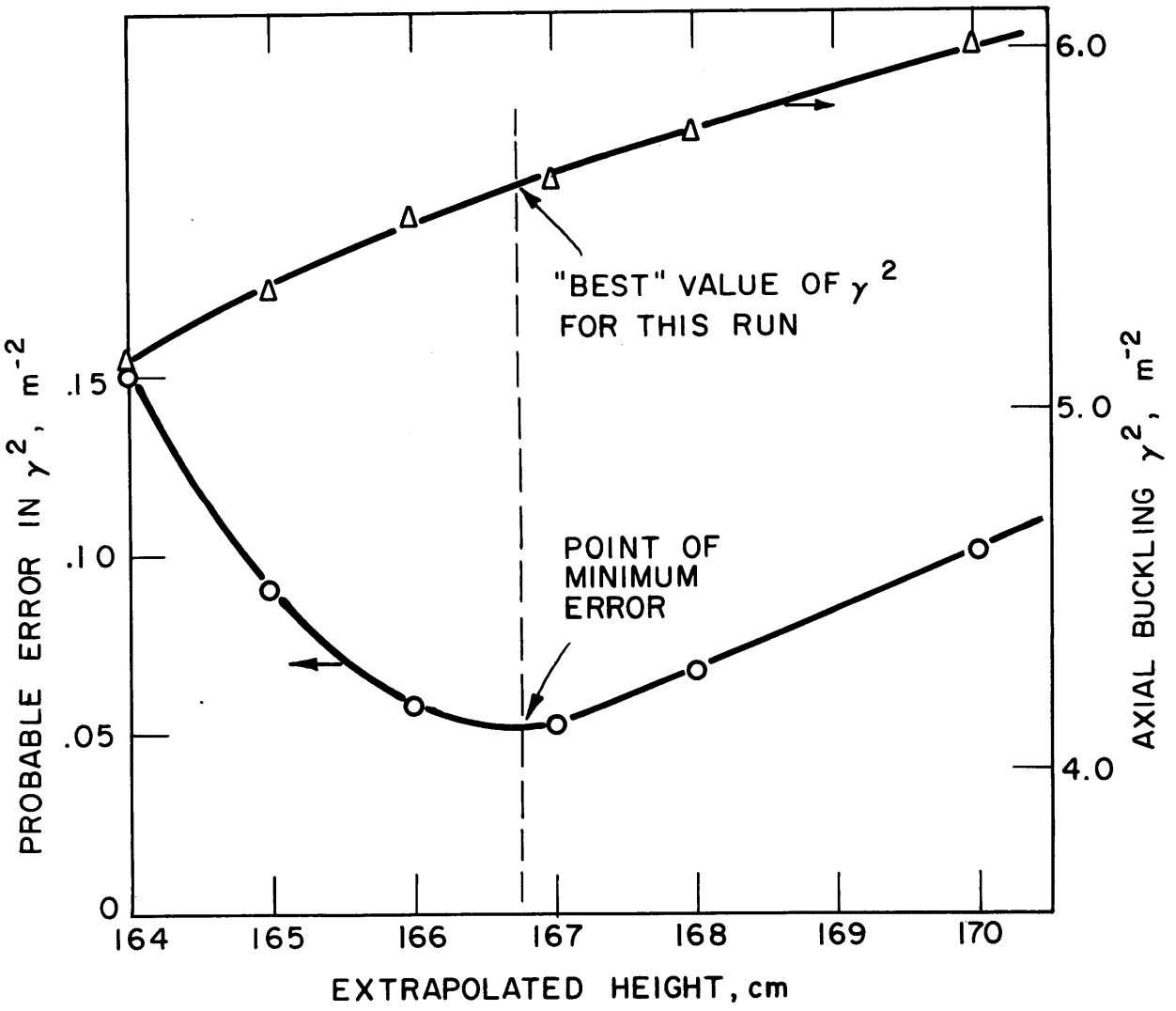

FIG. 7.15 VARIATION OF THE FITTED AXIAL BUCKLING AND ITS PROBABLE ERROR WITH EXTRAPOLATED HEIGHT - RUN 29

also be expected to produce a nonrandom distribution of residuals. Figure 7.16 shows the basis for such an analysis for the same run used in Fig. 7.15. It can be seen that with an h′ of 164 cm, the residuals near the center of the tank are almost all negative and, with an h′ of 170 cm, they are all positive. However, with h′ = 167 cm, the residuals are randomly distributed. These analyses were applied to each run and the most consistent value of h′ determined for each lattice. The axial bucklings reported in the next section were those corresponding to that value of the extrapolated height.

7.4 MATERIAL BUCKLING MEASUREMENTS

7.4.1 Experimental Results

The analytical techniques having been described and exemplified in detail above, this section presents the results of the measurements of the axial and radial bucklings and, thus, of the material bucklings.

4-1/4-inch Spacing Lattice

Table 7.5 summarizes the radial buckling measurements.

TABLE 7.5 MEASURED RADIAL BUCKLING, α^2, OF 4-1/2-INCH SPACING LATTICE

Run	α^2	Remarks
20	14.14 m^{-2}	1/4-inch bare Au foils
23	14.04 m^{-2}	1/2-inch foils
25	14.23 m^{-2}	Cd-covered 1/2-inch foils
26	14.16 m^{-2}	Duplicates the conditions of Run 20
50	14.10 m^{-2}	Used 10 dilute U foils, Cd-covered
Average	14.11 ± .06 m^{-2}	

The average value was obtained from Runs 20, 23 and 26. Runs 25

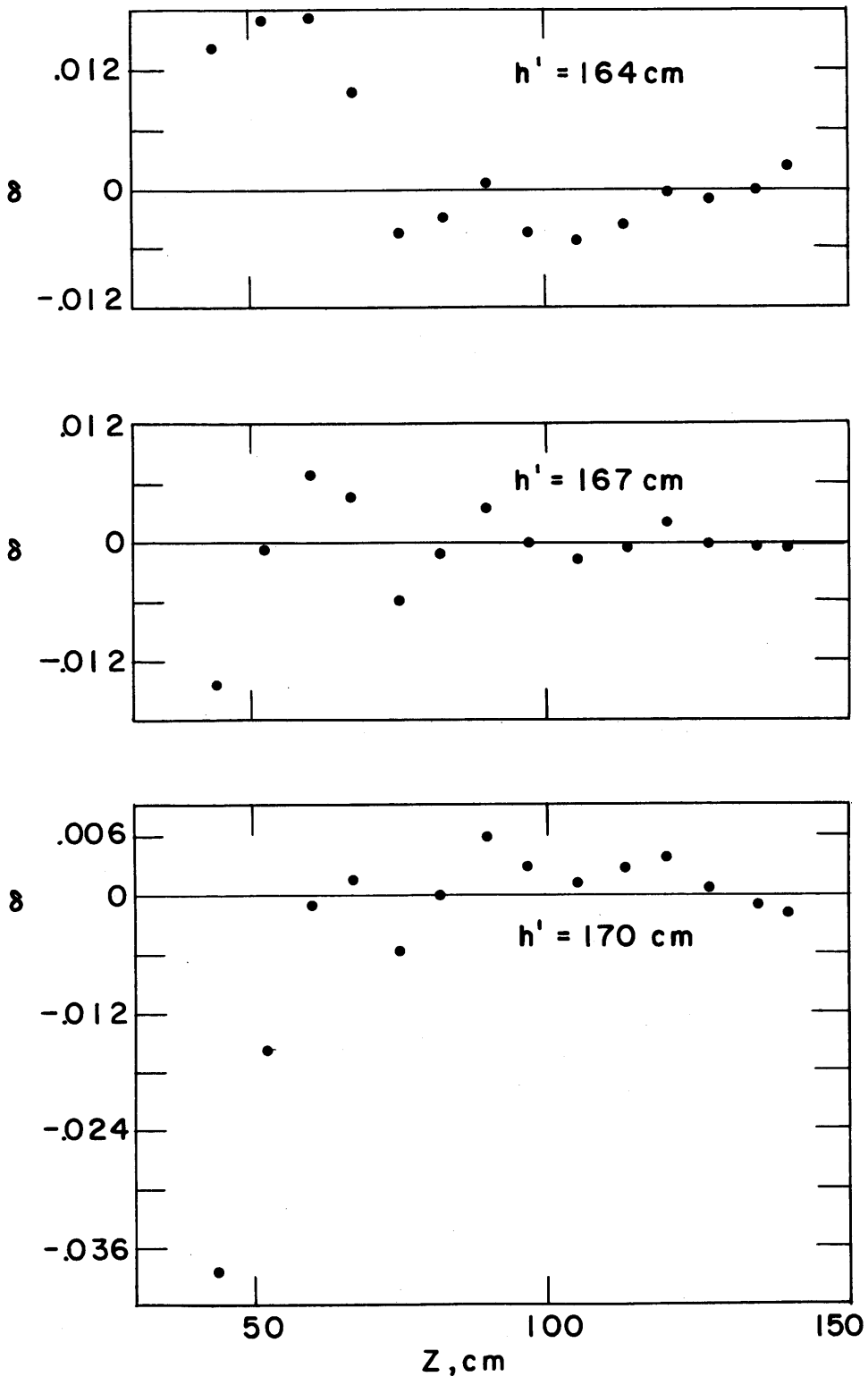

FIG. 7.16 AXIAL DISTRIBUTION OF RESIDUALS WITH THREE DIFFERENT VALUES OF THE EXTRAPOLATED HEIGHT. RUN 29 - 4 1/2 INCH LATTICE

and 50 were made to check the energy-space separability of the radial flux distribution. Being made with a relatively small number of cadmium-covered foils, they did not yield as accurate values of the buckling as did the other runs. However, the bucklings from Runs 25 and 50 are included in the table for the sake of comparison. The quoted uncertainty is larger than that which would be derived in the averaging process and is an estimate based on the possibility of systematic as well as random, errors. A small systematic error may derive from the fact that all traverses were taken in the same location, although this possible effect was investigated separately, as discussed in section 7.3.1. The precision of the individual measurements with bare foils is indicated by the excellent agreement between Runs 20 and 26.

The axial buckling measurements are summarized in Table 7.6.

TABLE 7.6 MEASURED AXIAL BUCKLING, γ^2, OF 4-1/2-INCH SPACING LATTICE

Run	γ^2	Remarks
21	5.62 m^{-2}	Traverse at lattice center
22	5.72	Cd-covered 1/4-inch foils
24a	5.70	1/2-inch foils, off center
24b	5.55	1/2-inch foils, off center
29	5.60	Foils attached to central fuel rod
Average of all runs	5.63 ± .08 m^{-2}	

The quoted values of γ^2 are those for the best value of h' of 167 cm. The results represent a variety of experimental approaches; however, again, the standard deviation of the average is higher than the spread of data would require to allow for systematic effects.

5-inch Spacing Lattice

Tables 7.7 and 7.8 summarize the radial and axial bucklings obtained in the 5-inch spacing lattice.

TABLE 7.7 MEASURED RADIAL BUCKLING OF 5-INCH SPACING LATTICE

Run	α^2	Remarks
32	14.05 m^{-2}	In direction a of Fig. 7.3
35	14.21	In direction a of Fig. 7.3, height = 3 feet
37	14.10	In direction b of Fig. 7.3, height = 3-1/2 feet
Average of all runs	14.12 ± .06 m^{-2}	

TABLE 7.8 MEASURED AXIAL BUCKLING OF 5-INCH SPACING LATTICE

Run	γ^2	Remarks
31	5.39 m^{-2}	Measured near edge of lattice
33a	5.53	Foils at surface of central rod
34	5.36	1/2-inch diameter foils
Average of all runs	5.47 ± .08 m^{-2}	

The value of h′ was again 167 cm.

5-3/4-inch Spacing Lattice

TABLE 7.9 MEASURED RADIAL BUCKLING OF 5-3/4-INCH SPACING LATTICE

Run	α^2	Remarks
40	14.19 m^{-2}	Direction a of Fig. 7.4, height = 3 feet
41	14.29	Direction b
42	14.27	Direction c
46	14.13	Direction a′
60	14.10	Height = 2 feet
Average of all runs	14.20 ± .05 m^{-2}	

TABLE 7.10 MEASURED AXIAL BUCKLING OF 5-3/4-INCH SPACING LATTICE

Run	γ^2	Remarks
43	$5.98\ m^{-2}$	Off-center traverse
48	6.00	In-center cell, foils on A1 holder
49	6.08	1/2-inch foils on string holder
Average of all runs	$6.05 \pm .05\ m^{-2}$	

The best value of h′ for this lattice was 168 cm.

The material bucklings of the three lattices are given in Table 7.11, where $B_m^2 = \alpha^2 - \gamma^2$.

TABLE 7.11 MEASURED MATERIAL BUCKLINGS OF 1.010-INCH DIAMETER NATURAL U RODS IN D_2O

D_2O Purity: 99.75 per cent

Lattice Pitch	V_m/V_u	B_m^2
4-1/2 inches	21.0	$8.48 \pm 0.10\ m^{-2}$
5 inches	26.4	$8.65 \pm 0.10\ m^{-2}$
5-3/4 inches	35.6	$8.15 \pm 0.08\ m^{-2}$

Two remarks should be made concerning the probable errors specified in Table 7.11. The first has to do with the general program of experimentation employed. As was indicated in the first sections of this chapter, the investigation of experimental techniques and the exploration of general properties were carried on in the three lattices, concurrent to the measurements of the buckling. Thus, during the measurements, the details of the experimental and analytical techniques were still being perfected. The higher precision of the last buckling measured arises from this feature of the experimental program. The second remark to be made in this regard has to do with the conservatism of the quoted, estimated, probable errors.

If the probable errors are calculated from the standard deviations of the mean values of α^2 and γ^2 used to derive B_m^2, considerably smaller errors would be obtained. For example, the probable error of B_m^2 for the 5-inch spacing lattice would be 0.05 m^{-2}, and that for the 5-3/4-inch spacing lattice would be 0.03 m^{-2}.

The purity of the D_2O moderator was determined by means of mass spectroscopic measurements at the Savannah River Laboratory. At the termination of the experiments, the purity was 99.75 ± .02 mole per cent D_2O. The purity of the D_2O before it was inserted into the system was 99.77 ± .02 percent (S3). If any degradation occurred, it was assumed to take place in the filling process. In any case, correction to a buckling measured at 99.77 per cent, to bring it to a value for 99.75 per cent, is negligible (D3).

7.4.2 Comparison with Other Experimental Results

Lattices of natural uranium rods in D_2O have been studied at a number of laboratories over several years in both critical and exponential experiments. Figure 7.17 presents a compilation of these various experiments and includes the MIT results reported above. The line drawn through the points considers primarily the North American and Savannah River measurements. The Zebra experiments were conducted in a very small assembly and have recently been subjected to considerable revision (I1). Similarly, the Aquilon critical measurements are currently undergoing re-evaluation (C4). The MIT measurements are seen to be in good agreement with the other results reported when the errors of the measurements are taken into account. To the extent that a difference can be said to exist, the current results indicate slightly higher values of the bucklings than do the other measurements. To that extent, the MIT results support the measurements made at Savannah River and at North American Aviation over those from Zebra and Aquilon.

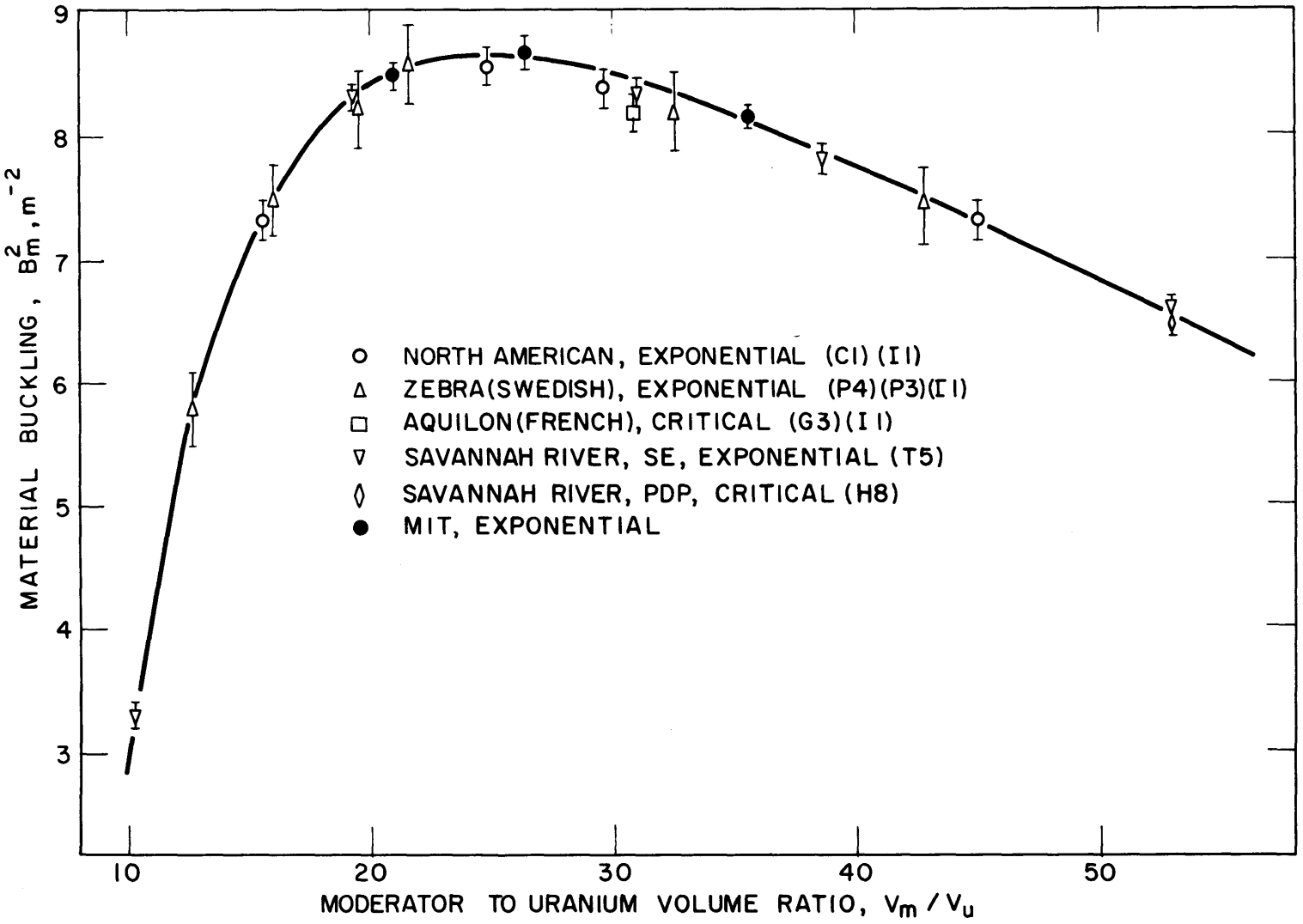

FIG. 7.17 BUCKLINGS OF 1.0 INCH DIAMETER, NATURAL URANIUM RODS IN D_2O – ALL MEASUREMENTS CORRECTED TO 99.75 MOLE % D_2O

CHAPTER VIII
CONCLUSIONS AND SUMMARY

8.1 GENERAL CONCLUSIONS

Several conclusions can be drawn from the work described in this report. These conclusions can be divided into four groups corresponding to four aspects of the investigation.

The first aspect of the work was the design of parts of the MIT lattice facility related to the measurement of bucklings. In particular, methods were investigated for adjusting the distribution and magnitude of the flux entering the experimental tank. Experiments on the flux-shaping pedestal below the tank were described in Chapter II. The results of preliminary flux distribution measurements were presented in that chapter, and the complete investigation of flux distributions in the tank and in lattices was described in Chapters III and VI. The flux-shaping results may be summarized by saying that the shape and magnitude of the incoming flux could be varied considerably by changing the pedestal configuration. A configuration was devised that provided an incoming flux appropriate for both macroscopic and microscopic measurements in lattices.

The second aspect of the work was the investigation of the analytical and experimental foundations of the measurement of material bucklings of subcritical assemblies. Chapters IV and V described the theoretical and experimental bases of the measurements. On the basis of the investigation, the techniques to be used in the MIT Lattice Project were chosen. The evolution of some of the experimental techniques was described in Chapter III, while Chapter VI included a discussion of the analytical and experimental methods finally employed. The experimental techniques described there were both easy to use and productive of accurate results. The computer codes that were developed were found to be well adapted to the experi-

mental techniques and efficient and accurate in deriving the buckling from measured flux traverses. Furthermore, the variety and flexibility of the codes made them well suited to the investigation of details of the flux distribution and of the fitting process. These uses of the codes were discussed in section 7.3. Section 8.2 summarizes the experimental techniques suggested for use in future buckling measurements.

The third aspect of the work described in this report was the investigation of some of the details of flux distributions in lattices as they applied to the measurement of bucklings. The experimental and analytical techniques used for these measurements were described in section 6.3, and the results were presented in section 7.3. Two conclusions of this study may be mentioned. First, it was shown that the macroscopic flux distribution, except for microscopic effects, had a simple form throughout most of the system. That is, in most of the lattices, the flux was describable by a single J_o function (radially) and a single hyperbolic sine function (axially). Negligible reflector effects were observed, and macroscopic energy-space separability held throughout most of the volume of the lattices studied. Second, it was shown that the macroscopic and microscopic distributions in the radial direction were not separable. This effect is small, however. It was shown that the microscopic distribution must be considered when over-all flux plots are made and that this can readily be accomplished with the experimental and analytical techniques developed.

Finally, the fourth aspect of the work was the determination of the material bucklings of three lattices of natural uranium rods in D_2O. These measurements served as a test of much of the work discussed above. The measured bucklings were reported and compared with previous measurements in section 7.4. These results were of high precision relative to previous measurements and in good agreement with the trend of those measurements.

In general, it may be concluded that the technical and analytical foundation has been laid for the future accurate investigation

of bucklings in the MIT lattice facility.

8.2 RECOMMENDED EXPERIMENTAL TECHNIQUES

The various experimental methods employed in the work have been described and discussed in sections 6.3, 6.4 and 7.3. A number of conclusions may be drawn from the experience gained from the experiments with regard to the general approach to be used in future buckling measurements.

In general, the recommended technique consists of two steps: a) determining the volume of the lattice in which a simple separable flux distribution exists, and b) using a convenient detector to determine flux distributions accurately in the acceptable volume. It was found that the most discriminating method of determining the useful volume was that of examining the gold-cadmium ratio as a function of position in the lattice. The techniques of examining residuals and successively dropping points are recommended as useful and informative checks, but they tend to provide more lenient, or less exact, criteria for determining the acceptable volume. Once the volume has been established, any convenient, accurate detector, such as the traveling fission counter described in section 6.3.3, can be used to determine the flux distributions and, thus, the buckling.

The advantage gained by using this general approach is one of accuracy. This can be made clear by comparing the method proposed with a possible alternative approach in a simplified case where foils are used as detectors. Let us consider the measurement of an axial traverse. The simplest form of the proposed method would entail the irradiation of two sets of foils, one bare and one Cd-covered. The cadmium ratio would be examined as a function of height, and then the bare foil data from the region of constant cadmium ratio would be used to obtain the relaxation length. Further bare foil measurements could be made, concentrating on the acceptable region, to increase the accuracy of the measurement. The alternative approach would be to examine the thermal activation (bare minus Cd-covered) as a function of height. However, the difference between the bare and

covered activity at a point is always less accurately known than the bare activity, so that a determination based on these differences is somewhat less accurate than one based on bare foil data. This example indicates the general advantage of separating the part of an experiment devoted to determining the valid region of investigation from the part devoted to measuring a property of that region.

When new types of lattices are studied, the radial buckling should be examined as a function of height and azimuth. For lattices such as those discussed above, radial buckling traverses should be made midway between rows of fuel rods to obtain the most accurate results. The use of 1/4-inch diameter, 0.010-inch thick, gold foils on thin, milled aluminum holders is recommended in situations when the use of the traveling counter is impossible or inconvenient.

8.3 GENERAL SUGGESTIONS

The future plans of the MIT Lattice Project include the study of lattices of partially enriched uranium rods of various diameters in D_2O (H6). The analytical and experimental techniques discussed above should provide the basis of the buckling measurements to be made in those systems. The experiments reported here also suggest other areas of investigation which might be interesting and fruitful for future study.

It has recently been observed at other laboratories that the radial bucklings of fully filled lattice tanks may vary with the lattice composition (C4). This possibility could be studied by measuring the radial bucklings of lattices of greatly varying degrees of homogeneity, i.e., large (one inch) rods at large spacings vs. small (1/4-inch) rods spaced close together. If such an effect exists, it may be of importance in the question of the difference between bucklings measured in exponential experiments and those measured in critical experiments.

Another interesting study could result from the investigation of the non-separability observed in the radial flux distribution. Theoretically, a small-source theory approach would probably be

fruitful. Experimentally, it would be of interest to study the variation in the microscopic properties of the lattices, particularly the thermal utilization, as a function of position. It would then be a question of whether the microscopic properties averaged over a finite system were independent of the size of the system.

The question of the difference between critical and exponential bucklings may be resolved by the investigations now being made. If not, it can best be decided by measuring the bucklings of lattices in the same facility, with both exponential and critical techniques. The MIT lattice facility could be easily adapted to such measurements.

APPENDIX A1
COMPUTER CODES

A1.1 INTRODUCTION

The availability of an IBM 709 Computer made possible a rapid, complete, and efficient analysis of the experimental data. This section deals with the various codes that were developed to perform different parts of that analysis. Such a description will serve to describe in detail the analytical methods employed in the interpretation of the experimental data, and will provide a guide to those who want to make use of the codes in this or a related type of experiment.

The ultimate purpose of the analysis, and thus of the codes, is to derive values of the material buckling from measured radial and axial flux distributions. The heart of the computer calculations is thus the least-squares fitting of a measured flux distribution to a J_o Bessel function in one case, and to a hyperbolic sine function in the other. Another important aspect of the measurements is the verification that certain theoretically important conditions hold with respect to the experimental data. For example, as has been discussed in chapter IV, it is important that the radial data that is analyzed correspond to a simple J_o distribution. The distribution should be contaminated neither by higher harmonics nor by reflector effects. Hence, two additional codes have been developed: one which analyzes a radial distribution for harmonic effects, and one which analyzes for an I_o reflector effect. Although the codes are designed to be used independently, the three radial codes may use the same basic input data. Some of the ancillary parts of the codes - the foil data reduction section, for example - are common to all the codes.

A1.2 FITTING TO A J_o BESSEL FUNCTION

A1.2.1 Foil Data Reduction

The first calculation made by all the codes is the reduction of the raw experimental data to quantities proportional to the flux. The data may be in the form of foil activities as measured at various times after an irradiation or in the form of count rates, or currents, from a neutron counter. The codes are written so as to deal with foil activities, since neutron chamber data may readily be cast in that form for input to the code. This part of the calculation proceeds as follows.

Let A_{ij} be the activity (i.e., the total number of counts recorded) of the i^{th} foil counted for the j^{th} time interval starting at a time, $T2_{ij}$, after the end of the irradiation. Consider the foil to be counted for a length of time given by $T1_{ij}$. The number of counts is first corrected for dead-time losses in the counter. The dead time is assumed to have the form

$$\tau = p + q \cdot C \qquad \text{(A1.1)}$$

where C is the count rate, found from A_{ij} and $T1_{ij}$, while p and q are specified in the input to the code. The next operation is to correct for the (measured) background count rate, B, to get a corrected activity, A'_{ij}. Decay, before and during counting, are corrected for to obtain a corrected activity, A''_{ij}, given by:

$$A''_{ij} = A'_{ij} e^{\lambda T1_{ij}} \left(1 - e^{-\lambda T2_{ij}}\right)^{-1} , \qquad \text{(A1.2)}$$

with

$$A'_{ij} = \frac{A_{ij}}{(1-\tau \cdot C)} - B \cdot T1_{ij}$$

where λ is the decay constant for the foil material being used. The average activity of the i^{th} foil is then obtained and corrected (with a quantity C_i) for any further corrections such as foil weight, etc.; C_i is a multiplicative correction factor for foil i and is part of the input to the code. Thus, a quantity, P_i, proportional to the flux is obtained

by forming the average:

$$P_i = \frac{1}{N} C_i \sum_{j=1}^{N} A''_{ij} \qquad \text{(A1.3)}$$

where each foil is considered as having been counted N times. For convenience in the other portions of the code, the P_i's are normalized, setting the largest equal to 1.0.

Several methods for testing for, and rejecting, bad foil data were considered, but none was found satisfactory. However, provision is made in all the codes to print out all the values of A''_{ij} so that a check can be made for wayward data.

Normally, in these experiments, flux distributions will not be made along a radius of a lattice, but along a chord. The code calculates the radial position from the position of the foil along the chord and the perpendicular distance from the chord to the center of the lattice.

A1.2.2 Theoretical Basis of the J_o Code

In the case of a measured radial distribution, the quantities, P_i, derived above correspond to values of the flux at various radial positions, r_i. Let us call these measured values of the flux $\phi_{ex}(r_i)$ (equal to the normalized P_i). The code described in this section fits these $\phi_{ex}(r_i)$ to the theoretical distribution given by

$$\phi(r_i) = AJ_o(\alpha r_i) \qquad \text{(A1.4)}$$

where the two parameters, A and α^2, the radial buckling, are to be fitted by the least-squares criterion. The possibility of including the center of the distribution in the fitting process (i.e., fitting to $AJ_o[\alpha(r-c)]$) was also investigated. However, to accomplish this, the convergence criterion had to be so loose as to be meaningless because of the flatness of the distribution at the center. Furthermore, in any reasonable experiment, the actual center of the lattice, or flux distribution, should be known. A provision in the code to allow a scan of various values of c is described below.

The least-squares process may be applied directly only to parameters in a linear relationship. In order to apply it to Equation (A1.4), we must linearize the equation by expanding in a Taylor series. (The mathematical technique employed here is similar to that described by Jedruch (J2) (J3)). We expand the "true" fitted flux at each point, $\phi_i(A,\alpha)$, in a series about A_o and α_o, the values of our first guesses of A and α, so that

$$\phi_i(A_o, \alpha_o) = A_o J_o(\alpha_o r_i) \tag{A1.5}$$

and

$$\phi_i(A, \alpha) = \phi_i(A_o, \alpha_o) + u_i a + v_i b + \ldots \tag{A1.6}$$

where a and b are the first-order correction terms to A_o and α_o, respectively, and

$$u_i \equiv \left.\frac{\partial \phi_i}{\partial A}\right|_o = J_o(\alpha_o r_i) \tag{A1.7}$$

$$v_i \equiv \left.\frac{\partial \phi_i}{\partial \alpha}\right|_o = -r_i A_o J_1(\alpha_o r_i) \, . \tag{A1.8}$$

Terminating the series of Equation (A1.6) at the first-order terms, the residuals, d_i, may be written

$$d_i = \phi_{ex}(r_i) - \phi_i(A_o, \alpha_o) - u_i a - v_i b \, , \tag{A1.9}$$

or

$$d_i = F_i - u_i a - v_i b \, , \tag{A1.10}$$

where

$$F_i = \phi_{ex}(r_i) - \phi_i(A_o, \alpha_o) \, . \tag{A1.11}$$

In the fitting process, it is the sum of the squares of the d_i's that is minimized with respect to A and α. That is, if

$$\delta^2 \equiv \sum_{i=1}^{M} d_i^2 \, , \tag{A1.12}$$

where M is the total number of experimental points, it is required that

$$\frac{\partial(\delta^2)}{\partial A} = \frac{\partial(\delta^2)}{\partial \alpha} = 0 \qquad \text{(A1.13)}$$

Putting Equations (A1.10) and (A1.12) into (A1.13), we obtain

$$\frac{\partial(\delta^2)}{\partial A} = \sum_{i=1}^{M} 2(F_i - u_i a - v_i b)(-u_i) = 0 \qquad \text{(A1.14)}$$

and

$$\frac{\partial(\delta^2)}{\partial \alpha} = \sum_{i=1}^{M} 2(F_i - u_i a - v_i b)(-v_i) = 0 \ , \qquad \text{(A1.15)}$$

or

$$\Sigma F_i u_i - a\Sigma u_i u_i - b\Sigma u_i v_i = 0$$

and

$$\Sigma F_i v_i - a\Sigma u_i v_i - b\Sigma v_i v_i = 0 \ ,$$

all summations being taken from i = 1 to M.
Hence,

$$a = \frac{\begin{vmatrix} \Sigma F_i u_i & \Sigma u_i v_i \\ \Sigma F_i v_i & \Sigma v_i v_i \end{vmatrix}}{D} \ , \qquad \text{(A1.16)}$$

where

$$D \equiv \begin{vmatrix} \Sigma u_i u_i & \Sigma u_i v_i \\ \Sigma u_i v_i & \Sigma v_i v_i \end{vmatrix} \ , \qquad \text{(A1.17)}$$

and

$$b = \frac{\begin{vmatrix} \Sigma u_i u_i & \Sigma F_i u_i \\ \Sigma u_i v_i & \Sigma F_i v_i \end{vmatrix}}{D} \ , \qquad \text{(A1.18)}$$

so that the next guesses to A and α may be obtained as $A_1 = A_o + a$ and $\alpha_1 = \alpha_o + b$, and the process repeated until adequate convergence has been obtained. If, for any reason, the convergence is to be slowed down or accelerated, a fraction (or multiple) of a and b, specified in the input, may be used as correction factors. Adequate convergence

is effectively defined as the satisfaction of the conditions:

$$\frac{a}{A} < \epsilon_1 \qquad \text{and} \qquad \frac{b}{\alpha} < \epsilon_2 \tag{A1.19}$$

where ϵ_1 and ϵ_2 are arbitrarily small quantities which may be specified in the code input.

Provision is made in the code for the weighting of the residuals in the fitting process, i.e., in Equations (A1.11) and (A1.12). In this case, it is the sum

$$\delta_1^2 \equiv \sum_{i=1}^{M} (w_i d_i)^2 \tag{A1.20}$$

that is minimized with respect to A and α. The weighting is effected in the code by multiplying each of the Equations (A1.7), (A1.8) and (A1.11) by the square root of the applicable weight, w_i (W13). The analysis remains as described above.

It is of interest to determine the standard deviations or probable errors of a and b, and thus of A and α. To do this, one can carry out the above analysis with $(a + \delta a)$ and $(b + \delta b)$ substituted for a and b (M2). Such a process gives for the standard deviations of A and α:

$$\sigma_A^2 = \frac{\Sigma v_i v_i}{D} \cdot \frac{\delta^2}{M - 2} \ , \tag{A1.21}$$

and

$$\sigma_\alpha^2 = \frac{\Sigma u_i u_i}{D} \cdot \frac{\delta^2}{M - 2} \ ,$$

so that the probable error of the radial buckling, ϵ_{α^2}, is given by

$$\epsilon_{\alpha^2} = 2\alpha \cdot \epsilon_\alpha$$

$$= 2\alpha \cdot \frac{\Sigma u_i u_i}{D} \cdot \frac{\delta^2}{(M-2)} \cdot 0.675 \ . \tag{A1.22}$$

As has been discussed above, variations in the J_o distribution are expected to exist near the boundary of the lattice. The J_o code is

therefore designed to perform the fitting process first with all experimental points, and then with all points except the outermost. This procedure is continued until a certain number of points (specified in the input to the code) has been used in the fit.

It is clear that in several places in the code it is necessary to have values of the J_o and J_1 Bessel functions. These are calculated by a subroutine, which may be "called" by the main program. Its call name is "BESSIE".

The calculations are based on the series representation of the Bessel functions of interest given by

$$J_p(x) = \sum_{k=0}^{\infty} \frac{(-1)^k \left(\frac{x}{2}\right)^{2k+p}}{k!(k+p)!} \quad . \tag{A1.23}$$

The code operates by calculating successive terms in the series until adequate convergence has been attained. Equation (A1.23) can be used to obtain the following recursion relations, where T_k is the k^{th} term in the particular series:

for J_o,

$$T_{k+1} = T_k \left[\frac{(-1)\left(\frac{x}{2}\right)^2}{(k+1)^2} \right] \tag{A1.24}$$

for J_1,

$$T_{k+1} = T_k \left[\frac{(-1)\left(\frac{x}{2}\right)^2}{(k+1)(k+2)} \right] \tag{A1.25}$$

A1.2.3 Outline of the J_o Code

The detailed operation of the code can best be understood by means of a schematic block diagram and a Fortran listing.

Figure A1.1 represents the logical operation of the J_o code. Input to the code is punched on cards. The quantities required as input and the formats in which they are to be punched are specified

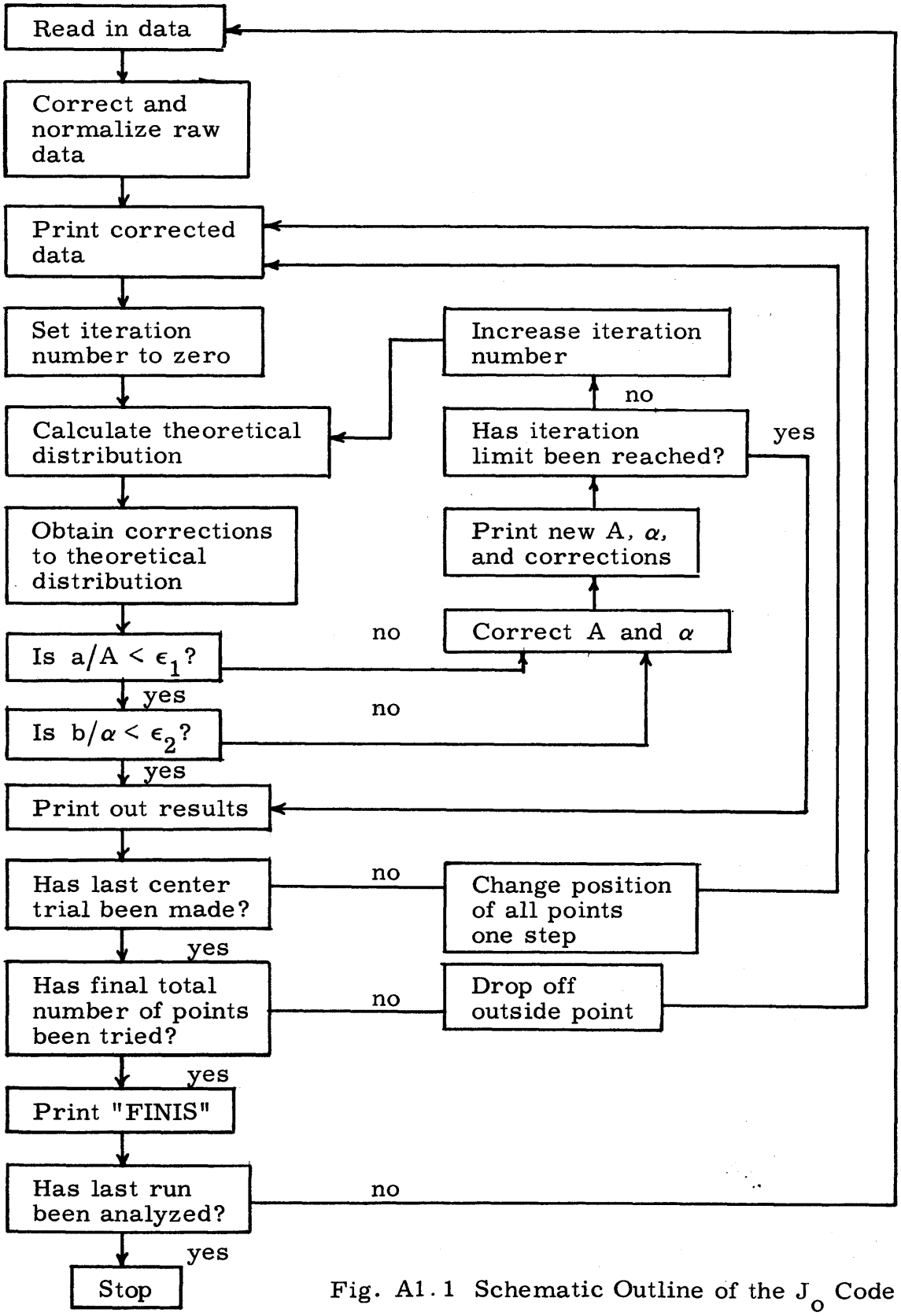

Fig. A1.1 Schematic Outline of the J_o Code

in the Fortran listings of section A1.2.4. It should be mentioned, however, that, because of the point-dropping process, data corresponding to outer points of the distribution should be read in last. The vocabulary of section A1.2.5 defines the terms used in the code language.

The first calculation made by the code is the calculation of normalized quantities proportional to the flux as described above The weighting factor for each point, w_i, is also calculated, where

$$w_i = \frac{[\phi_{ex}(r_i)]^R}{[\phi_{ex}(r_1)]^R} \quad ; \qquad \text{(A1.26)}$$

R is specified in the input.

The theoretical fluxes corresponding to the guessed values of A and α are then calculated by subroutine "BESSIE". In calling BESSIE, the call statement must specify:

a) The name in the main program of the quantities whose Bessel functions are to be calculated.

b) A quantity, Q. If $Q < 0$, the subroutine calculates only J_o; if $Q > 0$, only J_1 is calculated; and if $Q = 0$, both are calculated.

c) The name in the main program of the value of the J_o Bessel function.

d) The name in the main code of the J_1 Bessel function.

Correction factors to the guessed values of A and α of the distribution are then calculated as outlined in section A1.2.4. If both these corrections are not smaller than some specified fraction of A and α, respectively, the iteration is continued. The number of iterations that may be made is limited to a certain number specified in the input.

The fitting process can be repeated automatically with all the foils shifted in one direction and then the other, allowing a "search" for the center of the distribution. The amount of shift and the number of times the shift is to take place are input quantities.

The entire process is then repeated with successive outer points dropped. Whenever a value of the buckling is determined (or if the iteration limit is reached), the quantities of interest are printed out. An example of such a print-out is given below.

The first section of the print-out consists of the corrected activity of each foil each time it was counted. These quantities correspond to the A''_{ij} of Equation (A1.2) and are printed out to permit checking for inconsistencies in the basic input. There follow the values of A, α, a, and b (of Equations (A1.4), (A1.16) and (A1.18)) used in the fitting process at successive iterations.

Print-out from J_o Code:

RUN NUMBER 4004

FOIL ACTIVITIES

0.9924E 08	0.9966E 08	0.9789E 08
0.1022E 09	0.1026E 09	0.1012E 09
0.1029E 09	0.1027E 09	0.1024E 09
0.1010E 09	0.1002E 09	0.1000E 09
0.9990E 08	0.1003E 09	0.9850E 08
0.9206E 08	0.9201E 08	0.9171E 08
0.9027E 08	0.9181E 08	0.9051E 08
0.8956E 08	0.9062E 08	0.9027E 08
0.8935E 08	0.8901E 08	0.8963E 08
0.8289E 08	0.8276E 08	0.8304E 08
0.8238E 08	0.8189E 08	0.8337E 08
0.7156E 08	0.6002E 08	0.7104E 08
0.7097E 08	0.7059E 08	0.7081E 08
0.6489E 08	0.6398E 08	0.6478E 08

0.1006E 01	0.3836E-01	0.3028E-02	0.2585E-03
0.1005E 01	0.3841E-01	-0.1480E-02	0.4879E-04
0.1004E 01	0.3842E-01	-0.2816E-03	0.9064E-05
0.1004E 01	0.3842E-01	-0.5239E-04	0.1661E-05

RUN NUMBER 4004 (continued)

X POSITION	R POSITION	EXP. FLUX	FIT FLUX	DELTA
0.5000	4.2426	1.000000	0.997761	0.002239
4.3680	6.0687	0.982022	0.990816	-0.008794
5.3680	6.8238	0.988499	0.987234	0.001265
9.2360	10.1515	0.966412	0.966581	-0.000169
10.2360	11.0691	0.958564	0.959512	-0.000948
14.1040	14.7198	0.929521	0.925692	0.003829
15.1040	15.6806	0.918490	0.915320	0.003170
18.9720	19.4341	0.867890	0.869216	-0.001326
19.9720	20.4115	0.859980	0.855811	0.004168
23.8400	24.2094	0.798069	0.798624	-0.000555
24.8400	25.1947	0.794675	0.782536	0.012139
28.7080	29.0155	0.682697	0.715748	-0.033051
29.7080	30.0052	0.715599	0.697393	0.018207
33.5760	33.8393	0.621434	0.622728	-0.001294

RADIAL BUCKLING = 0.14763E-02 CM.SQ. -2
EXTRAPOLATED RADIUS = 62.5882 CM. A = 1.0044
POINTS USED = 14 EPSILON A = 0.5101E-02
EPSILON BSQ = 0.2193E-04 WEIGHTING EXPONENT = 0.
4 ITERATIONS WERE USED

The results of the final iteration are then printed out. Both the position of the foil (or chamber) along the chord and its radial position are listed. The experimental values of the flux, corresponding to the normalized P_i of Equation (A1.3), and the derived theoretical values of the flux at the same points are printed, along with the residuals (the differences between the two). Because of the processes of normalization and point-dropping, the points are listed in order of increasing distance from the center. Finally, the fitted value of the buckling and normalization constant are printed out along with their probable errors. Other quantities of interest printed out are: the extrapolated radius, the number of points used in the fit, the number of iterations used, and the weighting exponent (the R of Equation (A1.26)).

A1.2.4 Fortran Listing of the J_0 Code

```
      DIMENSION A1(40,5),T2(40,5),T1(40,5),PHI(40),CORR(40),
     A2(40,5),U(4X0),V(40),W(40),F(40),X(40),RO(40),ALPHA(40),
     BJO(40),BJ1(40), XACTY(5),FIT(40),XLOC(40),DIFFR(40),WT(40)
    1 FORMAT (I3,I3,I4,I4,I3)
    5 FORMAT (F10.7,F10.4,F10.4,E12.4,F8.6,F8.6)
    2 FORMAT (29H PALMEDO  BESSEL FUNCTION FIT)
    6 FORMAT (F10.4,F10.6)
    3 FORMAT (F10.0,F10.3,F10.3)
    7 FORMAT (12HORUN NUMBER I4)
      WRITE OUTPUT TAPE 2,2
    8 FORMAT (2E10.2)
    9 FORMAT (I3)
   10 FORMAT (3F5.2)
   11 FORMAT (2F5.2)
    4 READ INPUT TAPE 4,1,M,N,NORUN,LASTRN,MFINAL
      READ INPUT TAPE 4,9,ITSFNL
      READ INPUT TAPE 4,10, XTRA,XTRG,RISE
      READ INPUT TAPE 4,3,(( A1(I,J),T2(I,J),T1(I,J),J=1,N) I=1,M)
      WRITE OUTPUT TAPE 2,7,NORUN
      READ INPUT TAPE 4,5,ADAM,BKG,Y,BZERO,EPS1,EPS2
      READ INPUT TAPE 4,11,STEP,QUANTO
      READ INPUT TAPE 4,6,(X(I),CORR(I),I=1,M)
      READ INPUT TAPE 4,8,PX,QX
      SPIN=0.0
      DO27 I=1,M
      ASUM=0.0
      DO20 J=1,N
      CR=A1(I,J)/T2(I,J)
      TAU=PX+QX*CR
      A1K=(CR/(1.0-CR*TAU))*T2(I,J)-(BKG*T2(I,J))
      A2(I,J)=A1K*EXPF(ADAM*T1(I,J))/(1.0-EXPF(-ADAM*T2(I,J)))
   20 ASUM=ASUM+A2(I,J)
      FUNNY=N
   21 A2AV=(ASUM/FUNNY)*CORR(I)
      IF(I-1)25,25,26
   25 SPIN=A2AV
   26 PHI(I)=A2AV/SPIN
      WT(I)=PHI(I)**RISE/PHI(1)**RISE
   27 CONTINUE
   60 FORMAT (17HO FOIL ACTIVITIES)
   61 FORMAT (1H,6(4H,E10.4))
   47 WRITE OUTPUT TAPE 2,60
      DO 49 I=1,M
      DO 48 J=1,N
   48 ACTY(J)=A2(I,J)
   49 WRITE OUTPUT TAPE 2,61,(ACTY(J),J=1,N)
   28 AA=1.0
      C=0.0-QUANTO*STEP
      B=BZERO
```

```
 29   ITS=0
291   DO 30 I=1,M,2
 30   RO(I)=SQRTF(Y**2+(X(I)-C)**2)
      XLOC(I)=X(I)-C
      DO 33 I=2,M,2
 33   RO(I)=SQRTF(Y**2+(X(I)+C)**2)
      XLOC(I)=X(I)+C
 31   DO 32 I=1,M
 32  ALPHA(I)=B*RO(I)
     CALL BESSIE(ALPHA, 0.0,M,BJO,BJ1)
     SUMUU=0.0
     SUMUV=0.0
     SUMUF=0.0
     SUMVV=0.0
     SUMVF=0.0
     SSQRES=0.0
     DO 35 I=1,M
     U(I)=BJO(I)*WT(I)
     FIT(I)=AA*BJO(I)
     V(I)=-(RO(I))*AA*BJO(I)*WT(I)
     F(I)=(PHI(I)-FIT(I))*WT(I)
     DIFFR(I)=PHI(I)-FIT(I)
     SUMUU=SUMUU+U(I)**2
     SUMUV=SUMUV+U(I)*V(I)
     SUMUF=SUMUF+U(I)*F(I)
     SUMVF=SUMVF+V(I)*F(I)
     SUMVV=SUMVV+V(I)**2
     SSQRES=SSQRES+F(I)**2
 35   CONTINUE
      D1=SUMUF*SUMVV-SUMVF*SUMUV
      D2=SUMUU*SUMVF-SUMUV*SUMUF
     D33=SUMUU*SUMVV-SUMUV**2
      DELTAA=D1/D33
      DELTAB=D2/D33
      EM=M
      IF(ABSF(DELTAA)/AA-EPS1)36,36,38
 36   IF(ABSF(DELTAB)/B-EPS2)40,40,38
 38   AA=AA+XTRA*DELTAA
      B=B+XTRG*DELTAB
300   FORMAT (4E12.4)
      WRITE OUTPUT TAPE 2,300,(AA,B,DELTAA,DELTAB)
      IF(ITS-ITSFNL) 301,302,302
301   ITS=ITS+1
      GO TO 31
303   FORMAT (30HOTERMINATED ON ITERATION LIMIT)
302   WRITE OUTPUT TAPE 2,303
 40   DELA=SQRTF(SUMVV/D33)*SQRTF(SSQRES/(EM-2.0))*0.675
      DELB=(SQRTF(SUMUU/D33)*SQRTF(SSQRES/(EM-2.0))*0.675)*2.0*B
      EXRAD=2.4048/B
      B2=B**2
 41   FORMAT(58HO X POSITION R POSITION EXP. FLUX FIT FLUX DE
      1LTA)
 43   WRITE OUTPUT TAPE 2,41
```

```
 69   FORMAT (2F12.4,3F12.6)
      WRITE OUTPUT TAPE 2,69,(XLOC(I),RO(I),PHI(I),FIT(I),DIFFR
     (I),I=1,M)
 42   FORMAT (18HO RADIAL BUCKLING=E12.5,9H CM.SQ.-2,22H
      EXTRAPOLATED RADIUS=F10.4,4H CM.,4H A=F8.4,/13H
     POINTS USED=I2,11H EPSILON A = E11.4,13H EPSILON BSQ=E11.4)
 72   FORMAT (21HO WEIGHTING EXPONENT=F6.2)
 44   WRITE OUTPUT TAPE 2,42,(B2,EXRAD,AA,M,DELA,DELB)
421   FORMAT(I3,21H ITERATIONS WERE USED)
      WRITE OUTPUT TAPE 2,72,(RISE)
      WRITE OUTPUT TAPE 2,421,(ITS)
      IF (C-QUANTO*STEP) 401,402,402
401   C=C+STEP
      GO TO 29
402   IF (M-MFINAL) 452,452,46
 46   M=M-1
      C=-QUANTO*STEP
      GO TO 29
451   FORMAT (10HOF I N I S)
452   WRITE OUTPUT TAPE 2,451
 45   IF (LASTRN-NORUN) 51,51,50
 50   GO TO 4
 51   CALL EXIT
      END (1,1,0,0,0,0,0,0,0,0,0,0,0,0,0)
```

Subroutine BESSIE:

```
      SUBROUTINE BESSIE (X,Q,M,BJO,BJ1)
      DIMENSION X(40),BJO(40),BJ1(40),SQX(40)
      EPS=0.0001
      DO 100 I=1,M
100   SQX(I)=(X(I)**2)/4.0
      IF (Q)102,102,110
102   DO 109 I=1,M
      COUNT=1.0
      TERM=1.0
      BJ0(I)=1.0
103   TERM=-TERM*SQX(I)/COUNT**2
      BJ0(I)=BJ0(I)+TERM
      IF (TERM)105,104,104
104   IF (TERM-EPS)109,109,105
105   COUNT=COUNT+1.0
      GO TO 103
109   CONTINUE
110   IF (Q)121,111,111
111   DO 121 I=1,M
      COUNT=1.0
      TERM=X(I)/2.0
      BJ1(I)=X(I)/2.0
112   TERM=-TERM*SQX(I)/(COUNT*(COUNT+1.0))
      BJ1(I)=BJ1(I)+TERM
      IF (TERM)114,113,113
```

```
113   IF (TERM-EPS)121,121,114
114   COUNT=COUNT+1.0
121   CONTINUE
122   RETURN
      END (1,1,0,0,0,0,0,0,0,0,0,0,0,0,0)
```

A1.2.5 Vocabulary of the J_o Code

This section presents a list of all the important symbols of the J_o Code and an explanation of their use. Symbols clearly defined in the Fortran listings or those whose meanings are obvious are not listed.

Symbol in Code	Meaning	Corresponding Symbol in Appendix	Equation of Appendix	Input Quantity	Output Quantity
M	Number of points used	M	A1.11	*	*
N		N	A1.3	*	
NORUN	Run number			*	*
LASTRN	Last run of a series			*	
MFINAL	Last number of points to be used in fit			*	
ITSFNL	Limit of iterations			*	
RISE		R	A1.26	*	*
A1(I,J)		A_{ij}	A1.2	*	
T2(I,J)		$T2_{ij}$	A1.2	*	
T1(I,J)		$T1_{ij}$	A1.2	*	
ADAM		λ	A1.2	*	
BKG		B	A1.2		
Y	Perpendicular distance of experimental chord from center of lattice			*	
BZERO		α_o	A1.5	*	
EPS1		ϵ_1	A1.19	*	
EPS2		ϵ_2	A1.19	*	
STEP	Amount of shift of foil position in center search			*	
QUANTO	Number of times foils are to be shifted			*	

Symbol in Code	Meaning	Corresponding Symbol in Appendix	Equation of Appendix	Input Quantity	Output Quantity
X(I)	Original position along chord of i'th foil			*	*
CORR(I)		C_i	A1.3	*	
PX		p	A1.1	*	
QX		q	A1.1	*	
CR		C	A1.1		
A1K(I, J)		A'_{ij}	A1.2		
A2(I, J)		A''_{ij}	A1.2		*
PHI(I)	Normalized value of P_i	$\phi_{ex}(r_i)$	A1.9		*
WT(I)		w_i	A1.20		
AA		A	A1.4		*
B		α	A1.4		*
ITS	Iteration number				*
RO(I)		r_i	A1.9		*
XLOC(I)	Shifted chordal position of foil				*
BJ0(I)		$J_o(\alpha r_i)$	A1.4		
BJ1(I)		$J_1(\alpha r_i)$			
SUMUU		$\Sigma u_i u_i$	A1.15		
SSQRES		δ^2	A1.12		
FIT(I)		$AJ_o(\alpha r_i)$	A1.6		*
DIFFR(I)		F_i	A1.11		*
DELTAA		a	A1.16		*
DELTAB		b	A1.18		*
XTRA	Multiple of a to be used as correction factor to A			*	
XTRG	Multiple of b to be used as correction factor to α			*	

A1.3 RADIAL HARMONIC ANALYSIS CODE

A1.3.1 Theoretical Basis of the Code

The code designed to analyze the higher radial harmonic contributions to the fundamental mode is similar to the J_o code described in section A1.2. Again, a least-squares analysis is made to determine the coefficients of the functions describing the higher modes. In particular, we are interested in the lower order harmonics since any large distortion of the distribution from a simple J_o function would entail their presence. Furthermore, harmonics of higher orders attenuate more rapidly through the lattice and would not effect the distribution through any significant distance (see chapter IV). Thus, let us consider the flux distribution as composed of three harmonics in all so that we may write the theoretical distribution as:

$$\phi(r) = A_1 J_o(\alpha_1 r) + A_2 J_o(\alpha_2 r) + A_3 J_o(\alpha_3 r) \qquad \text{(A1.26a)}$$

where

$$\alpha_1 = \frac{2.4048}{R'} \quad , \quad \alpha_2 = \frac{5.5201}{R'} \quad , \quad \alpha_3 = \frac{8.6537}{R'} \quad ,$$

and

R' = the extrapolated radius which, in this case, is assumed known.

The sum of the squares of the residuals may then be written:

$$\delta^2 = \sum_{i=1}^{M} [\phi_i - A_1 J_o(\alpha_1 r_i) - A_2 J_o(\alpha_2 r_i) - A_3 J_o(\alpha_3 r_i)]^2 \qquad \text{(A1.27)}$$

and it is required that

$$\frac{\partial(\delta^2)}{\partial A_1} = \frac{\partial(\delta^2)}{\partial A_2} = \frac{\partial(\delta^2)}{\partial A_3} = 0 \qquad \text{(A1.28)}$$

In this case, the coefficients may be determined analytically; the three equations of (A1.28) become, upon expansion and substitution of Equation (A1.27),

$$A_1[\Sigma J_o^2(\alpha_1 r_i)] + A_2[\Sigma J_o(\alpha_1 r_i) J_o(\alpha_2 r_i)] + A_3[\Sigma J_o(\alpha_1 r_i) J_o(\alpha_3 r_i)] = \Sigma \phi_i J_o(\alpha_1 r_i)$$

$$A_1[\Sigma J_o(\alpha_1 r_i) J_o(\alpha_2 r_i)] + A_2[\Sigma J_o^2(\alpha_2 r_i)] + A_3[\Sigma J_o(\alpha_2 r_i) J_o(\alpha_3 r_i)] = \Sigma \phi_i J_o(\alpha_2 r_i)$$

$$A_1[\Sigma J_o(\alpha_1 r_i) J_o(\alpha_3 r_i)] + A_2[\Sigma J_o(\alpha_2 r_i) J_o(\alpha_3 r_i)] + A_3[\Sigma J_o^2(\alpha_3 r_i)] = \Sigma \phi_i J_o(\alpha_3 r_i) \qquad \text{(A1.29)}$$

Equation (A1.29) is readily solved for A_1, A_2, and A_3. For example:

$$A_1 = \frac{\begin{vmatrix} \Sigma \phi_i J_o(\alpha_1 r) & \Sigma J_o(\alpha_1 r) J_o(\alpha_2 r) & \Sigma J_o(\alpha_1 r) J_o(\alpha_3 r) \\ \Sigma \phi_i J_o(\alpha_2 r) & \Sigma J_o^2(\alpha_2 r) & \Sigma J_o(\alpha_2 r) J_o(\alpha_3 r) \\ \Sigma \phi_i J_o(\alpha_3 r) & \Sigma J_o(\alpha_2 r) J_o(\alpha_3 r) & \Sigma J_o^2(\alpha_3 r) \end{vmatrix}}{\begin{vmatrix} \Sigma J_o^2(\alpha_1 r) & \Sigma J_o(\alpha_1 r) J_o(\alpha_2 r) & \Sigma J_o(\alpha_1 r) J_o(\alpha_3 r) \\ \Sigma J_o(\alpha_1 r) J_o(\alpha_2 r) & \Sigma J_o^2(\alpha_2 r) & \Sigma J_o(\alpha_2 r) J_o(\alpha_3 r) \\ \Sigma J_o(\alpha_1 r) J_o(\alpha_3 r) & \Sigma J_o(\alpha_2 r) J_o(\alpha_3 r) & \Sigma J_o^2(\alpha_3 r) \end{vmatrix}} \qquad \text{(A1.30)}$$

A1.3.2 Outline of the Code

Since no iterational procedure is required in this code, its general format is more straightforward than that of the J_o Code. The input is very similar to that of the other codes, and the same data-reduction process is followed. With the extrapolated radius introduced as input to the code, and with the use of subroutine BESSIE, the code calculates directly the three coefficients, A_1, A_2, and A_3 of Equation (A1.26). An example of the output of the code is given below.

Harmonic Analysis Output:

```
PALMEDO    HARMONIC ANALYSIS
RUN NUMBER  506
R POSITION        EXP. FLUX        FIT FLUX
     1.5200          1.000000        0.999739
    11.6000          0.963727        0.958737
     9.6300          0.968125        0.971793
    22.4000          0.837616        0.842459
    19.9400          0.877098        0.875555
    32.5600          0.668860        0.669041
    30.3600          0.711582        0.711034
    43.8400          0.436438        0.430158
    41.8400          0.473633        0.474272
    54.2500          0.194574        0.201990
    53.1400          0.226093        0.225737
SUM OF THE SQUARES OF THE RESIDUALS = 0.1597E-03
P1 = 1.00585        P2 = 0.00785        P3 = 0.01325
FOIL ACTIVITIES
    0.72020E 08      0.72349E 08
    0.69729E 08      0.69403E 08
    0.69381E 08      0.70386E 08
    0.60921E 08      0.60005E 08
    0.63480E 08      0.63145E 08
    0.48364E 08      0.48199E 08
    0.51363E 08      0.51367E 08
    0.31629E 08      0.31379E 08
    0.34155E 08      0.34223E 08
    0.14131E 08      0.13959E 08
    0.16313E 08      0.16328E 08
```

A1.3.3 Fortran Listing of the Harmonic Analysis Code

```
P.F. PALMEDO HARMONIC ANALYSIS
      DIMENSION A1(40,5),T2(40,5)T1(40,5),PHI(40),CORR(40),A2(40,5),
     X(40),RO(40),ALPHA (40),BJ01(40),BJ11(40),BJ02(40),BJ12(40),
     ACTY(5),FIT(40),BJ03(40),BJ13(40),ALPHA1(40),ALPHA2(40),
     ALPHA3(40),F(40)
      DET3F(A11,A12,A13,A21,A22,A23,A31,A32,A33)=A11*(A22*A33
     -A23*A32)-A12*(A21*A33-A23*A31)+A13*(A21*A32-A22*A31)
    1 FORMAT(I3,I3,I4,I4)
    4 READ INPUT TAPE 4,1,M,N,NORUN,LASTRN
    2 FORMAT(28H PALMEDO  HARMONIC ANALYSIS)
      WRITE OUTPUT TAPE 2,2
    7 FORMAT (12H RUN NUMBER I4)
      WRITE OUTPUT TAPE 2,7,NORUN
    3 FORMAT (F10.0,F10.3,F10.3)
```

Fortran Listing of the Harmonic Analysis Code (continued)

```
      READ INPUT TAPE 4,3,((A1(I,J),T2(I,J),T1(I,J),J=1,N)I=1,M)
    6 FORMAT (F10.4,F10.6)
      READ INPUT TAPE 4,6,(X(I),CORR(I),I=1,M)
    5 FORMAT (F10.7,3F10.4)
      READ INPUT TAPE 4,5,ADAM,BKG,Y,EXRAD
      SPIN=0.0
      DO 27 I=1,M
      ASUM=0.0
      DO 20 J=1,N
      A1K=A1(I,J)-(BKG*T2(I,J))
      A2(I,J)=A1K*EXPF(ADAM*T1(I,J))/(1.0-EXPF(-ADAM*T2(I,J)))
   20 ASUM=ASUM+A2(I,J)
      FUNNY=N
   21 A2AV=(ASUM/FUNNY)*CORR(I)
      IF (I-1)25,25,26
   25 SPIN=A2AV
   26 PHI(I)=A2AV/SPIN
   27 CONTINUE
      B1=2.4048
      B2=5.520
      B3=8.654
      SKIP=0.0
      DO 30 I=1,M
   30 RO(I)=SQRTF(Y**2+X(I)**2)
   31 DO 32 I=1,M
      ALPHA1(I)=B1*RO(I)/EXRAD
      ALPHA2(I)=B2*RO(I)/EXRAD
   32 ALPHA3(I)=B3*RO(I)/EXRAD
      CALL BESSIE (ALPHA1,-1.0,M,BJ01,BJ11)
      CALL BESSIE (ALPHA2,-1.0,M,BJ02,BJ12)
      CALL BESSIE (ALPHA3,-1.0,M,BJ03,BJ13)
      ZFJ1=0.0
      ZFJ2=0.0
      ZFJ3=0.0
      ZFF=0.0
      ZJ1J1=0.0
      ZJ1J2=0.0
      ZJ1J3=0.0
      ZJ2J2=0.0
      ZJ2J3=0.0
      ZJ3J3=0.0
      DO 35 I=1,M
      F(I)=PHI(I)
      ZFJ1=ZFJ1+F(I)*BJ01(I)
      ZFJ2=ZFJ2+F(I)*BJ02(I)
      ZFJ3=ZFJ3+F(I)*BJ03(I)
      ZFF=ZFF+F(I)**2
      ZJ1J1=ZJ1J1+BJ01(I)**2
      ZJ1J2=ZJ1J2+BJ01(I)*BJ02(I)
```

```
      ZJ1J3=ZJ1J3+BJ01(I)*BJ03(I)
      ZJ2J2=ZJ2J2+BJ02(I)**2
      ZJ2J3=ZJ2J3+BJ02(I)*BJ03(I)
      ZJ3J3=ZJ3J3+BJ03(I)**2
   35 CONTINUE
      DEM=DET3F(ZJ1J1,ZJ1J2,ZJ1J3,ZJ1J2,ZJ2J2,ZJ2J3,ZJ1J3,ZJ2J3,
        ZJ3J3)
      P1=DET3F(ZFJ1,ZJ1J2,ZJ1J3,ZFJ2,ZJ2J2,ZJ2J3,ZFJ3,ZJ2J3,
        ZJ3J3)/DEM
      P2=DET3F(ZJ1J1,ZFJ1,ZJ1J3,ZJ1J2,ZFJ2,ZJ2J3,ZJ1J3,ZFJ3,
        ZJ3J3)/DEM
      P3=DET3F(ZJ1J1,ZJ1J2,ZFJ1,ZJ1J2,ZJ2J2,ZFJ2,ZJ1J3,ZJ2J3,
        ZFJ3)/DEM
      ZFFT=0.0
      ZFTFT=0.0
      DO 36 I=1,M
      FIT(I)=P1*BJ01(I)+P2*BJ02(I)+P3*BJ03(I)
      ZFFT=ZFFT+FIT(I)*PHI(I)
   36 ZFTFT=ZFTFT+FIT(I)**2
      ZRESSQ=ZFF-2.0*ZFFT+ZFTFT
   63 FORMAT (38H SUM OF THE SQUARES OF THE RESIDUALS=E10.4)
   41 FORMAT (F12.4,2F12.6)
   46 FORMAT (36HO R POSITION   EXP. FLUX   FIT FLUX)
   61 FORMAT (1H,6(4H,E11.5))
   47 FORMAT (4HOP1=F8.5,10H    P2=F8.5,10H    P3=F8.5)
   62 FORMAT (17HO FOIL ACTIVITIES)
      WRITE OUTPUT TAPE 2,46
      WRITE OUTPUT TAPE 2,41,(RO(I),PHI(I),FIT(I),I=1,M)
      WRITE OUTPUT TAPE 2,63,ZRESSQ
      WRITE OUTPUT TAPE 2,47,P1,P2,P3
      WRITE OUTPUT TAPE 2,62
      DO 49 I=1,M
      DO 48 J=1,N
   48 ACTY(J)=A2(I,J)
   49 WRITE OUTPUT TAPE 2,61,(ACTY(J),J=1,N)
      IF (LASTRN-NORUN)51,51,50
   50 GO TO 4
   51 CALL EXIT
      END (1,1,0,0,0,0,0,0,0,0,0,0,0,0,0)
```

A1.3.4 Vocabulary of the Harmonic Analysis Code

Many of the symbols used in this code are the same, and have the same meaning, as those used in the J_o code. The other symbols of importance, and their meaning, are defined below.

Symbol in Code	Meaning	Corresponding Symbol in Appendix	Equation in Appendix	Input Quantity	Output Quantity
EXRAD		R'	A1.26a	*	
BJ01 (I)		$J_o(\alpha_1 r_i)$	A1.27		
BJ02 (I)		$J_o(\alpha_2 r_i)$	A1.27		
BJ03 (I)		$J_o(\alpha_3 r_i)$	A1.27		
Z...	Summation of quantities whose symbols follow	$\sum_{i=1}^{M}$	A1.27		
ZJ1J3		$\Sigma J_o(\alpha_1 r_2)$ $\cdot J_o(\alpha_3 r_1)$	A1.29		
P1		A_1	A1.26		*
P_2		A_2	A1.26		*
P_3		A_3	A1.26		*
ZRESSQ		δ^2	A1.27		*

A1.4 RADIAL REFLECTOR EFFECT CODE

A1.4.1 Theoretical Basis of the Code

The second code, which provides a test of the radial distribution, analyzes for the possible effect of a reflector. In this case, the function to be fit is given by

$$\phi(r) = A_1 J_o(\alpha_1 r) + A_2 I_o(\alpha_2 r) \qquad \text{(A1.31)}$$

where the quantities A_1, A_2, α_1, and α_2 are solved for in the least-squares fitting process. The theoretical basis of this code is the same as that of the J_o code described in section A1.2. The data-reduction portions of the codes are identical. In this case, d_i, the i^{th} residual (see Equation A1.10), is given by

$$d_i = F_i - p_i a - q_i b - r_i c - s_i d \qquad \text{(A1.32)}$$

where

$$p_i \equiv \left.\frac{\partial \phi_i}{\partial A_1}\right|_o = J_o(\alpha_{10} r_i) \tag{A1.33}$$

$$q_i \equiv \left.\frac{\partial \phi_i}{\partial A_2}\right|_o = I_o(\alpha_{20} r_i) \tag{A1.34}$$

$$r_i \equiv \left.\frac{\partial \phi_i}{\partial \alpha_1}\right|_o = - r_i A_{10} J_1(\alpha_{10} r_i) \tag{A1.35}$$

and

$$s_i \equiv \left.\frac{\partial \phi_i}{\partial \alpha_2}\right|_o = r_i A_{20} I_1(\alpha_{20} r_i) \tag{A1.36}$$

δ^2 is then minimized with respect to A_1, A_2, α_1, and α_2, and equations for a, b, c, and d may be obtained corresponding to Equations (A1.16) and (A1.18). An iterative procedure must be followed until

$$\frac{a}{A_1} < \epsilon_1, \quad \frac{b}{A_2} < \epsilon_2, \quad \frac{c}{\alpha_1} < \epsilon_3, \quad \text{and} \quad \frac{d}{\alpha_2} < \epsilon_4 \tag{A1.37}$$

where the epsilons are input quantities.

The code uses the subroutine BESSIE described above to calculate J_o and J_1 Bessel functions. Another subroutine, BESIO, is used to calculate I_o and I_1 Bessel functions. The series representation which forms the theoretical basis of the code is

$$I_p(x) = \sum_{k=0}^{\infty} \frac{\left(\frac{x}{2}\right)^{2k+p}}{k!\,(k+p)!} \tag{A1.38}$$

The subroutine operates by calculating successive terms in the series expansion until adequate convergence is attained. The following recursion relations, derived from Equation (A1.38), are used in the code:

for I_o,

$$T_{k+1} = T_k\left[\frac{(x/2)^2}{(k+1)^2}\right] \qquad \text{(A1.39)}$$

for I_1,

$$T_{k+1} = T_k\left[\frac{(x/2)}{(k+1)(k+2)}\right] \qquad \text{(A1.40)}$$

where T_k is the k^{th} term in the particular series. The calling statement must include the same information as that required for BESSIE (with obvious changes of nomenclature).

A1.4.2 Outline of the Reflector Effect Code

The logical flow of the code is shown in Fig. A1.2. Because of the nature of the code, no search for the center of the distribution or dropping of outer points is included, although these can be effected by rerunning the code. An input quantity limiting the number of iterations is included to preclude excessively long runs.

An example of the output of the code is given below. The output is for a trial run in which $A_2/A_1 \cong 0.10$.

PALMEDO JO + IO FIT
RUN NUMBER 5
04 ITERATIONS WERE USED

R POSITION	EX. FLUX	FIT FLUX
5.0000	1.0000	1.0031
10.0000	0.9780	0.9826
15.0000	0.9451	0.9491
20.0000	0.9003	0.9035
25.0000	0.8381	0.8471
30.0000	0.8060	0.7815
35.0000	0.7365	0.7087
40.0000	0.6185	0.6308
45.0000	0.5389	0.5501
50.0000	0.4648	0.4691

B12 = 0.1291E-02 B22 = 0.1222E-02 AA1 = 0.9316 AA2 = 0.078315
EXTRAPOLATED RADIUS = 66.94171 ITERATIONS = 10.0
DELAA1 = 0.2845E-00 DELAA2 = 0.9348-01 DELB1 = 0.4337E-02
DELB2 = 0.1085E-00

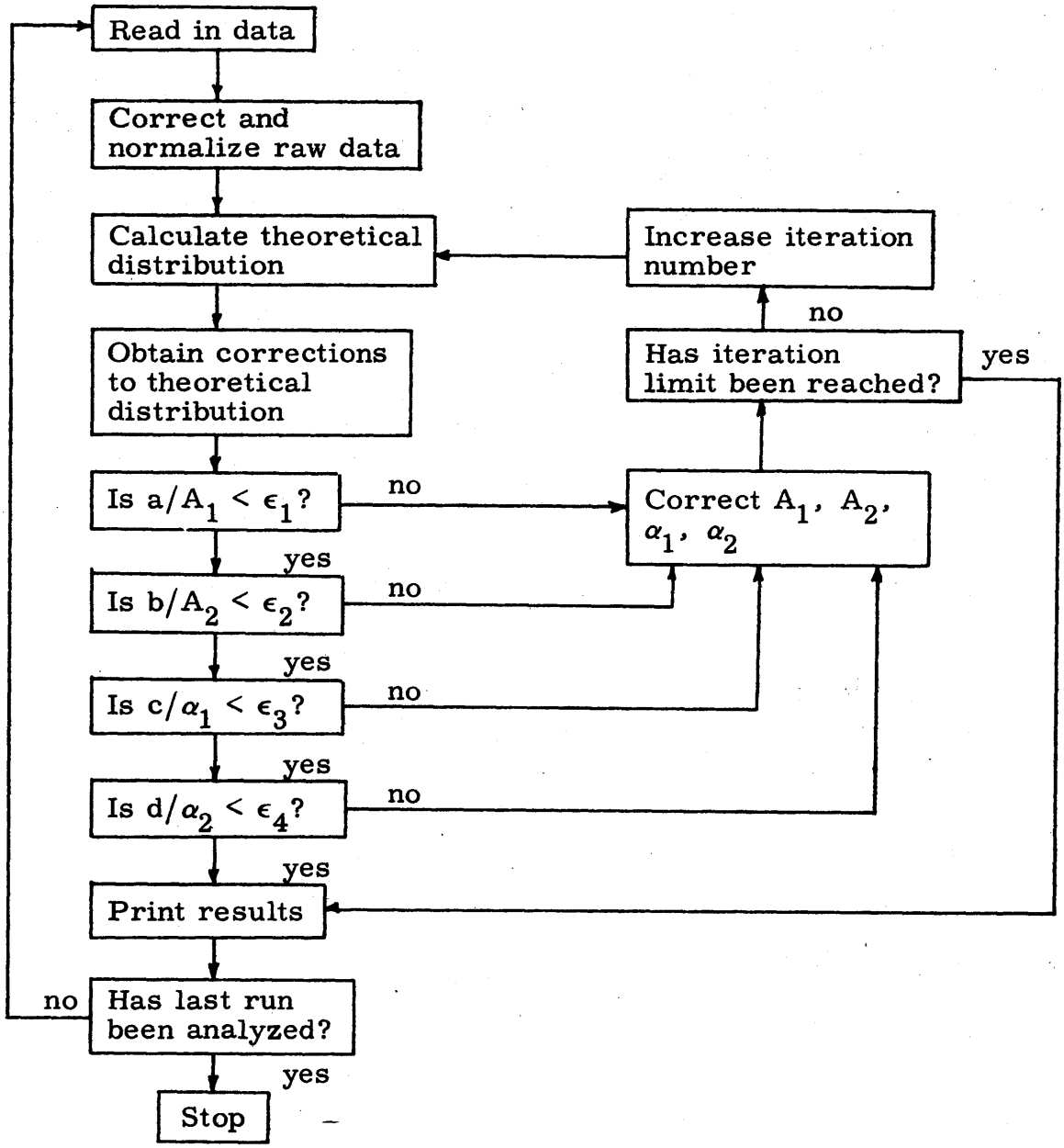

Fig. A1.2 Schematic Outline of the Reflector Effect Code

A1.4.3 Fortran Listing of the Reflector Effect Code

```
C  P. F. PALMEDO  PROB NO. M1297
   DIMENSION A1(40,5), T2(40,5), T1(40,5), PHI (41), CORR(40),
      A2(40,5), Q(40), R(40), S(40), F(40), X(40), RO(40), ALPHA(40),
      BJ0(40), BJ1(40), BI0(40), BI1(40), ACTY(40), FIT(40), P(40),
      ALPHA2(41)
   DET3F(A11,A12,A13,A21,A22,A23,A31,A32,A33)=A11*(A22*A33-
      A23*A32)-A12*(A21*A33-A23*A31)+A13*(A21*A32-A22*A31)
   DET4F(A11,A12,A13,A14,A21,A22,A23,A24,A31,A32,A33,A34,
      A41,A42,A43,A44)=A11*DET3F(A22,A23,A24,A32,A33,A34,
      A42,A43,A44)-A12*DET3F(A21,A23,A24,A31,A33,A34,A41,
      A43,A44)+A13*DET3F(A21,A22,A24,A31,A32,A34,A41,A42,
      A44)-A14*DET3F(A21,A22,A23,A31,A32,A33,A41,A42,A43)
 1 FORMAT (I3,I3,I4,I4)
 2 FORMAT (19HOPALMEDO  J0+I0 FIT)
 3 FORMAT (F10.0,F10.3,F10.3)
 5 FORMAT (F10.7,F10.4,F10.4,2F12.8)
 6 FORMAT (F10.4,F10.6)
 7 FORMAT (12H RUN NUMBER I4)
 8 FORMAT (2E10.2)
 9 FORMAT (4F8.6)
10 FORMAT (F5.0)
   WRITE OUTPUT TAPE 2,2
 4 READ INPUT TAPE 4,1,M,N,NORUN,LASTRN
   READ INPUT TAPE 4,10,ADLAST
   READ INPUT TAPE 4,3,((A1(I,J),T2(I,J), T1(I,J), J=1,N) I=1,M)
   WRITE OUTPUT TAPE 2,7,NORUN
   READ INPUT TAPE 4,5,ADAM, BKG, Y, BZERO, B2ZERO
   READ INPUT TAPE 4,9,EPS1,EPS2, EPS3, EPS4
   READ INPUT TAPE 4,6,(X(I),CORR(I),I=1,M)
   READ INPUT TAPE 4,9,PX, QX
   SPIN=0.0
   DO 27 I=1,M
   ASUM=0.0
   DO 20 J=1,N
   CR=A1(I,J)/T2(I,J)
   TAU=PX+QX*CR
   A1K=(CR/(1.0-CR*TAU))*T2(I,J)-(BKG*T2(I,J))
   A2(I,J)=A1K*EXPF(ADAM*T1(I,J))/(1.0-EXPF(-ADAM*T2(I,J)))
20 ASUM=ASUM+A2(I,J)
   FUNNY=N
21 A2AV=(ASUM/FUNNY)*CORR(I)
   IF (I-1)25,25,26
25 SPIN=A2AV
26 PHI(I)=A2AV/SPIN
27 CONTINUE
45 FORMAT (F12.4,F10.4,F10.4)
60 FORMAT (17H FOIL ACTIVITIES)
61 FORMAT (11E10.6)
```

Fortran Listing of the Reflector Effect Code (continued)

```
47  WRITE OUTPUT TAPE 2,60
    DO 48  I=1,M
    DO 49  J=1,N
49  ACTY(J)=A2(I,J)
48  WRITE OUTPUT TAPE 2,61,(ACTY(J),J=1,N)
28  AA1=1.0
    AA2=0.10
    B1=BZERO
    B2=B2ZERO
    ADDUP=1.0
    DO 30 I=1,M
30  RO(I)=SQRTF(Y**2+X(I)**2)
31  DO 32 I=1,M
    ALPHA(I)=B2*RO(I)
32  ALPHA(I)=B1*RO(I)
    CALL BESSIE (ALPHA,C.C,M,BJ0,BJ1)
    CALL BESIO (ALPHA2,C,C,M,BI0,BI1)
    SUMPF=0.0
    SUMQF=0.0
    SUMRF=0.0
    SUMSF=0.0
    SUMPQ=0.0
    SUMQQ=0.0
    SUMQR=0.0
    SUMQS=0.0
    SUMPR=0.0
    SUMQR=0.0
    SUMRR=0.0
    SUMRS=0.0
    SUMPS=0.0
    SUMSS=0.0
    SUMPP=0.0
    DO 35 I=1,M
    FIT(I)=AA1*BJ0(I)+AA2*BI0(I)
    P(I)=BJ0(I)
    Q(I)=BI0(I)
    R(I)=AA1*X(I)*BJ1(I)
    S(I)=AA2*X(I)*BI1(I)
    F(I)=PHI(I)-FIT(I)
    SUMPF=SUMPF+P(I)*F(I)
    SUMQF=SUMQF+Q(I)*F(I)
    SUMRF=SUMRF+R(I)*F(I)
    SUMSF=SUMSF+S(I)*F(I)
    SUMPQ=SUMPQ+P(I)*Q(I)
    SUMQQ=SUMQQ+Q(I)**2
    SUMQR=SUMQR+Q(I)*R(I)
    SUMRR=SUMRR+R(I)**2
    SUMRS=SUMRS+R(I)*S(I)
    SUMPS=SUMPS+P(I)*S(I)
```

Fortran Listing of the Reflector Effect Code (continued)

```
      SUMSS=SUMSS+S(I)**2
      SUMPP=SUMPP+P(I)**2
   35 CONTINUE
      DOO=DET4F(SUMPP,SUMPQ,SUMPR,SUMPS,SUMPQ,SUMQQ,
        SUMQR,SUMQS,SUMPR,SUMQR,SUMRR,SUMRS,SUMPS,SUMQS,
        SUMRS,SUMSS)
      DLTAA1=DET4F(SUMPF,SUMPQ,SUMPR,SUMPS,SUMQF,SUMQQ,
        SUMQR,SUMQS,SUMRF,SUMQR,SUMRR,SUMRS,SUMSF,SUMQS,
        SUMRS,SUMSS)/DOO
      DLTAA2=DET4F(SUMPP,SUMPF,SUMPR,SUMPS,SUMPQ,SUMQF,
        SUMQR,SUMQS,SUMPR,SUMRF,SUMRR,SUMRS,SUMPS,SUMSF,
        SUMRS,SUMSS)/DOO
      DLTAB1=DET4F(SUMPP,SUMPQ,SUMPF,SUMPS,SUMPQ,SUMQQ,
        SUMQF,SUMQS,SUMPR,SUMQR,SUMRF,SUMRS,SUMPS,SUMQS,
        SUMSF,SUMSS)/DOO
      DLTAB2=DET4F(SUMPP,SUMPQ,SUMPR,SUMPF,SUMPQ,SUMQQ,
        SUMQR,SUMQF,SUMPR,SUMQR,SUMRR,SUMRF,SUMPS,SUMQS,
        SUMRS,SUMSF)/DOO
  300 FORMAT (4E12.4)
      WRITE OUTPUT TAPE 2,300,(AA1,AA2,B1,B2)
      WRITE OUTPUT TAPE 2,300 (DLTAA1,DLTAA2,DLTAB1,DLTAB2)
      IF (ABSF(DLTAA1)/AA1-EPS1)36,36,38
   36 IF (ABSF(DLTAA2)/AA2-EPS2)37,37,38
   37 IF (ABSF(DLTAB1)/B1-EPS3)39,39,38
   39 IF (ABSF(DLTAB2)/B2-EPS4)40,40,38
   38 AA1=AA1+DLTAA1
      AA2=AA2+DLTAA2
      B1=B1+DLTAB1
      B2=B2+DLTAB2
      IF (ADDUP-ADLAST) 301,302,302
  301 ADDUP=ADDUP+1.0
      GO TO 31
  303 FORMAT (I3,21H ITERATIONS WERE USED)
  302 WRITE OUTPUT TAPE 2,303,(ADDUP)
   40 DELA1=SQRTF(DET3F(SUMQQ,SUMQR,SUMQS,SUMQR,SUMRR,
        SUMRS,SUMQS,SUMRS,SUMSS)/DOO)
      DELA2=SQRTF(DET3F(SUMPP,SUMPR,SUMPS,SUMPR,SUMRR,
        SUMRS,SUMPS,SUMRS,SUMSS)/DOO)
      DELB1=SQRTF(DET3F(SUMPP,SUMPQ,SUMPS,SUMPQ,SUMQQ,
        SUMQS,SUMPS,SUMQS,SUMSS)/DOO)
      DELB2=SQRTF(DET3F(SUMPP,SUMPQ,SUMPR,SUMPQ,SUMQQ,
        SUMQR,SUMPR,SUMQR,SUMRR)/DOO)
      EXRAD=2.4048/B1
      B12=B1**2
      B22=B2**2
   41 FORMAT (32H R POSITION EX. FLUX  FIT FLUX)
   42 FORMAT (5H B12=E13.4,5H B22=E13.4,5H AA1=F10.4,5H AA2=
        F10.6//21H EXTRAPOLATED RADIUS=F12.5,12H ITERATIONS=
        F6.1//8H DELAA1=E12.4,8H DELAA2=E12.4,7H DELB1= E12.4,
        7H DELB2=E12.4)
```

```
      WRITE OUTPUT TAPE 2,41
      WRITE OUTPUT TAPE 2,45,(RO(I),PHI(I),FIT(I),I=1,M)
      WRITE OUTPUT TAPE 2,42,(B12,B22,AA1,AA2,EXRAD,ADDUP,
         DELA1,DELA2,DELB1,DELB2)
      IF (LASTRN-NORUN)51,51,50
   50 GO TO 4
   51 CALL EXIT
      END (1,1,0,0,0,0,0,0,0,0,0,0,0,0,0)
```

Subroutine BESIO:

```
      SUBROUTINE BESIO (X,Q,M,BI0,BI1)
      DIMENSION X(40),BI0(40),BI1(40),SQX(40)
      EPS=0.0001
      DO 200 I=1,M
  200 SQX(I)=(X(I)**2)/4
      IF (Q)202,202,210
  202 DO 219 I=1,M
      COUNT=1.0
      TERM=1.0
      BI0(I)=1.0
  203 TERM=TERM*SQX(I)/COUNT**2
      BI0(I)=BI0(I)+TERM
      IF (TERM-EPS)209,209,205
  205 COUNT=COUNT+1.0
      GO TO 203
  209 CONTINUE
  210 IF (Q)221,211,211
  211 DO 221 I=1,M
      COUNT=1.0
      TERM=X(I)/2.0
      BI1(I)=X(I)/2.0
  212 TERM=TERM*SQX(I)/(COUNT*(COUNT+1))
  213 IF (TERM-EPS)221,221,214
  214 COUNT=COUNT+1
      GO TO 212
  221 CONTINUE
  222 RETURN
      END
```

A1.4.4 Vocabulary of the Reflector Effect Code

There follows a list of symbols used in the code which have not been defined before and are not defined clearly in the Fortran listing of the code.

Symbol in Code	Corresponding Symbol in Appendix	Equation in Appendix	Input Quantity	Output Quantity
BZERO First guess at α_1	α_{10}	A1.33	*	
B2ZERO First guess at α_2	α_{20}	A1.34	*	
AA1	A_1	A1.31		*
AA2	A_2	A1.31		*
B1	α_1	A1.31		*
B2	α_2	A1.31		*
P(I)	p_i	A1.33		
Q(I)	q_i	A1.34		
R(I)	r_i	A1.35		
S(I)	s_i	A1.36		
ADDUP Iteration number				*
ADLAST Iteration limit			*	

A1.5 FITTING TO THE AXIAL SINH DISTRIBUTION

A1.5.1 Theoretical Basis of the Code

The axial distribution code again uses the same data analysis section as is used by the codes described above. In this case, the quantities, P_i, of Equation (A1.3) correspond to values of the flux at various axial positions, z_i. The axial distribution code fits the measured values of the flux, $\phi_{ex}(z_i)$, to the theoretical distribution given by

$$\phi(z_i) = A \sinh \gamma(h'-z_i) \ , \qquad \text{(A1.41)}$$

where the normalizing constant, A, and the buckling, γ^2, are determined in the least-squares fitting process; h' is the extrapolated height of the tank.

Again, a linearization of the fitting equation must be performed to allow application of the least-squares method. Expanding the expression for the flux about the initial guessed values of A, A_o, and γ, γ_o, one obtains

$$\phi_i(A, \gamma) = \phi_i(A_o, \gamma_o) + u_i a + v_i b + \ldots \tag{A1.42}$$

where a and b are the first order correction terms to A_o and γ_o, respectively, and

$$u_i \equiv \left.\frac{\partial \phi_i}{\partial A}\right|_o = \sinh \gamma_o(h' - z_i) \tag{A1.43}$$

$$v_i \equiv \left.\frac{\partial \phi_i}{\partial \gamma}\right|_o = A_o(h' - z_i) \cosh \gamma_o(h' - z_i) \tag{A1.44}$$

The theoretical development follows the same lines from this point as that for the J_o code described in section A1.2.2. The corrections to A_o and γ_o may be a given fraction (or a multiple) of a and b, so that the new A, A_j, is given by

$$A_j = A_{j-1} + a \cdot x_a \tag{A1.45}$$

and

$$\gamma_j = \gamma_{j-1} + b \cdot x_b \tag{A1.46}$$

where x_a and x_b are specified in the code input.

As in the J_o code, the residuals may be weighted in the fitting process with a power of the flux specified as input. This is of particular importance in this code because of the large range of values of the experimental flux. With no weighting function, the points near the bottom of the tank are automatically weighted too heavily in the fitting process.

A1.5.2 Outline of the Axial Code

Figure A1.3 represents the logical flow of the axial code. The iterative procedure is followed until either adequate convergence is

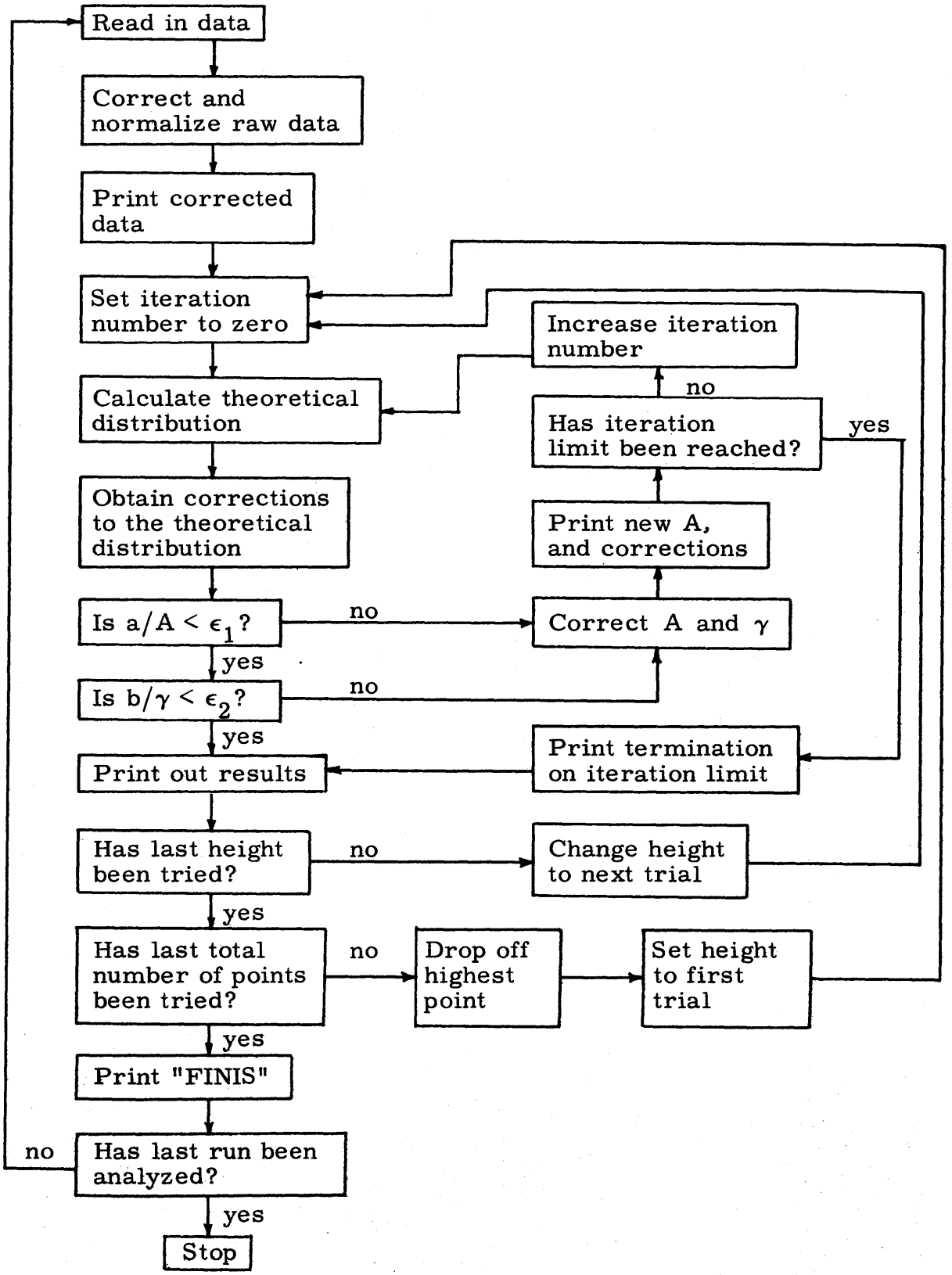

Fig. A1.3 Schematic Outline of Axial Sinh Code

attained or the limit of iterations is reached. It is possible to try several different values of the extrapolated height, h'. This is accomplished by means of the input quantities, q' and s', along with the estimated extrapolated height, h'_o; s' specifies the amount that the h' is to be varied at each trial and q', the number of times h' is to be varied in each direction. Thus, the first trial of h' is given by

$$h' = h'_o - q' \cdot s' \tag{A1.47}$$

and the last trial is given by

$$h' = h'_o + q' \cdot s' \tag{A1.48}$$

It is possible that, owing to harmonic effects, the points taken near the bottom of the tank do not actually correspond to a sinh function. To study this effect, provision is made in the code to repeat the fitting process, using successively fewer points (down to some present, i.e., input, number). When this aspect of the code is being used, the input data should be given starting with points at the top of the tank. An example of the output of the code is given below.

Print-out from Axial Code:

RUN NUMBER 3106

FOIL ACTIVITIES

0.96697E 07	0.96401E 07	0.96459E 07
0.11012E 08	0.11186E 08	0.11038E 08
0.12924E 08	0.12648E 08	0.12659E 08
0.14621E 08	0.14764E 08	0.14600E 08
0.16931E 08	0.16948E 08	0.16802E 08
0.19129E 08	0.19171E 08	0.18999E 08
0.22049E 08	0.21991E 08	0.22372E 08
0.24857E 08	0.24540E 08	0.25013E 08
0.28854E 08	0.28549E 08	0.29017E 08
0.32705E 08	0.33093E 08	0.33116E 08
0.38165E 08	0.37896E 08	0.37502E 08
0.42626E 08	0.42928E 08	0.42224E 08
0.50509E 08	0.50175E 08	0.49445E 08
0.57232E 08	0.57261E 08	0.56371E 08

Print-out from Axial Code (continued)

```
0.3923E-00  0.2358E-01  0.1690E 03  0.1337E-00  -0.5185E-02  0.
0.4467E-00  0.2322E-01  0.1690E 03  0.5438E-01  -0.3585E-03  0.
0.4471E-00  0.2325E-01  0.1690E 03  0.3507E-03   0.3091E-04  0.
```

Z POSITION	EXP. FLUX	FIT FLUX	DELTA
102.8700	1.000000	0.991900	0.008100
97.1600	1.147816	1.145502	0.002314
91.4400	1.320341	1.319643	0.000698
85.7300	1.519052	1.516786	0.002266
80.0100	1.750288	1.741114	0.009174
74.3000	1.978840	1.995800	-0.016960
68.5800	2.293578	2.286248	0.007330
62.8700	2.569817	2.616566	-0.046749
57.1500	2.984586	2.993762	-0.009176
51.4400	3.416041	3.423173	-0.007132
45.7200	3.921943	3.913909	0.008035
40.0000	4.412869	4.473956	-0.061088
34.2900	5.184760	5.112040	0.072720
28.5700	5.900889	5.841699	0.059189

```
EXTRAPOLATED HEIGHT = 169.00000  CM.
AXIAL BUCKLING = 0.000540458 INV. SQ. CM.
A=0.4471  DELA=0.7844E-04  DELG=0.3778E-02  DELC=0.
3 ITERATIONS WERE USED
14 POINTS WERE USED
WEIGHTING EXPONENT = -1.00
EPSILONS USED = FOR A 0.000010  FOR GAMMA 0.000010
```

A1.5.3 Fortran Listing of the Axial Code

```
PHILIP F. PALMEDO  AXIAL FIT TO GAMMA AND A
SINHF(Q)=0.5(EXPF(Q)-EXPF(-Q))
COSHF(Q)=0.5(EXPF(Q)+EXPF(-Q))
DIMENSION A1(50,5),T2(50,5),T1(50,5)PHI(50),A2(50,5),U(50),
   W(50),X(50),F(50),Z(50),FIT(50),HYSINE(50),HYCOS(50),ACTY(5),
   WT(50),DIFFR(50)
 1 FORMAT (I3,I3,I4,I4,I4)
 3 FORMAT (F10.0,F10.3,F10.3)
 5 FORMAT (F10.7,F10.4,F12.5,F10.4,2F8.6)
 2 FORMAT (32H PALMEDO AXIAL DISTRIBUTION FIT)
 6 FORMAT (F10.4,F10.6)
 7 FORMAT (12HORUN NUMBER I4)
 8 FORMAT (2E10.2)
 9 FORMAT (I3)
10 FORMAT (3F5.2)
11 FORMAT (2F5.2)
   WRITE OUTPUT TAPE 2,2
 4 READ INPUT TAPE 4,1,M,N,NORUN,LASTRN,MFNL
```

```
      READ INPUT TAPE 4,9,ITSFNL
      READ INPUT TAPE 4,10,XTRA,XTRG,RISE
      READ INPUT TAPE 4,3,((A1(I,J),T2(I,J),T1(I,J),J=1,N)I=1,M)
      WRITE OUTPUT TAPE 2,7,NORUN
      READ INPUT TAPE 4,5,ADAM,BKG,GZERO,CZERO,EPS1,EPS2
      READ INPUT TAPE 4,11,STEP,QUANTO
      READ INPUT TAPE 4,6,(Z(I),CORR(I),I=1,M)
      READ INPUT TAPE 4,9,PX,QX
      SPIN=0.0
      DO 27 I=0,M
      ASUM=0.0
      DO 20 J=1,N
      CR=A1(I,J)/T2(I,J)
      TAU=PX+QX*CR
      A1K=(CR/(1.0-CR*TAU))*T2(I,J)-(BKG*T2(I,J))
      A2(I,J)=A1K*EXPF(ADAM*T1(I,J))/(1.0-EXPF(-ADAM*T2(I,J)))
   20 ASUM=ASUM+A2(I,J)
      FUNNY=N
   21 A2AV=(ASUM/FUNNY)*CORR(I)
      IF (I-1)25,25,26
   25 SPIN=A2AV
   26 PHI(I)=A2AV/SPIN
      WT(I)=PHI(I)**RISE/PHI(1)**RISE
   27 CONTINUE
   60 FORMAT (17HO FOIL ACTIVITIES)
   61 FORMAT (1H,6(4H,E11.5))
   47 WRITE OUTPUT TAPE 2,60
      DO 49 I=1,M
      DO 48 J=1,N
   48 ACTY(J)=A2(I,J)
   49 WRITE OUTPUT TAPE 2,61,(ACTY(J),J=1,N)
      FITTING PROCESS IS TO BEGIN
   28 AA=2.0*EXPF(-GZERO*(CZERO-Z(1)))
      G=GZERO
      C=CZERO-QUANTO*STEP
   29 ITS=0
  291 DO 30 I=1,M
      ALPHA=G*(C-Z(I))
      HYSINE(I)=SINHF(ALPHA)
   30 HYCOS(I)=COSHF(ALPHA)
      SUMUU=0.0
      SUMUW=0.0
      SUMWW=0.0
      SUMFU=0.0
      SUMFW=0.0
      SSQRES=0.0
      DO 35 I=1,M
      U(I)=HYSINE(I)*WT(I)
      W(I)=AA*(C-Z(I))*HYCOS(I)*WT(I)
      FIT(I)=AA*HYSINE(I)
      DIFFR(I)=PHI(I)-FIT(I)
```

Fortran Listing of the Axial Code (continued)

```
      F(I)=(PHI(I)-FIT(I))*WT(I)
      SUMUU=SUMUU+U(I)**2
      SUMUW=SUMUW+U(I)*W(I)
      SUMWW=SUMWW+W(I)**2
      SUMFU=SUMFU+F(I)*U(I)
      SUMFW=SUMFW+F(I)*W(I)
      SSQRES=SSQRES+F(I)**2
   35 CONTINUE
      DOM=SUMUU*SUMWW-SUMUW**2
      DELTAA=(SUMFU*SUMWW-SUMFW*SUMUW)/DOM
      DELTAG=(SUMUU*SUMFW-SUMFU*SUMUW)/DOM
      IF ((ABSF(DELTAA)/AA-EPS1)36,36,39
   36 IF (ABSF(DELTAG)/G-EPS2)40,40,39
   39 AA=AA+XTRA*DELTAA
      G=G+XTRG*DELTAG
  369 FORMAT (6E12.4)
      WRITE OUTPUT TAPE 2,369,(AA,G,C,DELTAA,DELTAG,DELTAC)
      IF (ITS-ITSFNL)391,392,392
  391 ITS=ITS+1
      GO TO 291
  393 FORMAT (30HOTERMINATED ON ITERATION LIMIT)
  392 WRITE OUTPUT TAPE 2,393
   40 EM=M
      ZIP=SQRTF(SSQRES/(EM-2.0))*0.675
      DELA=SQRTF(SUMUU/DOM)*ZIP
      DELG=SQRTF(SUMWW/DOM)*ZIP
      GAMMA2=G**2
   70 FORMAT (I3,21H ITERATIONS WERE USED)
   41 FORMAT (F12.4,3F12.6)
   46 FORMAT (45HO Z POSITION EXP. FLUX  FIT FLUX  DELTA)
   42 FORMAT (21HO EXTRAPOLATED HEIGHT=F10.5,4H CM.,17H
         BUCKLING=12.9,11H INV.SQ.CM.,//4H  A=F0.4,  6H  DELA=
         E12.4,6H DELG=E12.4,6H DELC=E12.4)
   71 FORMAT (23H EPSILONS USED=FOR A,F8.6,11H FOR GAMMA,F8.6)
   72 FORMAT (21HOWEIGHTING EXPONENT=F6.2)
  721 FORMAT (I3,17H POINTS WERE USED)
      WRITE OUTPUT TAPE 2,46
   43 WRITE OUTPUT TAPE 2,41,(Z(I),PHI(I),FIT(I),DIFFR(I),I=1,M)
   44 WRITE OUTPUT TAPE 2,42,(C,GAMMA2,AA,DELA,DELG,DELC)
      WRITE OUTPUT TAPE 2,70,(ITS)
      WRITE OUTPUT TAPE 2,721,(M)
      WRITE OUTPUT TAPE 2,72,(RISE)
      WRITE OUTPUT TAPE 2,71,(EPS1,EPS2)
      IF (C-CZERO-QUANTO*STEP)401,402,402
  401 C=C+STEP
      GO TO 29
  402 IF (M-MFNL)404,404,403
  403 M=M-1
      C=CZERO-QUANTO*STEP
```

```
    GO TO 29
404 CONTINUE
405 FORMAT (10HOF I N I S)
    WRITE OUTPUT TAPE 2, 405
45  IF (LASTRN-NORUN)51, 51, 50
50  GO TO 4
51  CALL EXIT
    END(1, 1, 0, 0, 0, 0, 0, 0, 0, 0, 0, 0, 0, 0, 0)
```

A1.5.4 Vocabulary of the Axial Code

The Axial Code once more uses much of the vocabulary common to the other codes. New symbols, not otherwise defined, are listed below.

Symbol in Code	Meaning	Corresponding symbol in Appendix	Equation of Appendix	Input Quantity	Output Quantity
GZERO		γ_o	A1.41	*	
XTRA		x_a	A1.44	*	
XTRG		x_b	A1.45	*	
CZERO		h'_o	A1.46	*	
QUANTO		q'	A1.46	*	
STEP		s'	A1.46	*	
U(I)		u_i	A1.41		
W(I)		v_i	A1.41		
SINHF(x)	sinh x				
COSH(x)	cosh x				
DELA	probable error of A				*
DELG	probable error of γ				*

APPENDIX A2
TWO-GROUP REFLECTOR ANALYSIS

During the design of the lattice facility, considerable attention was directed toward the flux shape that would exist in the experimental tank. In particular, since the theoretical analysis was to be made in terms of a bare system, the back-scattering of fast leakage neutrons by the surrounding shielding seemed to be a possible problem. One of the methods suggested for avoiding such "room return", if necessary, was to fill the outer tank of the facility with borated H_2O. The calculations made to evaluate this scheme, as performed by Mr. F. Becker, are summarized in this appendix.

For a first, rough treatment, the following assumptions were made.

1. The physical situation could be represented as a two-region system, a cylindrical core surrounded by an annular reflector to which an absorber can be added. The shielding around the facility is neglected, mainly to avoid the need for a three-region treatment. This assumption is justified by the fact that, for the fast group, the thickness of the reflector (12 inches) is large, compared to $\sqrt{\tau}$ where τ is the Fermi age of fission neutrons in the borated water, or about 5.5 centimeters. In the thermal group, likewise, the assumption is justified by the fact that, due to the boron loading, the thickness of the reflector is large in comparison with the thermal mean free path.

2. Two-group diffusion theory could be applied to the problem. This assumption finds its justification in the exploratory nature of the calculation.

Fast neutrons back-scattered into the outer region should be slowed down and absorbed in that region, while slow neutrons should simply be absorbed. The problem, then, is to examine the theoretical form of the slow neutron flux in the core to see how the buckling

can be obtained from the flux distribution.

Two-region, two-group diffusion theory has been treated in so many places (W7), (H4), (G1), that we need only summarize its results. The standard assumption of the separability of the axial, azimuthal, and radial components of the flux is made. Only the radial component of the fast and slow fluxes will interest us here. The fast and thermal fluxes in the core are given respectively by

$$\phi_{1c}(r) = AJ_o(\alpha r) + CI_o(\beta r) \quad , \tag{A2.1}$$

and

$$\phi_{2c}(r) = a_1 AJ_o(\alpha r) + a_2 CI_o(\beta r) \quad , \tag{A2.2}$$

where

$$a_1 = \frac{p\Sigma_{1c}}{D_{2c}B_1^2 + \Sigma_{2c}} = \frac{D_{1c}B_1^2 + \Sigma_{1c}}{\frac{k}{p}\Sigma_{2c}} \quad , \tag{A2.3}$$

and

$$a_2 = \frac{p\Sigma_{1c}}{D_{2c}B_2^2 + \Sigma_{2c}} = \frac{D_{1c}B_2^2 + \Sigma_{1c}}{\frac{k}{p}\Sigma_{2c}} \quad . \tag{A2.4}$$

The symbols have their usual meanings with subscripts 1 and 2 referring to the fast and thermal groups, respectively, and c referring to the core. The "resonance" capture is assumed to occur in a small energy band between the fast and the thermal groups. The functional dependence of the fluxes has been obtained by assuming that they both satisfy the Helmholtz equation, i.e., that

$$\nabla^2 Z + B^2 Z = 0 \quad , \tag{A2.5}$$

where Z is either $\phi_{1c}(\vec{r})$ or $\phi_{2c}(\vec{r})$. The quantities, B_1^2 and B_2^2, are the two solutions of the two-group criticality equations. They can be expressed in the form

$$\mu^2 = \alpha^2 - \gamma^2 \qquad \text{and} \qquad \nu^2 = -\beta^2 - \gamma^2 \quad , \tag{A2.6}$$

where γ^2 is the axial buckling and $\mu^2 = B_1^2$, $\nu^2 = -B_2^2$. The solution

of the criticality equation gives

$$\mu^2 = \frac{1}{2}\left\{-\left(\frac{1}{L_1^2}+\frac{1}{L_2^2}\right)+\sqrt{\left(\frac{1}{L_1^2}+\frac{1}{L_2^2}\right)^2+\frac{4(k-1)}{L_1^2L_2^2}}\right\}, \quad (A2.7)$$

(a relatively small but positive quantity) and

$$\nu^2 = -\frac{1}{2}\left\{+\left(\frac{1}{L_1^2}+\frac{1}{L_2^2}\right)-\sqrt{\left(\frac{1}{L_1^2}+\frac{1}{L_2^2}\right)^2+\frac{4(k-1)}{L_1^2L_2^2}}\right\} \quad (A2.8)$$

(a relatively large but negative quantity). It also follows from (A2.6), (A2.7) and A2.8) that

$$\mu^2 - \nu^2 = \alpha^2 + \beta^2 \qquad \text{and} \qquad \mu^2 + \nu^2 = -\left(\frac{1}{L_1^2}+\frac{1}{L_2^2}\right). \quad (A2.9)$$

The fast and thermal fluxes in the reflector are given by

$$\phi_{1r}(r) = SK_o(\kappa_{1r}r) \quad (A2.10)$$

and

$$\phi_{2r}(r) = TK_o(\kappa_{2r}r) - a_3SK_o(\kappa_{1r}r)\ , \quad (A2.11)$$

with

$$a_3 = \frac{pr(\Sigma_{1r}/D_{2r})}{\kappa_{1r}^2-\kappa_{2r}^2} = -\frac{pr(D_{1r}/\Sigma_{2r})}{L_{1r}^2-L_{2r}^2}\ , \quad (A2.12)$$

where

$$\kappa_{1r}^2 = \frac{1}{L_{1r}^2} - \gamma^2 \qquad \text{and} \qquad \kappa_{2r}^2 = \frac{1}{L_{2r}^2} - \gamma^2\ . \quad (A2.13)$$

The conditions that have been assumed in the derivation of the above equations are that the flux be finite and non-negative in the core, and that it vanish at $r = \infty$. Four other boundary conditions are imposed; namely, that the fast and thermal fluxes, and the fast and thermal net currents, are continuous across the core-reflector interface. I.e., that

$$\phi_{1c}(R) = \phi_{1r}(R)\ , \quad (A2.14)$$

$$\phi_{2c}(R) = \phi_{2r}(R) \quad , \tag{A2.15}$$

$$D_{1c} \left.\frac{\partial \phi_{1c}}{\partial r}\right|_R = D_{1r} \left.\frac{\partial \phi_{1r}}{\partial r}\right|_R \quad , \tag{A2.16}$$

and

$$D_{2c} \left.\frac{\partial \phi_{2c}}{\partial r}\right|_R = D_{2r} \left.\frac{\partial \phi_{2r}}{\partial r}\right|_R \quad , \tag{A2.17}$$

where R is the core radius. By substituting the relations for the fluxes, Equations (A2.1), (A2.2), (A2.10) and (A2.11), into Equations (A2.14) - (A2.17), we obtain a determinantal equation. It is this equation that is usually solved to obtain a value for the critical radius.

The determinantal equation can be reduced to the form:

$$P \cdot Q = R \cdot S \tag{A2.18}$$

where

$$P = -D_{1c} \frac{\alpha J_1(\alpha R)}{J_o(\alpha R)} + D_{1c} \frac{\kappa_{1r} K_1(\kappa_{1r} R)}{K_o(\kappa_{1r} R)} \quad ,$$

$$Q = a_2 D_{2c} \frac{\beta I_1(\beta R)}{I_o(\beta R)} + a_3 D_{2r} \frac{\kappa_{1r} K_1(\kappa_{1r} R)}{K_o(\kappa_{1r} R)} - (a_2 - a_3) D_{2r} \frac{\kappa_{2r} K_1(\kappa_{2r} R)}{K_o(\kappa_{2r} R)} \quad ,$$

$$R = D_{2c} \frac{\beta I_1(\beta R)}{I_o(\beta R)} + D_{1r} \frac{\kappa_{1r} K_1(\kappa_{1r} R)}{K_o(\kappa_{1r} R)} \quad ,$$

and

$$S = -a_1 D_{2c} \frac{\alpha J_1(\alpha R)}{J_o(\alpha R)} + a_3 D_{2r} \frac{\kappa_{1r} K_1(\kappa_{1r} R)}{K_o(\kappa_{1r} R)} + (a_1 - a_3) D_{2r} \frac{\kappa_{2r} K_1(\kappa_{2r} R)}{K_o(\kappa_{2r} R)} \quad .$$

Our primary interest is in the thermal flux in the core. It is convenient to recast Equation (A2.2) in the form

$$\phi_{2c}(r) = \phi_{2c}(o) \frac{J_o(\alpha r) + \lambda I_o(\beta r)}{1 + \lambda} \quad , \tag{A2.19}$$

where

$$\lambda = \frac{C}{A} \cdot \frac{a_2}{a_1} \quad . \tag{A2.20}$$

The ratio C/A can be obtained from the following equations derived from (A2.14), (A2.15), and (A2.16):

$$AJ_o(\alpha R) + CI_o(\beta R) = SK_o(\kappa_{1r}R) \ ,$$

$$a_1AJ_o(\alpha R) + a_2CI_o(\beta r) = TK_o(\kappa_{2r}R) - a_3SK_o(\kappa_{1r}R) \ ,$$

and

$$D_{1c}A\alpha J_1(\alpha R) - D_{1c}C\beta I_1(\beta R) = D_{1r}S\kappa_{1r}K_1(\kappa_{1r}R) \ . \qquad (A2.21)$$

Solving these, we get

$$\frac{C}{A} = \frac{D_{1c}K_o(\kappa_{1r}R)\ \alpha J_1(\alpha R) - J_o(\alpha R)\ D_{1r}\kappa_{1r}K_1(\kappa_{1r}R)}{\kappa_{1r}I_o(\beta R)\ D_{1r}K_1(\kappa_{1r}R) + K_o(\kappa_{1r}R)\ D_{1c}\beta I_1(\beta R)} \ . \qquad (A2.22)$$

We are now in a position to use the above equations to examine the problem at hand. Basically, we would like to determine λ, and examine Equation (A2.19) for various values of the boron concentration in the water of the reflector region. As an example, the numbers were calculated for a lattice of 0.50 inch diameter, 1 per cent enriched rods, with a value of 23.66 for the ratio of the volume of moderator to the volume of uranium. The quantities needed for the calculation and their derivation are given below:

$\underline{p_r}$

Basis of Calculation:

$$\ln p = -\frac{1}{\xi\Sigma_s}\int_E^{E_o}\frac{\Sigma_a}{1+\Sigma_a/\Sigma_s}\frac{dE'}{E'} \qquad (A2.23)$$

Even for quite large concentrations of B in H_2O, the epithermal flux varies as 1/E (P7). We calculate p from 20 kev to thermal with the following data (H5):

$\sigma_{sH} = 20b$	$\sigma_{aH} = 0.3b$
$\sigma_{aB}(th) = 755b$	(1/v dependence)
$\sigma_{sB} = 3.8b$	
$\sigma_{aO} = 0$	$\sigma_{sO} = 3.8b$

The results of the calculation are shown in Fig. A2.1.

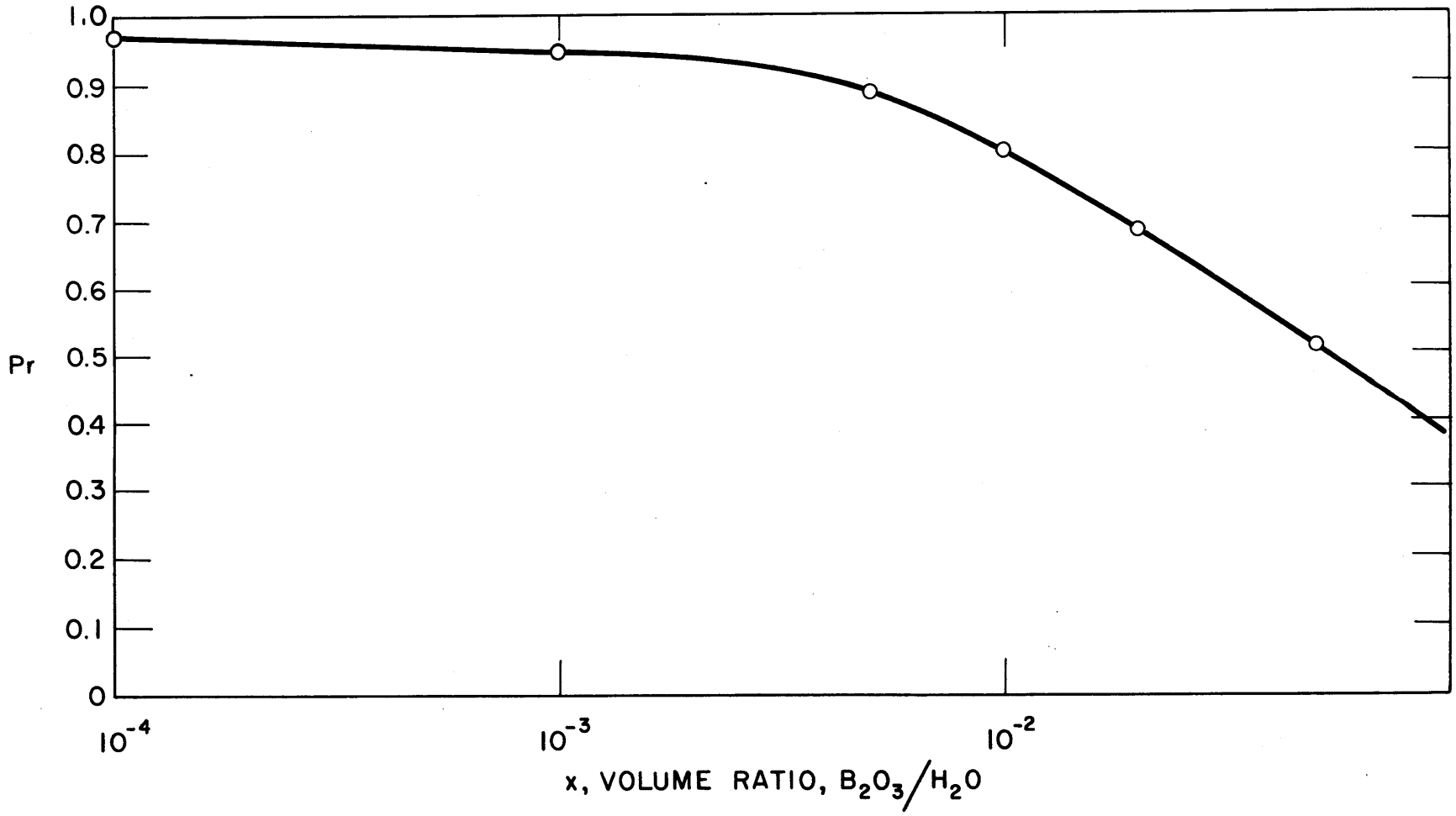

FIG. A2.1 VARIATION OF Pr WITH BORON CONCENTRATION

$\underline{D_{2r}}$

Basis of Calculation:

$$D_{2r} = \frac{1}{3} \frac{1}{\Sigma(1-\mu)\left(1-\frac{4}{5}\frac{\Sigma_a}{\Sigma}+\frac{\Sigma_a}{\Sigma}\frac{\mu_o}{1-\mu_o}\right)} \qquad \text{(A2.24)}$$

Data:

$$\mu_H = 0.333 \qquad \mu_O = 0.958$$

$$\mu_B = 0.944$$

and the cross section given above.

The results of the calculation are shown in Fig. A2.2.

$\underline{L^2_{2r}}$

Basis of Calculation:

$$L^2_{2r} = D_{2r}/\Sigma_a \qquad \text{(A2.25)}$$

The cross sections given above were used, and the resultant diffusion areas are shown in Fig. A2.3.

$\underline{D_{1r}}$

Basis of Calculation:

$$D_{1r} = \frac{\int_{E_{th}}^{E_o} D(E)\,\phi(E)\,dE}{\int_{E_{th}}^{E_o} \phi(E)\,dE} \qquad \text{(A2.26)}$$

Assumptions:

$\phi \propto \frac{1}{E}$ (see ref. P7)

$E_o = 2$ Mev, $E_{th} = 0.025$ ev

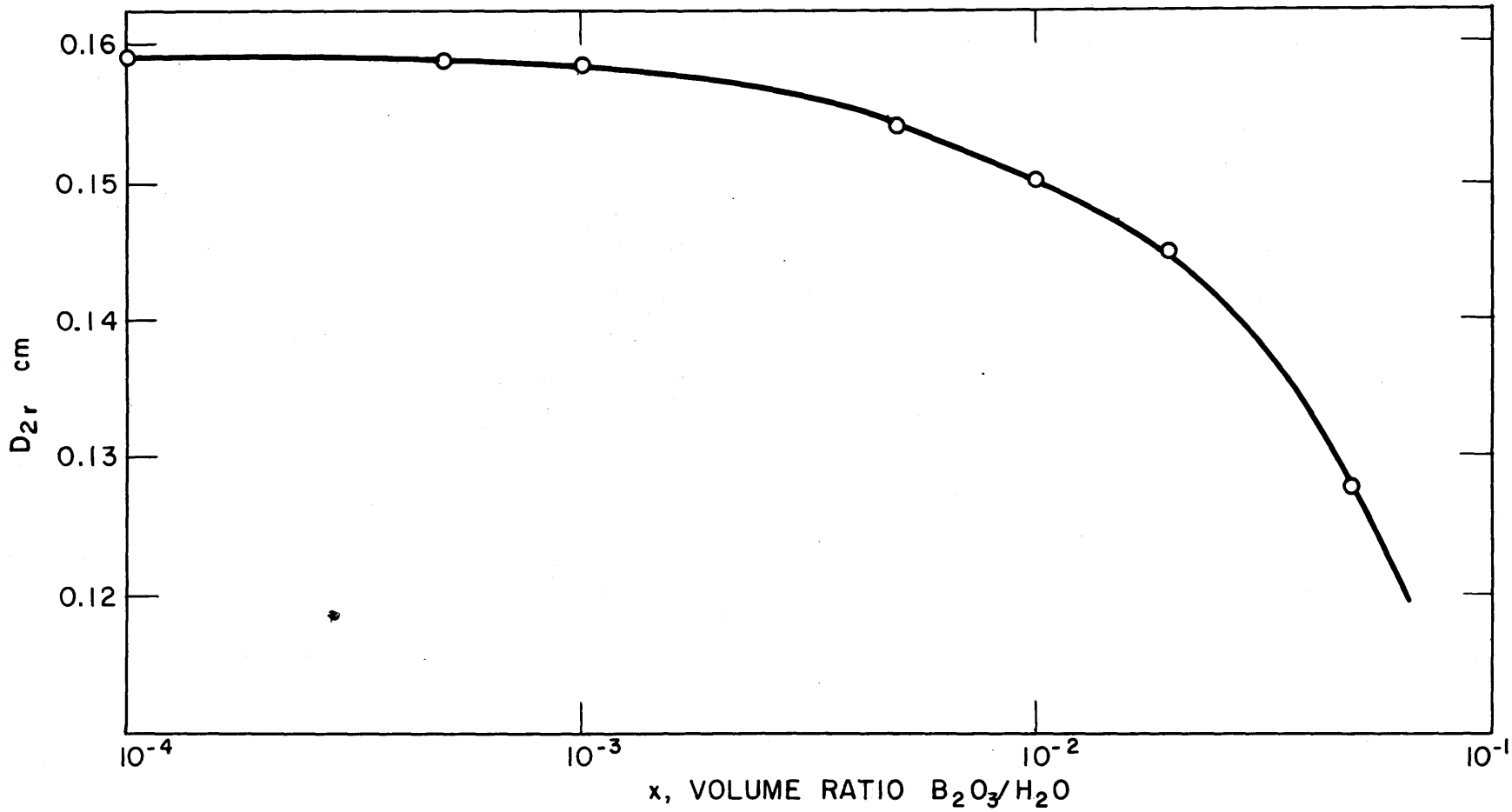

FIG. A2.2 VARIATION OF D_{2r} WITH BORON CONCENTRATION

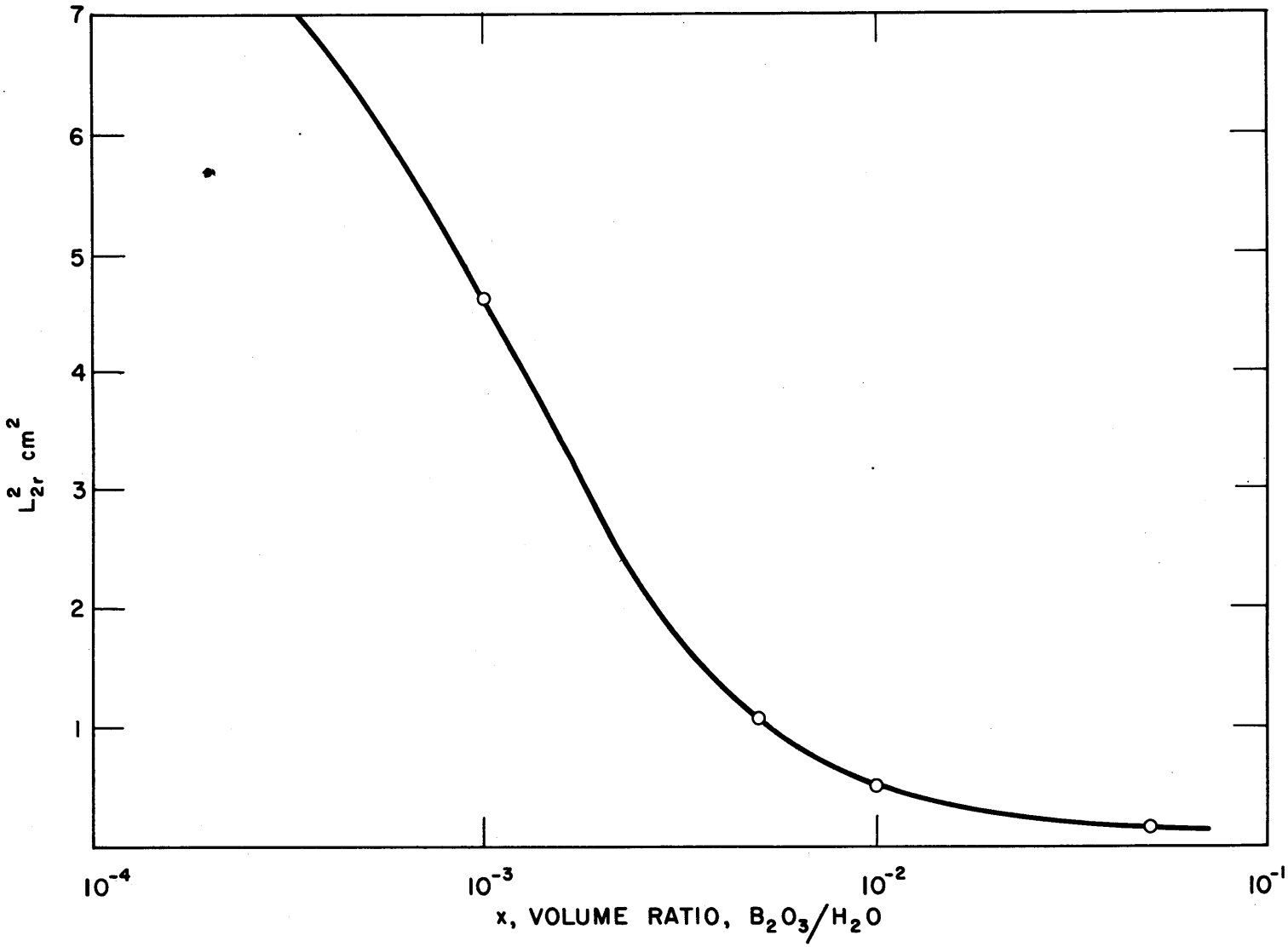

FIG. A2.3 VARIATION OF L^2_{2r} WITH BORON CONCENTRATION

$$D(E) = 1/3\Sigma(E)\,[1-\mu(E)]\left[1 - \frac{4}{5}\,\frac{\Sigma_a(E)}{\Sigma(E)} + \frac{\Sigma_a(E)\,\mu(E)}{\Sigma(E)\{1-\mu(E)\}}\right]$$

Data:

$\mu(E)$ constant for all materials other than H

$\mu_H(E) = 0.0656$ $\qquad 0.088 \text{ ev} < E < 2 \text{ Mev}$

$\mu_H(E) = \frac{E - 0.025}{0.063}\,(0.45) + 0.15$ $\qquad 0.025 \text{ ev} < E < 0.088 \text{ ev}$

(from reference D5)

$\sigma_{aB} = 1.8b$	$1 \text{ kev} < E < 2 \text{ Mev}$
$\sigma_{aB} = 755b$	$E = 0.025 \text{ ev}$
$\sigma_{aB} \propto 1/v$	$0.025 \text{ ev} < E < 1 \text{ kev}$
$\sigma_{aO} = 0$	
$\sigma_{aH} = 0.3b$	
$\sigma_{sB} = 3.8b$	$1 \text{ kev} < E < 2 \text{ Mev}$
$\sigma_{sB} = 4.0b$	$1 \text{ ev} < E < 1 \text{ kev}$
$\sigma_{sB} = 4.2b$	$0.025 \text{ ev} < E < 1 \text{ ev}$
$\sigma_{sO} = 3.7b$	
$\sigma_{sH} = 2.5b$	$E = 2 \text{ Mev}$
$\sigma_{sH} = 20b$	$E = 10 \text{ kev}$
$\sigma_{sH} \propto 1/v$	$10 \text{ kev} < E < 2 \text{ Mev}$
$\sigma_{sH} = 20b$	$1 \text{ ev} < E < 10 \text{ kev}$
$\sigma_{sH} = 32b$	$E = 0.025 \text{ ev}$
$\sigma_{sH} \propto E^{-5.3}$	$0.025 \text{ ev} < E < 1 \text{ ev}$

The above cross sections are taken from BNL-325 (H5). The results of the calculation are shown in Fig. A2.4.

$\underline{\tau_r}$

Basis of Calculation:

$$\tau = L_{1r}^2 = D_{1r}/\Sigma_{a1r} \qquad \text{(A2.27)}$$

The data for this calculation have been given above, and the results of the calculation are shown in Fig. A2.5.

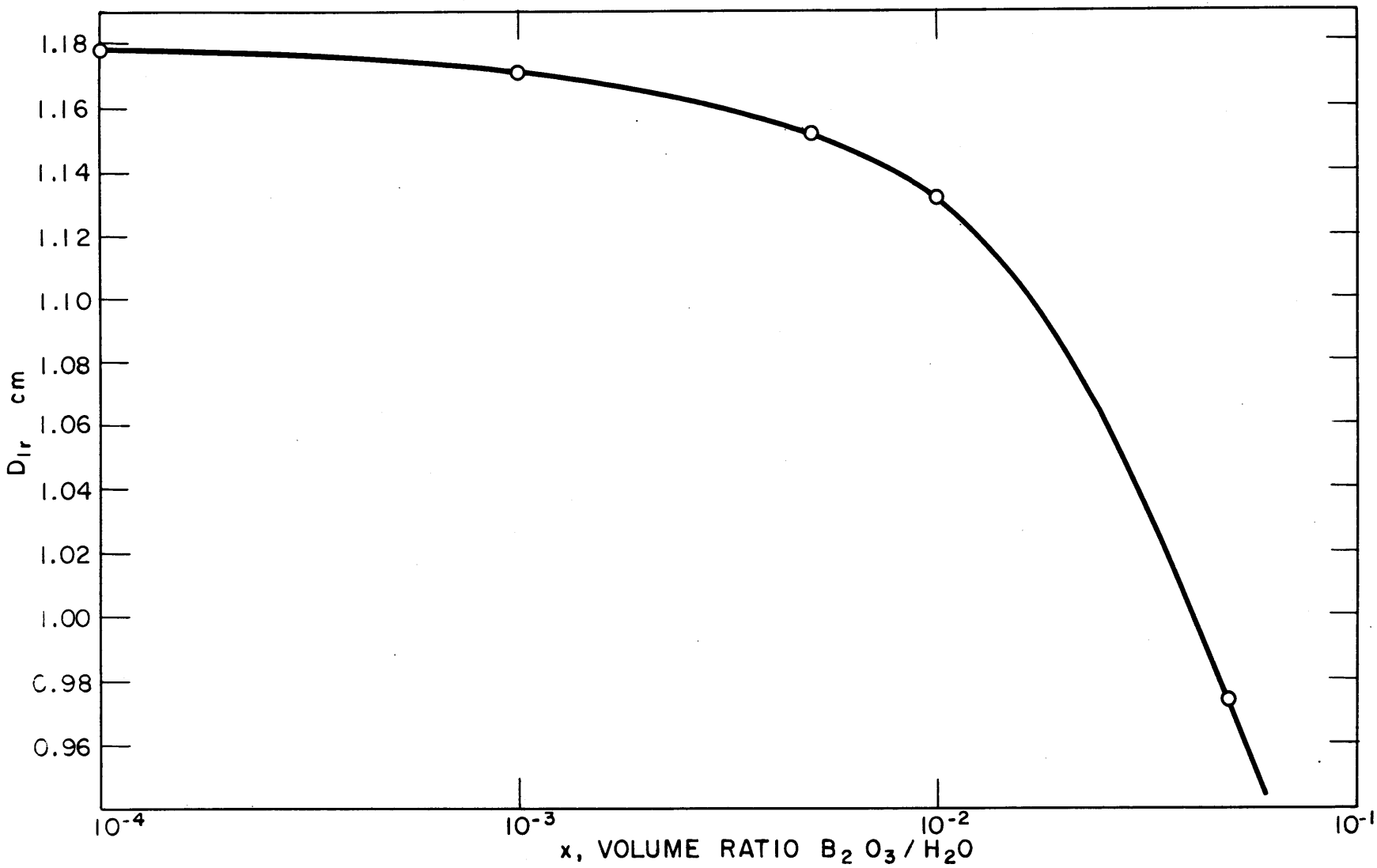

FIG. A2.4 VARIATION OF D_{lr} WITH BORON CONCENTRATION

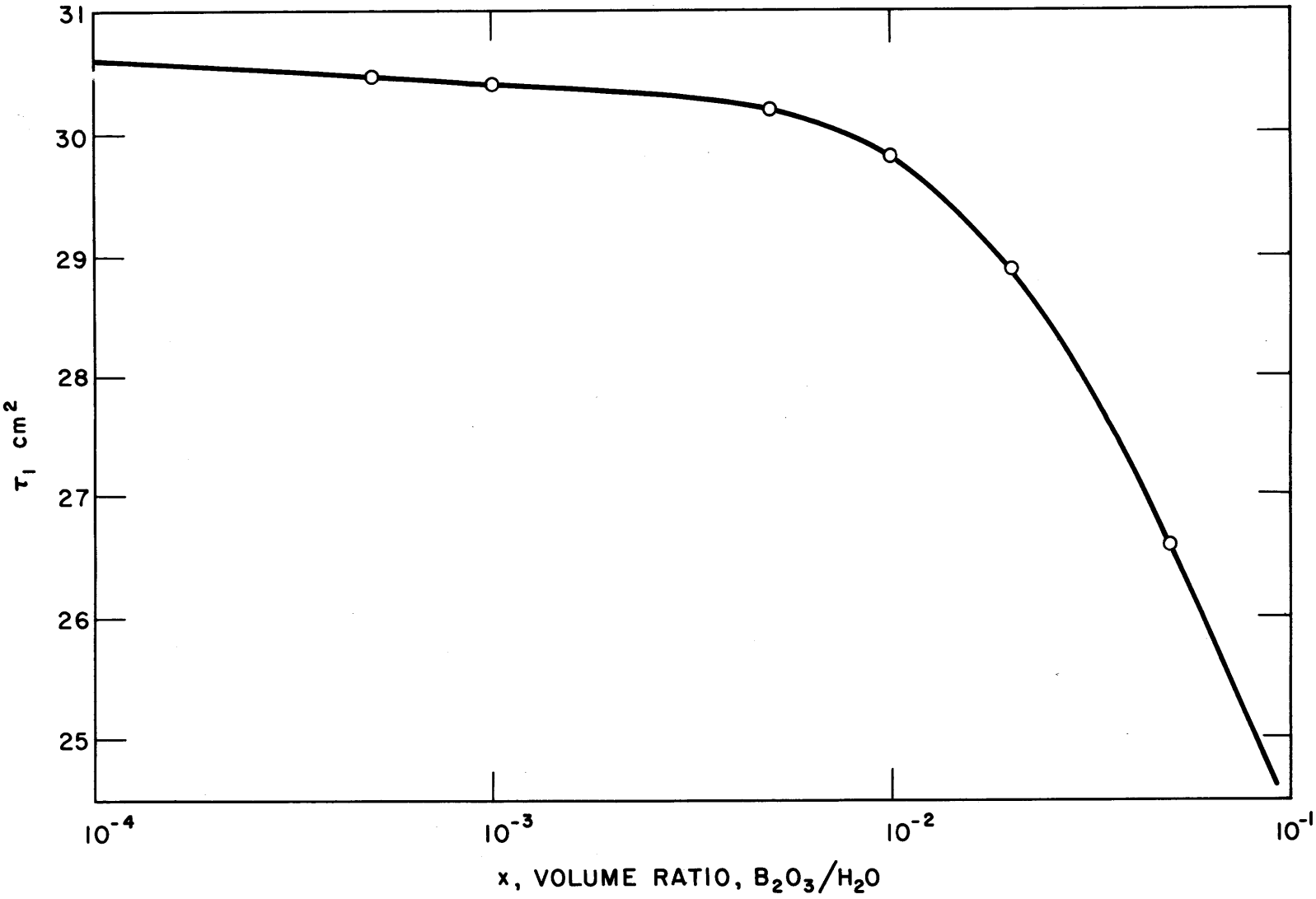

FIG. A2.5 VARIATION OF τ_f WITH BORON CONCENTRATION

It is now possible to calculate the fast-thermal coupling coefficient, a_3, as given by Equation A2.12. The dependence of a_3 on boron concentration is shown in Fig. A2.6. The fast-thermal coupling coefficients for the core, a_1 and a_2, as defined by Equations (A2.3) and (A2.4) can be calculated by using the following data (from references R2, E4, and H5):

$p = 0.863$ $\qquad B_1^2 = 12.81\ cm^{-2}$

$L_{2c}^2 = 66.2\ cm^2$ $\qquad \Sigma_a(D_2O) = 10^{-4}\ cm^{-1}$

$L_{1c}^2 = 123.8\ cm^2$ $\qquad \Sigma_a(U) = 0.405\ cm^{-1}$

$\xi(D_2O) = 0.509$ $\qquad \Sigma_s(D_2O) = 0.351\ cm^{-1}$

$\xi(U) = 0.0084$ $\qquad \Sigma_s(U) = 0.264\ cm^{-1}$

These data lead to

$a_1 = 0.489$ and $a_2 = -0.855$

Other data used are:

$D_{1c} = 1.29\ cm$ $\qquad D_{2c} = 1.092\ cm$

With the above data, the variation of λ with boron concentration in the reflector may be calculated as follows: A value of x, the boron concentration, is chosen. Try a value of α. From Equations (A2.9), (A2.7) and (A2.8), deduce the corresponding value of β. The right and left hand sides of Equation (A2.18) are then evaluated. This is repeated for different α's until Equation (A2.18) is found to be satisfied. The process is then repeated for other values of x. The variation of λ with x is then found by using Equations (A2.20) and (A2.22). The results of this calculation are shown in Fig. A2.7.

It is now straightforward to calculate the thermal flux distributions that would exist in the tank with various concentrations of boron in the reflector. The results of this calculation are shown in Fig. A2.8.

It should be noted, first of all, that an appreciable boron concentration is required before the flux assumes a pure Bessel function shape. At a B_2O_3/H_2O volume ratio of $5X10^{-2}$, the boron

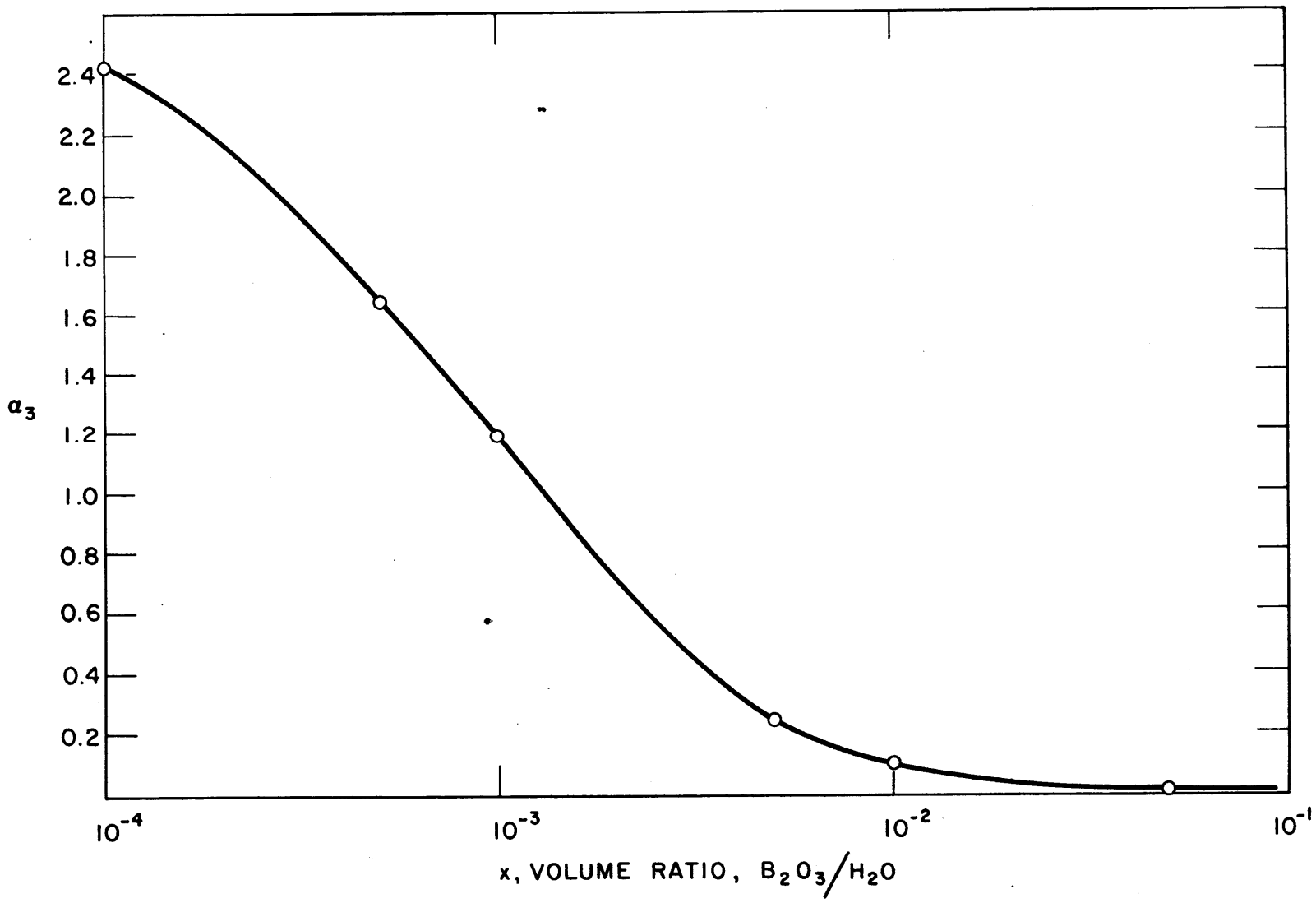

FIG. A2.6 FAST-THERMAL COUPLING COEFFICIENT IN REFLECTOR AS A FUNCTION OF BORON CONCENTRATION

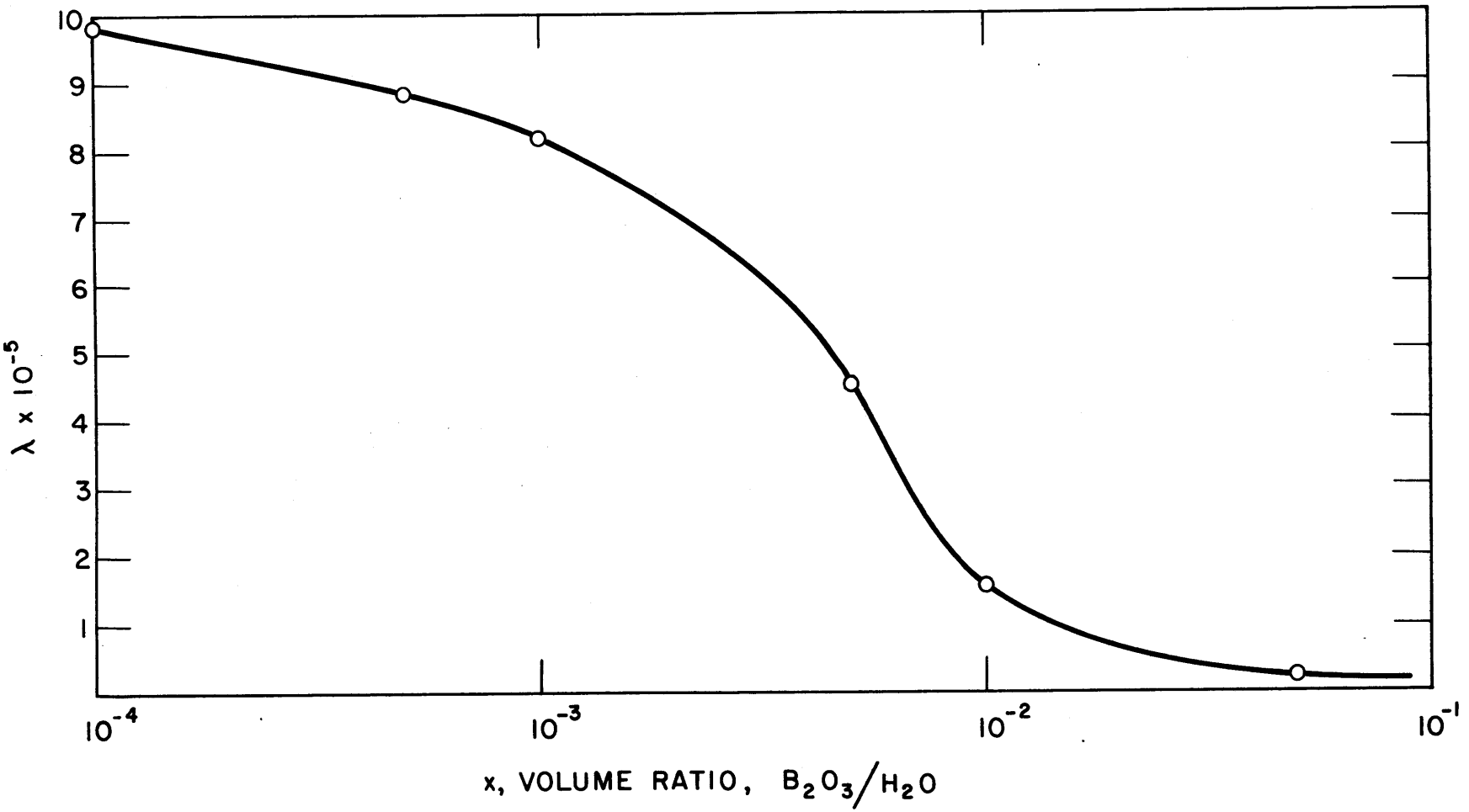

FIG. A2.7 VARIATION OF λ WITH BORON CONCENTRATION IN REFLECTOR

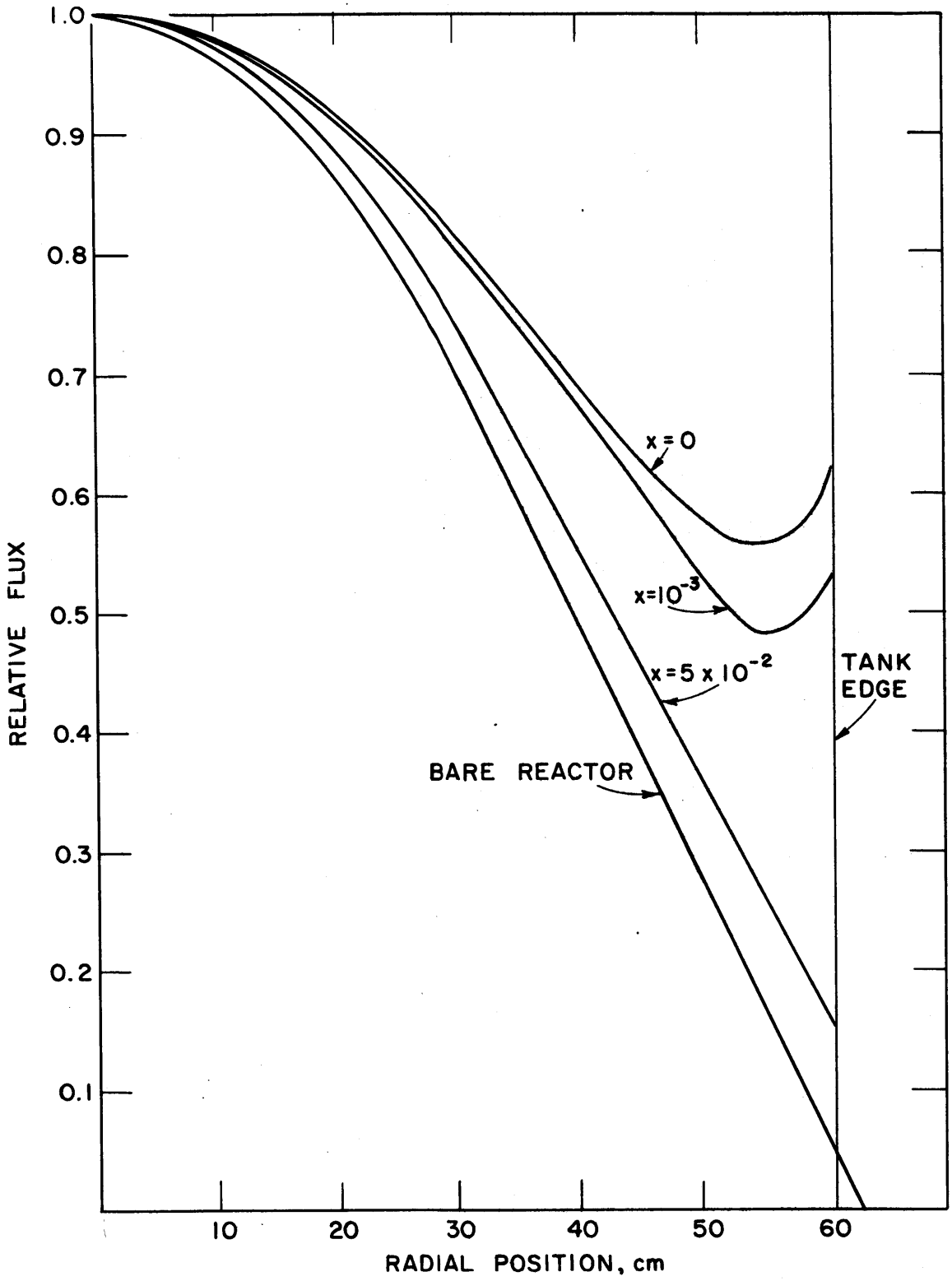

FIG. A2.8 RADIAL DISTRIBUTION OF THERMAL FLUX IN CORE AS A FUNCTION OF BORON CONCENTRATION IN REFLECTOR

concentration is 90 gm./liter. Even at this concentration, the I_o term is 3 per cent of the total value of the flux at 60 cm. The necessity for very high boron concentrations in order to obtain a pure J_o flux can be understood by examining the curves of Figs. A2.1 - A2.5. Many of the important parameters are strongly affected only at x values of 10^{-3} to 10^{-2}. This fact is further displayed by the shape of the curve for λ of Fig. A2.7.

Secondly, it should be noted that even at very high boron concentrations, the flux distribution does not correspond to that for a bare reactor. The reason for this is, of course, that the boron has very little effect in the fast groups. The reflector, although it may be a sink for thermal neutrons, still acts as a good reflector for epithermal neutrons.

In conclusion, it may be said that the method discussed above for dealing with the problem of fast reflection is, at best, difficult and, at worst, not feasible. It is doubtful whether sufficiently high boron concentrations can be obtained, for example. In any case, if such a method were used, the flux in the core would have to be fitted to an expression such as (A2.1)) to obtain the buckling.

Despite the complexity of even the straightforward approach used here, it would probably be advisable to examine fast reflection effects from shielding with a three-region, multigroup treatment. Only in such a calculation can a sufficiently accurate picture of fast neutron effects be obtained.

APPENDIX A3
REFERENCES

In the following list of references, the proceedings of the first and second International Conferences on the Peaceful Uses of Atomic Energy, held at Geneva, are referred to as ICPUAE, (1955) and (1958).

A1 T. Arnette, et al., "Exponential Experiments with Water-Metal Rod Lattices" CP-2048 (1944)

A2 D. G. Andrews and A. R. Dastur, "Flux Plotting in Source-Fed Subcritical Assembly", Can. Nucl. Tech., Summer, 1961, 14

A3 E. Anderson and O. Aspelund, "Exponential Experiments with Uranium Oxide Clusters in Heavy Water", ICPUAE, (1958) P/575, 12, 374

B1 P. Brown, "Measurement of the Spatial and Energy Distribution in Heavy Water-Uranium Reactor Lattices", Ph.D. Thesis, Nuclear Engineering Department, M.I.T., to be completed in June, 1962, and published as an NYO report.

B2 A. T. Biehl and E. R. Cohen, "The N.A.A. Exponential Assembly - Part I Apparatus and Preliminary Procedure", NAA-SR-103 (1951)

B3 J. R. Brown, et al., "Kinetic and Buckling Measurements on Lattices of Slightly Enriched Uranium and UO_2 Rods in Light Water" WAPD-176 (1958)

B4 W. Bothe, "Zur Methodik der Neutronensonden", Zeits. fur Physik 120, 437 (1943)

B5 D. F. Babcock, "Heavy Water Moderated Power Reactors Quarterly Progress Report, November, 1958 through January, 1959" DP-375 (1959)

B6 D. F. Babcock, "Heavy Water Moderated Power Reactors Quarterly Progress Report, February, March and April, 1958", DP-295 (1958)

B7 D. F. Babcock, "Power Reactor Studies Quarterly Progress Report, February, March, and April, 1957", DP-232 (1957)

C1 E. R. Cohen, "Exponential Experiments on D_2O - Uranium Lattices", ICPUAE (1955) P/605, 5, 268

C2 E. Critoph, "Comparison of Theory and Experiment for a) Lattice Properties of D_2O - U Reactors, b) Central Rod Experiments, c) Foreign Rod Experiments" CRRP-655 (1956)

C3 B. M. Carmichael and G. F. O'Neill, "Measurements of Lattice Constants in a Two-Region Critical Facility", Nuclear Eng., Part IV. Chemical Engineering Progress Symposium Series, 52, 173 (1956). No. 19. Am. Inst. Chem. Eng.

C4 J. Crandall, personal communication, November, 1961.

D1 G. von Dardel and N. G. Sjöstrand, "Diffusion Parameters for Thermal Neutrons in Water", Phys. Rev. 96, 1945 (1954)

D2 B. Davison, "Effective Thermal Diffusion Length in a Sandwich Reactor", J. Nucl. Energy 7, 51 (1958)

D3 G. Dessauer, "Physics of Natural Uranium Lattices in Heavy Water" ICPUAE (1958) P/590, 12, 320

D4 K. W. Downes, and H. J. Kouts, "Reactivity Coefficient Measurements of Buckling" BNL-1785 (1954)

D5 S. I. Drozdov, et al, "On the Formation of a Thermal Neutron Spectrum" Progress in Nuclear Energy Series I, Physics and Mathematics, Pergamon Press, 1959, 3, 207

E1 F. B. Estabrook, "Foil Activation by Neutron Currents", NAA-SR-259 (1953)

E2 F. B. Estabrook, "Single Rod Exponential Experiments", ID in NAA-SR-854 (1953)

E3 F. B. Estabrook, "Single Rod Exponential Experiments", ID in NAA-SR-925 (1954)

E4 H. Etherington, Nuclear Engineering Handbook, McGraw-Hill, N.Y., (1958)

F1 S. M. Feinberg, "Heterogeneous Methods for Calculating Reactors", ICPUAE (1955) 5, 484

G1 S. Glasstone and M. C. Edlund, The Elements of Nuclear Reactor Theory, D. von Nostrand Co., Inc., Princeton, N.J. (1952), p. 198

G2 S. Gallone, Nuovo Cim., 10, 1495 (1953)

G3 Y. Girard, et al., "Natural Uranium, Heavy Water Lattices", ICPUAE (1958) P/336, 12, 281

G4 A. D. Galanin, Thermal Reactor Theory, Pergamon Press, 1960, p. 362

G5 A. D. Galanin, "Critical Sizes of Heterogeneous Reactor with a Small Number of Rods", ICPUAE (1955), 5, 462

H1 W. Heisenberg and K. Wirtz, "Grossversuche zur Vorhereitung der Konstruktion eines Uranbrenners", Section 7.1 in FIAT Review of German Science, 1939-1946, Nuclear Physics and Cosmic Rays, Part II; W. Bothe and S. Flugge, Dieterich'sche Verlagsbuchhandlung, Weisbaden, Germany (1948)

H2 D. W. Hone, et al., "Natural Uranium Heavy-Water Lattices, Experiment and Theory", ICPUAE (1958), P/212 12, 351

H3 D. R. Harris, "Neutron Flux Mapping by Large Detectors", WAPD-TM-91 (1957)

H4 J. F. Hill, "One and Two Group Theory of Cylindrical Piles", AERE T/R-170 (1949)

H5 D. J. Hughes and R. B. Schwartz, "Neutron Cross Sections", BNL-325, Second Edition, (1958)

H6 "Heavy Water Lattice Research Project Annual Report", September 30, 1961, NYO-9658

H7 W. A. Horning, "A Summary of Small Source Theory Applied to Thermal Reactors", HW-34021 (1954)

H8 T. J. Hurley, Jr., H. R. Fike, and G. F. O'Neill, "Natural Uranium - D_2O Bucklings over an Extended Range of Pitch and Fuel Assembly Size", Transactions, Am. Nucl. Soc., 4, No. 1, 103 (1961)

H9 R. E. Heineman, "Experience in the Use of the Physical Constants Testing Reactor", ICPUAE (1958) P/1929, 12, 650

I1 International Atomic Energy Agency, Heavy Water Lattices, Vienna, 1960

J1 L. M. Johnson, "A Traveling Monitor for an Exponential Pile", DP-51 (1955)

J2 J. Jedruch, "Jofit - A Least Squares Bessel J_o Fitting Program for the IBM-704 Computer" YAEC-86 (1958)

J3 J. Jedruch and C. Saalbach, "Dared-1, an IBM-704 Program for Reducing Data from Foil Irradiations and Fitting by Least Squares to Bessel J_o or Cosine Function", YAEC-104 (1959)

K1 H. Kouts, G. A. Price, K. Downs, R. Sher, and V. Walsh, "Exponential Experiments with Slightly Enriched Uranium Rods in Ordinary Water" ICPUAE (1955), P/600, 5, 183

K2 S. W. Kash, "Buckling Measurements of Thermal Neutrons in Natural Uranium - D_2O Square Lattices" in NAA-SR-1432 (1955)

K3 H. Kouts and R. Sher, "Exponential Studies of Slightly Enriched Uranium, Water Moderated Lattices", BNL-486 (1955)

K4 A. E. Klickman, et al., "A Wire-Activation Technique for Reactor-Flux-Profile Measurements", BMI-1086 (1956)

K5 S. W. Kash, "Correction for Epithermal Neutrons in Diffusion Length Measurements" IB in NAA-SR-925 (1954)

K6 S. W. Kash, "Epithermal Neutron Attenuation Factor in D_2O", ID in NAA-SR-1016 (1954)

K7 S. W. Kash, "Effect of Neutron Source Gammas on the Buckling Measurements in D_2O Lattices" I in NAA-SR-209 (1955)

K8 S. W. Kash, E. Martin, and E. R. Cohen, "Neutron Production Reactor Experiments in the Exponential Assembly", NAA-SR-104 (1956)

L1 D. C. Leslie, "The Method of Feinberg-Galanin", AEEW-M18 (1959)

M1 J. Madell, "Spatial Distribution of the Neutron Flux on the Surfaces of a Graphite-Lined Cavity", Ph.D. Thesis, Nuclear Engineering Dept., M.I.T., Cambridge, Mass. To be published as NYO-9657. (1961)

M2 M. Merriman, A Textbook on the Methods of Least Squares, John Wiley, N.Y. (1892), p. 43

P1 R. Persson, "Criticality of Normal-Water Natural-Uranium Lattices", Nucleonics 12, No. 10, 26 (1954)

P2 R. J. Preston, "The MTR Automatic Wire Scanner", IDO-16243

P3 R. Persson, E. Blomsjo, M. Bustraan, and R. Meier, "Exponential Pile Experiments with Natural Uranium and Heavy Water", J. Nucl. Energy, 3, 188 (1956)

P4 R. Persson, et al., "Exponential Experiments on Heavy Water Natural Uranium Metal and Oxide Lattices", ICPUAE (1958) P/160, 12, 364

P5 R. Persson, "Exponential Pile Measurements on R3a Fuel Elements" AEF 65 (1956), AEC-Tr-3362

P6 R. Persson, "Exponential Measurements on Clusters of 19 UO_2-Rods, Diameter 15 mm" AEF-86 (1957)

P7 M. J. Poole, M. S. Nelkin and R. S. Stone, "The Measurement and Theory of Reactor Spectra" in Progress in Nuclear Energy Series I, 2, 91

Q1 M. Quinteiro Blanco, "Design and Construction of an Automatic Neutron Flux Scanner for the MIT Heavy Water Lattice Facility", M.S. Thesis, Nuclear Engineering Department, M.I.T., February, 1962

R1 J. H. Rush, "Range of Ra-α-Be Neutrons in Water", Phys. Rev. 73, 271 (1948)

R2 D. H. Roy, "The Physics of Slightly Enriched Uranium-Heavy Water Lattices", S.M. Thesis, Nuclear Engineering Department, M.I.T., 1959

S1 N. G. Sjöstrand, "Measurement of the Geometric Buckling Using the Pulsed Neutron Source Technique", ICPUAE (1958) P/161

S2 L. Seren and D. Tsakarissianos, "Analysis of Neutron Flux Data for Accurate Determination of Relaxation Lengths", Nucl. Sci. and Eng., 7, 277 (1960)

S3 W. D. Sandberg, Savannah River Laboratory, Personal Communications to Miss Barbara Kelly, M.I.T., March and November, 1961

T1 C. W. Tittle, "Slow Neutron Detection by Foils II", Nucleonics, 9, No. 1, 60 (July, 1951)

T2 R. J. Tuttle, "Technique for Gross Flux Measurements in the OMR Critical Assembly", NAA-SR-Memo 4263 (1959)

T3 R. J. Tuttle, "Preliminary Gross Neutron Flux Distribution Measurements in the OMR Critical Assembly", NAA-SR-Memo 4266 (1959)

T4 E. Teller, "Influence of the Lattice Structure on the Exponential Experiment", CP-165 (1942)

T5 O. A. Towler, et al., "Exponential Measurements in Heavy-Water Systems", Chem. Symposium Series, 52, No. 19, 177 (1956)

U1 R. E. Uhrig, "Material Buckling Measurements in a Subcritical Assembly" Paper 8-1, Trans. Am. Nucl. Soc. 2, No. 1 U959

U2 R. E. Uhrig, "Material Buckling Measurements in a Subcritical Assembly", Nucl. Sci. and Eng. 5, 530 (1959)

W1 A. M. Weinberg and E. P. Wigner, The Physical Theory of Neutron Chain Reactors, The University of Chicago Press, Chicago (1958)

W2 Ibid, p. 429

W3 Ibid, p. 430

W4 Ibid, p. 727

W5 Ibid, p. 382

W6 Ibid, p. 432

W7 Ibid, p. 501

W8 D. E. Wood, "Small Source Theory Oscillations in Exponential Pile Flux Distributions", HW-70716, 22 (1961), also Transactions, Am. Nucl. Soc., 4, No. 2, 284 (1961)

W9 E. C. Wingfield and E. J. Hennelly, "Comparison of Exponential and Critical Bucklings for Natural Uranium Rods in Heavy Water", Transactions, Am. Nucl. Soc., 4, No. 2, 296 (1961)

W10 J. R. Wolberg, "A Study of the Fast Fission Effect in Lattices of Uranium Rods in Heavy Water", Ph.D. Thesis, Nuclear Engineering Department, M.I.T., 1962, to be published as NYO-9661

W11 A. Weitzberg, "Measurements of Neutron Capture in U^{238} in Lattices of Uranium Rods in Heavy Water", Ph.D. Thesis, Nuclear Engineering Department, M.I.T., February, 1962, to be published as NYO-9659

W12 E. Weinstock, personal communication, Brookhaven National Laboratory, December, 1959

W13 E. Whittaker and G. Robinson, The Calculus of Observations, Blackie and Sons, London (1958) p. 222

W14 C. Wikdahl, A. B. Atomenergi, Sweden, personal communication, 1961

W15 A. Weitzberg, "Studies of Resonance Capture in U^{238}", in Heavy Water Lattice Research Annual Report, NYO-9658 (1961), p. 54

W16 E. C. Wingfield and E. J. Hennelly, "Comparison of Exponential and Critical Bucklings for Natural Uranium Rods in Heavy Water", Transactions, Am. Nucl. Soc., 4, No. 2, 296 (1961)

Z1 J. W. Zink and G. W. Rodeback, "Determination of Lattice Parameters by Means of Measurements on a Single Fuel Element", Nucl. Sci. and Eng., 9, 16 (1961)